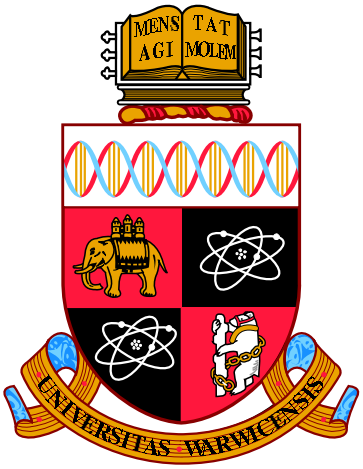

Collective Photo-Thermophoresis

by

Arran Tamsett

Thesis

Submitted to the University of Warwick

for the degree of

Doctor of Philosophy in Physics and Complexity Science

Centre for Complexity Science

November 2017

THE UNIVERSITY OF WARWICK

Declarations

This Thesis is submitted to the University of Warwick in support of my application for the degree of Doctor of Philosophy. I have read and understood the rules on cheating, plagiarism and appropriate referencing as outlined in my handbook and I declare that the work contained in this assignment is my own. No substantial part of the work submitted here has also been submitted by me in other assessments for this or previous degree courses, and I acknowledge that if this has been done an appropriate reduction in the mark I might otherwise have received will be made.

Abstract

The stationary distributions of thermally interacting thermophoretic colloids under illumination are studied by mathematical analysis of mean field models. This work generalises the model of Golestanian by explicitly modelling the non-local and non-pairwise effect of shading on the collective dynamics. Golestanian's solutions are recovered in the transparent limit, and the effect of shading is revealed to be two-fold: in the opaque limit in 1D all the heating occurs in the edges of the swarm which means the shaded centre of the colloid distribution is uniform and confined by exponentially decaying tails where the heating occurs; in 2D, hysteresis occurs of discontinuous transitions between dense, opaque distributions and diffuse, transparent distributions as the incident power is tuned. These results provide insight into systems governed by non-local line-of-sight based interactions which may illuminate other active matter systems, such as phototaxis of micro-organisms or flocking in birds.

Contents

List of Figures

1

Introduction

Since the birth of mathematical physics, with Newton's mathematical theories explaining the phenomenology of planetary orbits, there has been much interest in the collective behaviour of systems consisting of many interacting components. Since exact analyses are usually only possible with two-particle systems (with rare exceptions [1]), physicists, for many decades, employed numerical methods (calculated by hand) to study the dynamics of several interacting particles, which gets increasingly complicated and increasingly unreliable as more particles are considered. That is until the late nineteenth century where the development of statistical mechanics enabled physicists to understand the behaviour of systems consisting of very many interacting particles, and indeed to explain thermodynamics (a discovery of the early nineteenth century) as the so called thermodynamic limit of infinitely many particles, where the distributions in statistical mechanics can be replaced by the average of those distributions. The use of statistical physics methods to study systems in thermodynamic equilibrium has been of great utility over the twentieth century in explaining the properties of materials (i.e. systems composed of many interacting molecules), the emergent phenomena of such systems, and the phase transitions between different modes of emergent collective behaviour [2–4].

Over recent decades there has been a lot of interest in understanding the collective

behaviour of non-equilibrium systems [5–9], which are composed of many interacting particles which do not, over the time-scales of interest, reach a state of thermodynamic equilibrium. Any object which is alive must be a non-equilibrium system, since being alive involves extracting free energy from the environment in order to perform various functions. Since the state of minimum free energy is fundamentally the definition of thermodynamic equilibrium, living systems cannot be in such a state and so are fundamentally non-equilibrium phenomena. Of the many functions performed by living systems, active motion [10]- the directed movement of the object due to processes in or on the object converting free-energy in the environment (or stored energy in the object) to motion- is almost ubiquitous, occurring on length scales from micrometres, in the swimming of bacteria and eucharia [11], to tens of metres in the largest mammals. Of particular interest to physicists is the collective behaviour of many such active particles, mutually interacting with one another, a type of system known as active matter [12–19]. Active matter also occurs on a wide range of length scales, from micro-organism colonies on the micron scale [11, 20], to bird flocks [21] on the scale of hundreds of metres, to large mammal herds or fish shoals on the scale of tens of kilometres [22, 23]. Indeed, as ubiquitous as active motion is *per se*, active matter may be more ubiquitous in the sense that though different physical mechanisms produce active motion of individual particles on different scales, the phenomenology of their collective behaviour may be universal, meaning that the same, or similar, collective dynamics may appear in bird flocks as bacteria colonies. In contrast with many other non-equilibrium systems where an externally applied field globally perturbs a system from equilibrium, in active matter each particle is a local source of non-equilibrium behaviour, such as motion. This means that non-equilibrium collective behaviour of active matter is truly emergent: rather than being the collective response to a common external stimulus, collective dynamics in active matter are the result of the single particle dynamics and inter-particle interactions.

Following on from the use of probability theory in the formulation of statistical mechanics, and especially the mathematical theory of stochastic processes in the analysis of Brownian motion (an equilibrium phenomenon), the methods of stochastic dynamics have been extensively employed in the study of non-equilibrium phenomena [24–27] and active matter in particular [28]. A model typically is structured by specifying the state of the system as the microstate: this is the state of each particle individually, which is almost always a position variable and usually an orientation variable, and possibly other internal variables. The dynamics of the system are then defined by the increment on each particle (in theory one can define a continuous time

stochastic process, though in practice these are often discrete time processes) which usually includes a single particle self-interaction term (e.g. the directed motion of the particles along its own orientation, or the autonomous dynamics of other internal variables) plus a multi-particle interaction term plus a stochastic noise term. One of the first in the physics community to study such systems was Tamas Vicsek [29] who proposed the eponymous Vicesk model, which arguably laid the foundations for most computational studies of active matter since, many of which are formulated in the same way as the Vicsek model or as variations thereof.

The Vicsek model [30] consists of N particles whose state is defined by a position in a finite two dimensional space with periodic boundary conditions, and an orientation, that is an angle $\theta \in [0, 2\pi]$. The particles move at a fixed speed and interact via alignment interactions, so the orientation of the particle at the next time step is the average orientation of all the particles within some interaction radius, $\theta_i\left(t+\delta t\right) = \left\langle \theta_j\left(t\right)\right\rangle_R$ where R is the interaction radius and the index $i \in [1, N]$ labels the particle, plus a stochastic noise term (uniformly distributed in $[-\eta, \eta]$), and then the increment in position is a step in this direction at the fixed speed, $\vec{x}_i\left(t+\delta t\right) = \vec{x}_i\left(t\right) + v\left(\cos\theta_i, \sin\theta_i\right)$. In this original formulation of the Vicsek model there is no self-interaction; the model can be modified [31] to include, for example, an inertial effect so that particles tend to move in the direction they are currently moving, modified by a tendency to align with their neighbours. Indeed the most common concept of an active particle is one which moves along the direction of its internal orientation axis (perhaps with additional Brownian motion superimposed on this ballistic motion) with orientational Brownian motion acting to randomly re-orient the particle [10].

Vicsek interpreted his original model as a kinetic XY ferromagnet [32]: the alignment interactions as ferromagnetic interactions, the random noise term as analogous to the effect of temperature, and kinetic in the sense that the spins are moving. The Vicsek model exhibits a non-equilibrium phase transition: for low density (relative to interaction radius) and high noise a disordered gaseous phase occurs with particles moving randomly and no persistent alignment; for high density and low noise a globally ordered phase occurs with all particles moving in the same (spontaneously chosen) direction. In Vicsek's original paper this was understood to be a second order, continuous phase transition to a globally ordered collective phase with long-range order in a two-dimensional system- a significant contrast to equilibrium phenomena in which the Mermin-Wagner theorem [30, 32] prohibits long range order of spontaneously broken symmetry in two dimensions. It has subsequently been

shown to be a first order discontinuous phase transition induced by an instability at high enough density [33, 34]. The instability that creates the first-order character of the phase transition is due to the density dependent alignment interactions (i.e interact with *all* particles within some radius and *no* particles outside) of the original Vicsek model. A Vicsek-like model can be constructed to be incompressible (by, for example, introducing strong repulsive interactions). In this case the phase transition *is* continuous [35]. This constitutes a new universality class not found in equilibrium systems. Alternatively, if the interactions are metric-free (i.e. interactions are with the nearest n neighbours, or with Voronoi neighbours) then the phase transition is also continuous [36, 37]. In the case of compressible active matter of the Vicsek model type, as density is increased close to the critical point the system becomes unstable with respect to local fluctuations in density: a fluctuation creates a locally dense region which becomes locally ordered (at least partially) and moves together as a swarm; if the overall density of the system is too low then this will disintegrate over some time scale, but if the overall density is high enough then before this local swarm disintegrates it sweeps up more particles and grows becoming more dense and eventually spreading laterally, which makes it more ordered resulting in a positive feedback. Eventually the system phase separates, forming a narrow (in the direction of motion), dense, strongly ordered band that repeatedly cycles around the system sweeping up particles from a low density, disordered gas at it's leading edge, and losing particles to the disordered gas at its trailing edge [33, 34, 38]. As the overall density of the system is increased the band widens until it fills the system. This is the principal phenomenology of the Vicsek model, which is highly robust with respect to changes in the details of the model [39, 40], and which has been observed in synthetic experimental systems [41] and living systems [42, 43].

In contrast to the Vicsek model, in which the self-propelled particles interact via alignment rules, an alternative model has been extensively studied in which the particles have finite size and interact via volume exclusion rules (without alignment) [44, 45]. In such models the state of each particle is defined by its position and orientation; the system dynamics are single particle rules plus interaction rules, where the single particle rule is the standard active Brownian motion of moving along the particle's orientation at fixed speed with Brownian rotation of the particle and isotropic Brownian motion superimposed on this; and the interaction rule is hard core repulsion, which can be implemented most simply by, at each increment in the simulation, displacing particles along the line connecting their centres whenever they overlap, or else with an (almost hard) soft-core repulsion such as a Weeks-Chandler-Anderson potential [46] (which is the Lennard-Jones potential cut off at

the minimum). The principal phenomenology of this model is mobility induced phase separation [47–49]: at low densities and low activity a disordered gas occurs in which each particle undergoes active Brownian motion without alignment or other collective effects; whereas, at high density and strong activity (i.e fast propelling speed), a phase separation occurs in which many clusters form (or one large cluster, at the highest overall density) surrounded by a low density disordered gas. The clusters, or 'active crystals', can move or rotate, grow and shrink by single particles joining the cluster or leaving, or else two clusters can merge or one cluster can separate into smaller ones. Phase separation is also seen in non-active colloids even without attractive interactions, however this only occurs at high density whereas active crystals can form when the overall density is much lower [46, 50, 51]. In equilibrium colloidal systems phase separation (fluid and crystal) of spherical colloids occurs at a packing fraction of 0.494 and the transition to purely crystal phase at a packing fraction of 0.545 (to put this in context the maximal packing fraction is 0.74, and the random close packing fraction is 0.64) [50], whereas active crystals have been shown to form at a packing fraction of 0.14 [19, 52].

In equilibrium, the crystal formation is due to maximisation of entropy i.e. the colloids arrange in a crystal in order to maximise the free volume that each particle moves in- the reduced macroscopic entropy of the crystal formation is compensated by the increased microscopic entropy of mixing [51, 53]. In contrast the living crystals form by the self-propelled particles "pushing" against one another [19]: as two particles collide head on they stop each other, a state which persists for a time of the order of the rotational time scale. After this time one of the particles rotates and moves away. However, if more particles collide with the first two before they rotate then, by the time they have rotated, they are "boxed in"; if this persists then a crystal forms where the particles on the edge are pointing inwards, and new particles join the cluster before the edge particles have a chance to turn and leave; that is until the rate at which new particles join becomes low enough for the cluster to begin to disintegrate. This is a non-equilibrium phenomenon, due to the active movement of the particles, which can violate detailed balance (clusters steadily grow and then collapse). This can also be understood as an instability in a system where an effective diffusivity is a function of local density [47, 48, 54]: active Brownian particles have, over long time scales, an enhanced effective diffusivity determined by their propulsion speed; repeated collisions between particles slows them on average, thus reducing their effective diffusivity, resulting in a density dependent diffusivity which, under an appropriate parameter regime, is unstable with respect to density fluctuations. This phenomenon has been realised in experiments on active colloids

[52, 55–57], and has been observed in bacterial systems [58–60]. Active crystals have also been found in nature on macroscopic scales in emperor penguin huddles [61].

Aside from stochastic models, usually studied using agent based computer simulations, the other important tool for theoretical studies of active matter has been continuum mean field models. Mean field models have been used to model many different physical phenomena: distributions of diffusing particles, the evolution of temperature fields, atmospheric fluid dynamics and the magneto-hydrodynamics of the solar atmosphere- all systems out of thermodynamic equilibrium. The first continuum mean field model of active matter was proposed, shortly after Vicsek's seminal publication, by Toner and Tu [62, 63] and many others have followed [12, 15]. These models usually take the form of Navier-Stokes type equations (according to symmetry requirements) with unknown coefficients, or Fokker-Planck type equations [64, 65]. Such models have been generalised to model active forms of other emergent phenomena, such as nematic or smectic fields, and have been interpreted as models of various physical systems from acto-myosin dynamics inside living cells [66, 67] on the smallest scales, to flocks of birds on the largest scales.

The Vicsek type transition to polar ordered active fluid whenever alignment interactions dominate, and the active crystal phase separation transition, whenever steric repulsion dominates, are arguably the most fundamental and important phenomena discovered in studies of active matter over the past couple of decades. However, many other phenomena have been revealed in experiment, simulation, and mathematical analysis: nematic and smectic ordered active matter [12, 15, 68], circulation and vortices (including vortex lattices) [69, 70], lane formation [71, 72], travelling active crystals and clusters [73, 74], turbulence [75, 76], the emergence of localised polar ordered swarms [77, 78].

Active matter systems have been studied experimentally with microscopic artificial active colloids [11, 46]. Active colloids can be synthesised by exploiting various physical phenomena: the phenomenon of Quincke rotation has been exploited to create self-propelling and interacting colloids under an applied electric field [41, 79]; recoil from bubble release has been used to create self-propelling particles- hollow micro-tubes have been constructed such that the inside surfaces catalyse the decomposition of H_2O_2 into oxygen and water causing the formation of bubbles which detach from a spontaneously selected side of the tube creating a jet-like propulsion [80–82]; biomimetic microswimmers have been synthesised to imitate the beating flagella [83, 84] or beating cilia [85–88] of living micro-organisms; the most common physical mechanisms exploited to create active colloids are phoretic processes.

Phoresis is a hydrodynamic process in which an effective slip flow is induced close to the surface of a colloid in response to gradients of some field (temperature, solute concentration, electric potential) which, since the system is overall force free, results in the colloid moving in the opposite direction [89–91]. If the phoretic colloid can be constructed in such a way as to induce a local field gradient around itself (along an axis determined by the axially-symmetric structure of the colloid) then the colloid will also drift by phoresis in response to this field gradient along the direction of its own orientation, hence it has induced its own movement and is self-propelling. This phenomenon is called self-phoresis [92–94]. Perhaps the most common form used to create self-propelled colloids is self-diffusiophoresis [95–98] (although it is not always clear exactly which phoretic mechanism is occurring in a given experiment) achieved by making Janus colloids which are spherical particles (usually polystyrene or silica beads) half coated with a metal that catalyses some chemical reaction in the fluid (for example, a platinum cap catalysing the breakdown of hydrogen peroxide into oxygen and water) thus inducing a local chemical gradient around the colloid, which responds to this gradient by diffusiophoresis. Such particles are autonomous, self-propelling when in the presence of the chemicals that they catalyse; moreover self-diffusiophoresis can be used in colloids which have hematite cubes attached so that the reaction catalyses only when under illumination [52, 55] so that the self-propulsion can be optically activated or de-activated. The second kind of phoretic mechanism used to synthesise self-propelled colloids is electrophoresis [99], indeed this was one of the first mechanisms used in creating colloidal self-propelled particles [100, 101]. The third phoretic mechanism is thermophoresis, the drift of colloids in response to temperature gradients [102–104]. Self-thermophoretic colloids can be created by making Janus particles where non-metallic colloids (e.g. silica beads) are half coated in metal (e.g. gold) and illuminated by laser radiation so that the metallic side heats more than the non-metallic side creating a local temperature gradient that the colloids can then drift along by thermophoresis [105–109]. Unlike diffusio- and electro-phoresis, thermophoresis is not well understood (though there have been some attempts [103, 110]) and seems to be highly chemistry specific. The thermophoretic mobility depends on the type of solvent, the detailed nature of the particle-solvent interactions, the absolute temperature (broadly, this dependence is thermophobic at higher temperatures and thermophilic at lower temperatures)[102, 106]. Nevertheless, self-thermophoresis has been experimentally realised and has been exploited to gain considerable control over individual colloids [111–115] which has great potential for future development of nano-technology or as tools for studying other systems [116–119].

The collective behaviour of self-thermophoretic colloids under light irradiation has been theoretically analysed by Golestanian et al in [64] and [120]. In the first of these publications Golestanian began with a Langevin model of the stochastic dynamics of the Janus colloids accounting for Brownian motion, self-propulsion and Brownian rotation, and inter-particle interactions via temperature in which the temperature field induced by each particle (due to light radiation that it absorbs) is a monopole temperature field inversely proportional to distance from the particle, and the speed of each particle is proportional to the gradient of the overall temperature field. Golestanian then derived, via Fokker-Planck equations, a continuum model for the system in terms of a mean field density and temperature. He analysed the system for the cases of both thermophobic and thermophilic colloids in one, two, and three dimensional symmetric systems. For the case of thermophobic particles he found a depletion in the centre of the system (the centre will always be hotter, so thermophobic colloids will drift outwards until this drift is balanced by diffusion). The magnitude of the depletion can be described by the relative size of central to edge density. In the strong coupling limit, that is when the colloids absorb a lot of energy and are strong sources of heat, the depletion grows with system size in 1D (rectangular symmetry), shrinks with system size in 3D (spherical symmetry), and is independent of system size in 2D (cylindrical symmetry). For the case of thermophilic particles, Golestanian found an accumulation of particles in the centre. As the coupling strength increased a point is reached beyond which the stationary distributions become unstable in all geometries (1D, 2D and 3D). The reason for this instability is the positive feedback between the density of colloids and temperature: as the density increases the centre becomes hotter, which draws more particles to the centre resulting in positive feedback. In this article Golestanian offered no analysis of system behaviour when this instability occurs as the system enters parameter regimes (of high density) beyond the validity of the model.

Golestanian's model makes the simplifying assumption that the light intensity is uniform everywhere, so every particle is a similar source of heat. The model includes an unknown coupling constant that describes the efficiency at which each particle absorbs energy from the radiation. The rate of production of heat per particle is proportional to the product of light intensity and this parameter, thus the strong coupling regime corresponds to either tuning this parameter or the light intensity (in the analysis what is actually tuned is the dimensionless ratio of various length scales which include this parameter). This model does not account for the possible shading of light by other particles closer to the light source. The source of energy is radiation which illuminates the system from the outside. Particles at the exterior of

the distribution will be irradiated by laser radiation at a high intensity, but precisely because these outer particles have absorbed some of the energy, the particles in the interior of the distribution will experience radiation at a lower intensity (or at least a lower overall power- the intensity may increase with geometric focusing but the energy present in the radiation at lower radii will decrease). The effect of shading is that not all particles will be equal sources of heat, in particular the heating per particle ought to be greatest in the least shaded regions and least in the most shaded regions, thus a very dense swarm should have the least heating per particle in the centre as this should be the most shaded area, which may arrest the instability of Golestanian's model. This is one of the key questions that I address in this thesis.

In [120] Golestanian and Cohen studied the collective dynamics of self-thermophoretic colloids under planar irradiation by agent based simulation. They modelled the particles as Brownian active particles undergoing isotropic Brownian motion together with self-propulsion along the direction of their internal axis, which itself undergoes rotational Brownian motion. They also included a drift along the gradient in the macroscopic temperature field. Excluded volume interactions were also included. The macroscopic temperature field is the sum of the temperature fields due to the heating of each particle, where each particle heats, and also self-propels, only when under direct illumination, and, indeed, the particles only heat from the surface on the side illuminated. In this way the effect of shading is explicitly accounted for in the model. In this model, a single particle would heat on the side facing the radiation. This generates a local gradient in temperature, not necessarily aligned with the particle's axis. This causes the particle to self-propel towards the radiation. The collective effect is the formation of comet-like swarms in which most of the heating in the swarm occurs at the front end by the unshaded, or partially shaded, colloids generating a high temperature in the centre of the swarm. This has the effect of radially constraining the swarm, and of creating a shaded region in the comet's wake of particles that do not heat but are drawn by the heating from the leading edge. The swarm as a whole is slowed due to collective thermal drag: individual particles at the front are drawn back by the heat produced by the particles behind them. Over time the swarm evaporates as particles in the tail diffuse radially outwards whereupon they become illuminated, self-propel vertically (faster than the comet) and are either drawn back into the swarm or else eventually by-pass it. The system exhibits many phenomena including circulating particles in the comet tail, strong density fluctuations in the comet head, and occasional ejection of mini-comets from the comet head. The non-local effect of shading is extremely significant in determining the collective dynamics of this system of optically driven active particles.

The mathematical theory developed in this thesis, which generalises Golestanian's mathematical model as discussed in the previous paragraph, could potentially be modified to model Golestanian and Cohen's agent based model, perhaps providing theoretical insights to the results of their simulations.

There have been relatively few studies of the collective behaviour of optically induced active matter systems where the effect of shading is taken into account. The simulations of Golestanian and Cohen have accounted for the effect of shading in a system of self-thermophoretic colloids, discussed above, but there have been few other such models. One other model of active matter where a shading-like effect determines the dynamics has been studied by Pearce et al [121]. They noticed that bird flocks are usually marginally opaque across a wide range of flock sizes even though there is ample room for the birds to spread into transparent flocks or to move together and form entirely opaque flocks. The opacity of a flock of birds, or of a distribution of any type of particle in which the individual particles do not transmit electromagnetic radiation, is the fraction of lines of sight through the distribution which are obstructed by at least one particle. An opaque distribution will obstruct almost all lines of sight, a transparent distribution will obstruct a small fraction of lines of sight, and a marginally opaque distribution is one in which a substantial fraction of sight-lines are obstructed but also a substantial fraction are unobstructed.

The Vicsek model produces polar ordered phases but only in a confined system where the global particle density is fixed. If the size of the (periodic) box confining the particles is increased at fixed number of particles, the polar ordered distribution will spread laterally, becoming a narrower band in the direction of motion until it becomes too narrow to sustain itself and the system transitions to the disordered phase. There is no mechanism in the original Vicsek model to produce stable, spatially localised swarms. Furthermore, field studies [21] suggest the interaction rules in bird flocks are topological rather than distance based, but though metric-free Vicsek-type models may produce ordered collective states even at low density, there is no mechanism in such models to regulate density and prevent the flock from spreading arbitrarily far in open space. Other models [77, 78] which are modifications of the Vicsek model can produce localised ordered swarms, but without regulation of density to produce the rather special state of a marginally opaque swarm (i.e. there are many ways to be transparent or opaque, but marginal opacity is a fine balance).

Pearce et al proposed an active particle model in which the self-propelled particles in-

teract via alignment interactions with Voronoi neighbours, and also by multi-particle interactions determined by the projection of the swarm onto each particle's field of view. In contrast to most active matter models this does not model interactions as the linear combination of pairwise interactions, but as a non-local, non-pairwise interaction of each particle with the whole swarm. In particular, particle dynamics determined by field of view based rules must incorporate the effect of shading. Their model produces flocks that self-organise into marginally opaque swarms across a broad range of flock sizes. The fact that the phenomenology of real bird flocks can most parsimoniously be explained by models that incorporate projection based interactions into the particle dynamics is strong evidence that the effects of non-local line-of-sight type interactions have important consequences for the collective dynamics of (at least some) active matter systems. By incorporating the effect of shading (which is so important in the self-organisation of bird flocks) into the dynamics of active thermophoretic colloids, the present work can be thought of as one of the first bridges between non-equilibrium thermodynamic systems and animal systems. Interestingly, the state of marginal opacity, an attractor in the model of Pearce et al, is also important in determining the self-organisation of thermophoretic colloids.

Another example of living systems responding to optical fields is the phototaxis of micro-organisms [122–125]. In [126] Vincent and Hill introduced a continuum mean field model of phototactic algae (which they have developed in [127, 128]). This model describes a continuous distribution of algae suspended in a fluid where the algae are slightly more dense than the fluid. These are confined in a container of finite depth and large (i.e. effectively infinite) horizontal extent, so that the gravitationally stable arrangement is for the algae to sink to the bottom. The system is irradiated vertically downward with uniform intensity. The algae are advected by the fluid flow which is influenced by the algae, which can be viewed as Stokeslets, due to their negative buoyancy. Aside from being advected by the fluid, the algae diffuse isotropically, and self-propel in response to light fields. The response of an algal cell is either photophilic or photophobic depending on the level of light intensity- photophobic when the intensity is too high, and photophilic when the intensity is too low [129]- where the precise intensity response is species dependent. In their model Vincent and Hill explicitly modelled the effect of shading whereby algae higher up shade the incoming light causing algae lower down to experience a lesser intensity. If the light intensity is very high then the algae move to the bottom of the container, whereas if the intensity is low then the algae move vertically up and accumulate close to the fluid surface. If the light intensity is tuned appropriately there will be a position in the algal distribution where the intensity is the critical

value that corresponds to the transition from photophilic to photophobic response. Above this height, the algae will respond photophobically swimming downwards, and below this point they will swim upwards towards the light. Hence, the effect of shading within the algal distribution is the self-organisation of a layer suspended in the fluid where the algae congregate. Since the algae are slightly more dense than the fluid, the fluid above the algal layer is gravitationally stable and the fluid below is potentially unstable. In certain parameter regimes the stationary distribution becomes unstable, and convection cells form (which bifurcate as the parameters are tuned. Eventually a Hopf bifurcation creates periodically evolving convection cells). This has been termed bioconvection.

In the Vincent-Hill model shading is explicitly included, and they analysed this in the limit of low shading, analytically computing the stationary distribution of algae. Interestingly this takes the form of the square of a hyperbolic secant function, which is precisely the functional form of the stationary distribution of thermophilic colloids in 1D in Golestanian's model [64]! These two models have very different mechanisms: in the thermophoresis case the colloids absorb energy from a common radiation field, heat the fluid and drift by thermophoresis according to the collectively produced temperature field; the phototactic algae move towards or away from the light dependent on the light intensity, where the collective effect is to modify the intensity in different positions by shading. Despite having very different physical mechanisms determining the interparticle interactions, these systems are both active, responding to optical stimulation which, in the low shading limit, produces very similar stationary distributions and even instabilities as the coupling strength (i.e. magnitude of activity) increases. This similarity of phenomenology may (tentatively) be taken as evidence that there may be universal phenomena in systems governed by shading interactions.

In the present work the collective stationary distributions of self-thermophoretic colloids under illumination are studied in rectangular and cylindrical symmetry. The analysis is essentially a generalisation of Golestanian's model that explicitly accounts for the effect of shading. The effects of shading are basically two-fold: first, not all particles are equal sources of heat, but rather the position of the colloid determines the heating that it generates. This has important consequences for the form of the resulting distributions. Second, the overall heating of the colloid distribution depends on its opacity, which, in dimensions higher than 1D, depends non-trivially on the density distribution which has important consequences for the ability of the system to self-organise. In [64] Golestanian assumed that every particle is an equal

source of heat, which is proportional to the light intensity. This model does not explicitly account for shading. If one does account for shading, and then analyses the solution in the low shading limit (that is, considering an almost transparent system), one obtains the same functional form (the square of the hyperbolic secant) found by Golestanian, and Vincent and Hill. As the system becomes more opaque, the effect is that the centre of the swarm becomes almost entirely shaded so that only particles at the edge are contributing to the heating. The collective heating is then at the edges of the swarm, creating a uniform temperature profile inside the swarm and a steeply decaying temperature outside of it, so particles inside can freely diffuse until they reach the edge at which point they are confined by steep temperature gradients. Hence, the distribution of particles is uniform up until the point where the outside becomes visible (that is the point where radiation from the outside can penetrate) at which point the density exponentially decays. In the cylindrical geometry, the opacity of the distribution depends on the particle distribution: a localised distribution can be opaque, but the same number of particles can alternatively be spread out to create a transparent distribution. An opaque distribution will absorb almost all of the radiation energy, whereas a transparent distribution will absorb almost none of it. This interplay between opacity and activity creates hysteresis in the stationary distributions: with low radiation power there is not enough energy for the system to form localised swarms, i.e. diffusion (entropy) dominates and the system becomes diffuse; for high power even the smallest fraction of this energy absorbed by the system is enough to overcome diffusion, so thermophoresis dominates, driving the colloids close to the origin, where a localised, opaque distribution forms. For intermediate laser power the system becomes bistable: a diffuse and transparent distribution absorbs so little of the available laser power that diffusion dominates and it remains diffuse and transparent; a sufficiently localised distribution will also be opaque and so must absorb most of the laser radiation, in which case it absorbs enough radiation to overcome diffusion and remain localised and opaque. The same analysis of shading can be employed in modelling phototaxis of colloids that move in response to light intensity differences as seen from either side (i.e. the colloid current is proportional to the vector sum of light intensity). The stationary distributions of this collective phototaxis system are *exactly the same* as those of the self-thermophoretic system! This is reminiscent of the similarity of stationary distributions as found by Golestanian and Vincent and Hill. Although we have not analysed the stability of the stationary distributions, it is plausible that the instabilities found by Golestanian, as coupling to the radiation is increased, are arrested by the effect of shading: Golestanian's instability occurs because a highly dense centre

becomes very hot which draws more particles in which becomes even more dense and even hotter; however, accounting for shading, if this increased central density makes the system more opaque at the centre then the heating region separates away from the centre thus limiting the condensation to the centre.

2

One Dimensional Model

2.1 The Model

Consider a system of N thermophoretic colloidal particles of radius r_0 enclosed in a 1D container of width $2x_b$, which has solid, transparent boundaries impermeable to the colloids and in contact with a heat bath at some temperature. The colloids are suspended in a fluid of specific heat capacity c and density ρ_f which conducts heat with thermal diffusivity κ; the colloids diffuse with diffusivity D (which is assumed to be independent of temperature) and exhibit a net drift along temperature gradients, where the drift is assumed to be linearly coupled to the temperature gradient [106], a phenomenon known as thermophoresis [102], with thermophoretic mobility D_T. Although most of the analysis applies to a purely 1D model (with the attendant implicit assumptions, i.e. phantom particles that can pass through one another), the system should really be thought of as quasi-1D. Janus colloids are small particles that have been half coated in a metal (usually gold), so that if illuminated by radiation (say, a laser) then their metallic side will heat up more than the non-metallic side, thereby creating a local temperature gradient around themselves oriented along their axis. If such colloids are thermophoretic then they will drift along this local temperature gradient and hence be self-propelling. This is called

self-thermophoresis [106]. Random reorientation of the particles will also occur as orientational Brownian motion. Janus colloids are active Brownian particles whose movement is determined simultaneously by two processes, Brownian motion and net drift along the particle's axis which itself undergoes Brownian re-orientation. The analysis that follows in this chapter applies to isotropic thermophoretic colloids that absorb light radiation and convert it to heat in the fluid, i.e. we do not explicitly model self-thermophoretic Janus colloids. However, this analysis could be interpreted as a first approximation to an analysis of the collective behaviour of self-thermophoretic Janus colloids where, in all subsequent results, the diffusivity is replaced with the effective diffusivity of active particles, $D \to D_{eff}$. In this case the effective diffusivity is $D_{eff} = D + \frac{v_0^2}{6D_R}$, where v_0 is the constant speed of the active particle and D_R is the rotational diffusivity of the particle. This follows the model of Golestantian in [64] in which he computed the particle speed to be $v_0 = \frac{\epsilon I D_T}{6k}$, where k is the thermal conductivity and ϵ is the coupling constant in his model that describes the efficiency with which colloids absorb light radiation, hence the speed of self-propulsion is proportional to light intensity. However, Golestanian's simplifying assumption that the light intensity is uniform, without accounting for shading, implies that all the particles have the same propulsion speed, which is not an assumption that can correctly be made when shading is taken into account. Thus, if the results of the following model are to be interpreted as corresponding to self-propelled particles (replacing diffusivity with effective diffusivity) then this must be understood as a first approximation, where a more exact analysis would account for spatially varying effective diffusivity.

We assume the system to be illuminated from both sides by laser radiation. If the laser light is intercepted by a colloid then it will either be absorbed by the colloid or scattered. Here we ignore the phenomenon of scattering[1] and assume all radiation is absorbed by the colloid, converted to heat which can then conduct into the fluid that the colloid is suspended in. The heat conducts through the fluid to the boundary where it conducts into the heat bath the system is connected to so that the temperature at the boundary of the system is the fixed temperature of the

[1] Golestanian's equation for the speed of a particle follows from the analysis of Jiang et al in [106] which includes a factor, ϵ, which they call the efficiency of laser absorption for which the amount of energy flux that contributes to heating is ϵI. This imperfect absorption of energy can be caused by a combination of partial transmission of light and partial reflection. Measurements of ϵ are not quoted by Jiang et al, but in [111] Qian et al do measure the absorbance and reflectance of their Janus colloids (the polystyrene sphere is mostly transparent and the gold cap is where most of the absorption occurs, and it matters which way through the radiation passes, i.e. medium $\to$ gold $\to$ polystyrene $\to$ medium or medium $\to$ polystyrene $\to$ gold $\to$ medium): absorbance $\sim 38\% \to 40\%$, reflectivity $\sim 43\% \to 47\%$, and transmittance $\sim 15\% \to 17\%$. The assumption of opaque colloids without scattering is a simplifying assumption that is not completely valid in general.

heat bath. The temperature profile in the system is the collective effect of the many colloids acting as heat sources and that heat conducting through the system subject to the boundary conditions. The collective heating of the colloid distribution will produce an inhomogeneous temperature profile, hottest in the bulk and decreasing to the boundary. If the colloids are thermophoretic then they will drift along the temperature gradients resulting in an inhomogeneous colloid density distribution, which will then modify the distribution of heat input, etc. The collective dynamics of heating, heat conduction, diffusion and thermophoresis are local effects; however, not all colloids are equal sources of heat, since they receive their heating energy from incident light radiation whose intensity may vary with position. In particular, the outer parts of the colloid swarm will shade the inner parts introducing a *nonlocal* effect into the dynamics. Following the models of Golestanian and Golestanian and Cohen we neglect hydrodynamic interactions between colloids.

The state of the system is characterised by a one dimensional mean field density, temperature, and light intensity distinguishing the radiation coming from the right, I_+, with that coming from the left, I_-. The number of particles, on average, inside some interval $x_1 < x < x_2$ is $\int_{x_1}^{x_2} \rho(x)\, dx$, so the density has dimensions $[\rho] = \frac{1}{L}$ reflecting the one dimensional nature of the system. The light intensity is the flux of radiation energy past a point and so has dimensions of energy per time, or power, $[I_\pm] = \frac{E}{T}$. More generally, the density has dimensions of number per volume, i.e. $[\rho] = \frac{1}{L^n}$, whereas the radiation intensity is a flow of energy across a surface, and so has dimensions of energy per time per cross-sectional surface area, i.e. $[I] = \frac{E}{TL^{n-1}}$, in an n dimensional space. The one dimensional system of finitely many particles considered here should really be understood as a two or three dimensional system in which the radiation is directed along only the x-axis, and all mean field quantities vary only along this same axis ($\frac{\partial}{\partial y}\phi = \frac{\partial}{\partial z}\phi = 0$ where ϕ is any mean field quantity). In such a system, the system may extend arbitrarily far in any perpendicular direction with arbitrarily many particles. To relate the purely 1D model with the reality of a higher dimensional experimental system, one must consider a slice of the higher dimensional system and multiply by the cross-sectional area of this slice. For example, if the system is really two dimensional then the particle distribution is described by the 2D density, $\rho_{2D}(x)$ with dimensions $[\rho_{2D}] = \frac{1}{L^2}$, and the 2D radiation intensity is I_{2D} with dimensions $[I_{2D}] = \frac{E}{TL}$; to relate this to the 1D model consider a slice of thickness Δy, then the 1D density is $\rho = \rho_{2D}\Delta y$, and the 1D intensity is $I = I_{2D}\Delta y$. The total number of particles in the slice is $N = \Delta y \int_{-xb}^{x_b} \rho_{2D} dx = \int_{-x_b}^{x_b} \rho dx$. The number of particles, N, which is a fixed physical parameter in the purely 1D model, is in reality not a fixed

parameter; rather the perpendicular density is the fixed physical parameter, i.e. in the 2D example, $\rho_y = \int_{-x_b}^{x_b} \rho_{2D} dx$ is the uniform density in the y-direction which can extend arbitrarily far, whereas the particle number, N, is the number in some section which depends on the width of the section, Δy.

2.2 General Equations of Motion

The current of particles is the density multiplied by the mean particle velocity, $\vec{j} = \rho \langle \vec{v} \rangle$. Diffusion follows from Fick's law, which assumes proportionality between the particle current and the density gradient ($\vec{j} = -D\nabla\rho$); similarly heat conduction is modelled by Fourier's law, which assumes the heat flux is proportional to the temperature gradient ($\vec{q} = -k\nabla T$, where k is the thermal conductivity of the fluid). In the case of diffusion, the average velocity of a particle is zero because the pressure fluctuations, which drive the Brownian motion, are isotropic, however the net flux of particles is due to relative numbers of particles moving from one direction compared to another, i.e. if the same proportion of particles in point A move to point B as move from point B to point A, but the total number of particles in A is greater than in B, then there will be a larger number moving from A to B and hence a net flux. The average velocity is not the time average of a single particle but the ensemble average over a distribution of particles, and is $\langle \vec{v} \rangle = -D\nabla \log \rho$, i.e. the average particle velocity is proportional to the gradient in entropy of mixing, where the proportionality constant, or diffusivity, can be derived from statistical mechanics. The diffusivity and rotational diffusivity of a spherical particle in three dimensional space are $D = \frac{k_b T}{6\pi\eta r_o}$ and $D_R = \frac{k_b T}{8\pi\eta r_o^3}$ [19]. In the case of thermophoresis, it is the time average of a single particle's velocity that is non-zero, and this is proportional to the temperature gradient ($\langle \vec{v} \rangle = D_T \nabla T$), but as yet the proportionality constant, the thermophoretic mobility D_T, has not been derived from statistical mechanics as there is no universally accepted theory to explain thermophoresis.

The mean field particle current is modelled by,

$$\vec{j} = -D\nabla\rho + D_T \rho \nabla T \tag{2.1}$$

The evolution of colloid density is determined by the current and the conservation of particle number,

$$\frac{\partial \rho}{\partial t} = -\nabla . \vec{j} \tag{2.2}$$

which leads to the general equation for particle density evolution,

$$\frac{\partial \rho}{\partial t} = D\nabla^2 \rho - D_T \nabla . (\rho \nabla T) \tag{2.3}$$

The temperature evolution shall be modelled by the heat equation with a source

term that is a (non-local) functional of density,

$$\frac{\partial T}{\partial t} = \kappa \nabla^2 T + \Gamma\left[\rho\right] \tag{2.4}$$

where κ is the thermal diffusivity of the fluid. The heating term, $\Gamma\left[\rho\right]$, is a functional of the particle distribution.This must reflect the physics that the more particles in some region the more heating in that region and also the non-local effects of shading. Moreover, the fact that the heating energy, at each point, comes from the energy lost from the radiation field, means that the heating term must balance the divergence of the intensity fields, i.e.

$$\Gamma\left[\rho\right] = -\frac{1}{c\rho_f}\nabla.\left(\vec{I}_+ + \vec{I}_-\right) \tag{2.5}$$

The boundary conditions on these equations must ensure that particles cannot leave or enter the system, i.e. the current must be zero on the boundary, $D\nabla\rho|_{boundary} = D_T\rho\nabla T|_{boundary}$, and that heat energy goes into the heat bath at the boundary, i.e. the temperature at the boundary must be the fixed temperature of the heat bath, $T|_{boundary} = T_{heatbath}$. Since the dynamics of the system depend only on *gradients* in temperature one can, without loss of generality, take the temperature of the heat bath to be zero. To compare with experiments one must simply add the absolute temperature of the heat bath. The boundary conditions on the intensity fields are simply the intensities of the light sources at the edge of the system. In general, almost all physical parameters (such as diffusivity, D, thermophoretic mobility, D_T, thermal diffusivity, κ etc) vary with temperature. For simplicity it is assumed the experiment is conducted within a temperature range that is small relative to the variation of these parameters, so that they may be assumed to be constants.

2.3 1D Equations of Motion

The dynamic variables in 1D are the density, $\rho\left(x\right)$, the temperature, $T\left(x\right)$, and the radiation intensities coming from the right and left, $I_{\pm}\left(x\right)$; such that the temperature is subject to the boundary condition $T\left(\pm x_b\right) = 0$, the radiation intensity is subject to the boundary conditions $I_+\left(x_b\right) = I_\infty$ and $I_-\left(-x_b\right) = I_{-\infty}$, and the density and temperature are subject to the joint boundary condition $D\frac{d\rho}{dx}|_{\pm x_b} = D_T\rho\left(\pm x_b\right)\frac{dT}{dx}|_{\pm x_b}$ which ensures a zero flux of particles across the boundaries. The general equations of motion are (2.3), (2.4), and (2.5). In the next section we address

the interception of light by the colloid distribution.

2.3.1 Light Interception (Shading) in 1D

At the microscopic level the passage of light rays through the colloid swarm can be considered binary. Considering a point in the interior, either a light ray has passed through from the edge of the system to the particular point without being intercepted, in which case the energy of the light ray is not reduced at all; or there is at least one particle obscuring the path, in which case that light ray has been intercepted and none of it's energy reaches the interior point. However, the time-averaged light intensity, seen from this point, exists on a continuum between zero and the maximum of the incident light ray. This reflects a probabilistic interpretation of the mean field density at a microscopic level. Similarly, if one measures the energy flow across a cross-sectional surface element which is wide compared to the length scale of the colloid diameter, but narrow compared to the length scale over which the colloid density varies , then some of that surface will be completely in shade and some illuminated at the unchanging light intensity, but the average over the surface will be on a continuum. Figure (2.2) illustrates this coarse-grained 1D shading of a 2D system with rectangular symmetry.

Consider a small interval, $x \in [x, x + \Delta x]$, over which the colloid density is effectively uniform. The interception of light is modelled by a reduction in the average light intensity as a Poisson process over the length of this interval: the probability that a light ray will be obstructed in this interval is proportional to the number of particles, on average, in the interval; hence the proportion of energy absorbed through the interval is proportional to the number of particles[2], i.e. for light coming from the right, $\frac{I(x+\Delta x)-I(x)}{I(x+\Delta x)} = \alpha\rho\left(x\right)\Delta x$. This is illustrated in figure (2.1). In the continuum limit,

$$\frac{dI}{dx} = \alpha\rho\left(x\right)I\left(x\right) \tag{2.6}$$

[2]If the colloid opacity assumption is relaxed such that the particles are partially transparent, then this corresponds to a reduction of the parameter α, but everything else is unchanged. If single particle scattering of opaque particles is accounted for then this model of the incoming and outgoing radiation remains valid (although the assumption that scattered light exits the system without encountering another particle is unreasonable), but if multiple scattering is accounted for then such a model must account for absorption and scattering of radiation in all directions (light intensity is initially directed radially, but then some of this is scattered in other directions, some of which is absorbed from non-radial directions, and some of which is re-scattered etc). One model for this is the radiative transfer equation [128, 130].

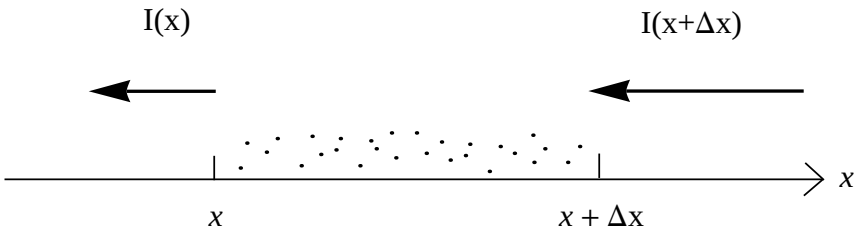

Figure 2.1: Schematic of light interception by colloids. The proportion of incident radiation that is absorbed over some distance is proportional to the number of particles in the interval.

This has the solution,

$$I\left(x\right) = I_{\infty} e^{-\alpha \int_{x}^{\infty} \rho dx'} \tag{2.7}$$

The derivation above, and the equation (2.6) which introduces an unknown dimensionless proportionality constant, are appropriate for a purely one dimensional model, but if the system is higher dimensional, with the radiation directed along the x-axis, then the derivation is more direct and no unknown parameter is introduced. Suppose the system is really two dimensional (with density and light intensity ρ_{2D} and I_{2D} respectively) and consider the cross-sectional surface of the back of a small interval in x of a strip of thickness Δy (see figure(2.2)): the fraction of radiation absorbed passing through this interval will be the fraction of the surface that is occluded by the particles in the interval (no proportionality constant introduced). The fraction of the surface occluded by the particles will be the number of particles ($\rho_{2D}\Delta x\Delta y$) multiplied by the fraction of the surface occluded per particle ($2r_0/\Delta y$), hence $\frac{\Delta I_{2D}\Delta y}{I_{2D}\Delta y} = \Delta x\Delta y\rho_{2D}\frac{2r_0}{\Delta y}$. In the continuum limit this is,

$$\frac{dI_{2D}}{dx} = 2r_0\rho_{2D}I_{2D} \tag{2.8}$$

This equation resembles equation (2.6) but with known proportionality constant, however to properly compare these two equations one must convert the 2D quantities in equation (2.8) to 1D quantities, i.e. the one dimensional density and intensity are $\rho = \rho_{2D}\Delta y$ and $I = I_{2D}\Delta y$. Re-writing equation (2.8) in terms of these one-dimensional quantities one obtains

$$\frac{dI}{dx} = \frac{2r_0}{\Delta y}\rho I \tag{2.9}$$

Thus the parameter α is revealed to be $\alpha = \frac{2r_0}{\Delta y}$. In the purely one dimensional model α is taken to be a fundamental property of the system, however if the system is truly two dimensional then α is determined by the arbitrary choice of Δy. Recall that the particle number, N, which is a fixed system parameter in the purely 1D model, is in fact not a fixed parameter if the system is higher dimensional, extending arbitrarily far in perpendicular directions, but rather the y density, ρ_y, is the fixed system parameter, i.e. $N = \int_{-x_b}^{x_b} \rho dx = \Delta y \int_{-x_b}^{x_b} \rho_{2D} dx = \Delta y \rho_y$. So two of the parameters of the purely one dimensional model actually depend upon the arbitrary choice of Δy if the system is really two dimensional ($\alpha = \frac{2r_0}{\Delta y}$ and $N = \Delta y \rho_y$). Consider the product of these: $\alpha N = 2r_0 \rho_y$. The product of the purely 1D system parameters depends on the product of the non-arbitrary 2D system parameters. A similar argument applies if the system is three dimensional with 1D symmetries (i.e. $\alpha N = \pi r_0^2 \rho_{yz}$). One expects in advance, therefore, that the analysis of the 1D model should depend only on the product of parameters, αN, and not on either of these independently.

In a two dimensional system with rectangular symmetry, the product, αN, can be interpreted as the perpendicular density in units of particle diameter, i.e. αN is the number of particles per particle diameter in the y direction. This can be greater than unity without particles overlapping since they can be spread out along the x direction. Notice that this determines the system opacity: if $\alpha N < 1$ then there are gaps in the projection of the particle distribution onto the field of view seen along the x direction from the side (as depicted in figure 2.2) and so the system is transparent; if $\alpha N > 1$ then the particles overlap in projection, on average, so the system is opaque; if $\alpha N \sim 1$ then on average every line of sight intercepts one particle, however, fluctuations in density will result in there being gaps as some lines of sight temporarily have more than one particle, and so this will be marginally opaque. Notice that the opacity of the system is determined by fixed system parameters and cannot change by changing the form of the distribution, a fact which applies only to quasi-one-dimensional systems in marked contrast to higher dimensional systems.

This result follows from the mean field assumption, which does not account for correlations in particle position, but may break if such correlations were to occur. For instance, consider a quasi-one-dimensional system in 2D with perpendicular density ρ_y: there may, over timescales which are long relative to the Brownian motion of single particles, be a tendency for particles to align along the x-axis, i.e for a colloid to be persistently shaded by its nearest (along the x-axis) neighbour. If the positions of nearby particles are correlated in this way then it must be that adjacent

to them (in the y direction) there is a persistent gap, hence this part of the swarm is less efficient at absorbing radiation than the mean field theory would predict. Or it could be that adjacent particles have a tendency to anti-align, spreading laterally such that the frequency with which adjacent particles shade one another is less than would occur with uncorrelated particles, and hence this part of the swarm is more opaque than the mean field theory predicts. In either case it could be that the effect of the correlations is to change the parameter α in the Poisson process model of light absorption, or it could be that the Poisson process model is no longer valid (i.e. the probability that a line intercepts a particle through some interval is now conditional on whether that line intercepted a particle through the previous interval, which is not the case in a Poisson process). It could be that the nature or strength of such correlations are a function of local particle density, so that the opacity of the swarm depends on the form of the distribution (i.e. a diffuse, low density swarm may be uncorrelated, but a localised, dense swarm may have position correlations in the centre which may modify the opacity of the swarm); or, given the non-local nature of the shading effect, it could be that there are non-local correlations in particle position. If correlations in particle position were to occur then the overall opacity of the system would depend not only on the fixed system parameters of particle radius and average perpendicular density, but also on the nature and strength of the correlations and the form of the distribution. Such hypothetical correlations are not considered here, we assume an uncorrelated distribution of particles for which the result holds that the opacity of the system is determined by fixed system parameters, αN, if the system is one-dimensional (or quasi-one-dimensional).

2.3.2 Conversion of Intercepted Energy to Heat

The conversion of the energy from intercepted radiation into heat in the fluid is described generally by equation (2.5) which equates the heating per fluid volume with the divergence of the intensity field. Specifically, in the one dimensional case, if an amount of energy ΔE is absorbed in the fluid in an interval of width Δx, then the change in temperature will be $\Delta T = \frac{1}{c\rho_f}\frac{\Delta E}{\Delta x}$. The rate of heating in the interval is the differential of radiation intensity entering and leaving the interval[3] (with a contribution from the radiation coming from each side), so

[3]If single scattering is taken into account then a ray of light intercepting a colloid is not completely absorbed, as is assumed in this analysis, but is partially scattered in which case a proportionality constant less than 1 should be introduced here, as the incoming radiation is reduced in part from absorption but also in part from scattering. However, if multiple scattering is accounted for then this point is moot as the model of heating must account for reduction of light intensity

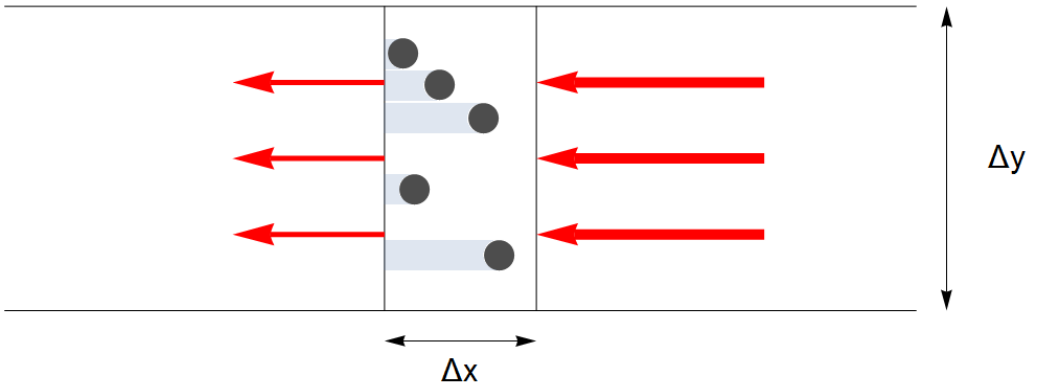

Figure 2.2: Schematic illustration of light interception in a 2D system with radiation directed uniformly along the x-axis. At an instant in time the particles in the interval, Δx, cast a pattern of light and shade. The coarse-grained light intensity is reduced over the interval by a factor equal to the proportion of the cross-section occluded by the particles.

$\dot{\Delta E} = (I_+(x+\Delta x) - I_+(x)) - (I_-(x+\Delta x) - I_-(x))$. The rate of temperature change per interval is then $\frac{\dot{\Delta T}}{\Delta x} = \frac{1}{c\rho_f}\left(\frac{\Delta I_+}{\Delta x} - \frac{\Delta I_-}{\Delta x}\right)$, and in the continuum limit

$$\Gamma(x) = \frac{1}{c\rho_f}\left(\frac{dI_+}{dx} - \frac{dI_-}{dx}\right) \tag{2.10}$$

which, by equation (2.6)- noting that the light intensity which comes from the left decreases towards the right- is $\Gamma(x) = \frac{\alpha\rho(x)}{c\rho_f}(I_+(x) + I_-(x))$, and substituting the solutions for light intensity,

$$\Gamma(x) = \frac{\alpha\rho(x)}{c\rho_f}\left(I_\infty e^{-\alpha\int_x^{x_b}\rho dx'} + I_{-\infty}e^{-\alpha\int_{-x_b}^{x}\rho dx'}\right) \tag{2.11}$$

$$= \frac{\alpha\rho(x)}{c\rho_f}\left(I_\infty e^{-\alpha\int_x^{x_b}\rho dx'} + I_{-\infty}e^{-\alpha N}e^{\alpha\int_x^{x_b}\rho dx'}\right) \tag{2.12}$$

The exponentials in equation (2.12) can be combined to give

$$\Gamma(x) = \frac{2\alpha}{c\rho_f}\sqrt{I_\infty I_{-\infty}}e^{-\alpha N/2}\rho(x)\cosh\left[\alpha\int_x^{x_b}\rho dx' - \frac{\alpha N}{2} - \frac{1}{2}\log\frac{I_\infty}{I_{-\infty}}\right] \tag{2.13}$$

Equation (2.13) describes the heating as a functional of the density. Notice that it has a factor of the density in front of the nonlinear term, a local effect (i.e. the more

from all directions across the interval.

sources of heat in a fluid element the more heating in that fluid), multiplied by a functional of the density, a non-local effect (i.e. the heating per particle depends where it is the swarm, in particular the integral from that point to the edge of the system, $\int_x^{x_b} \rho dx'$, accounts for the shading).

Previously, in mapping from a two dimensional system to a purely one dimensional model, the association between the absorption coefficient and particle number was noted: in order to map two dimensional mean field quantities to the one dimensional quantities of the purely 1D model an arbitrary perpendicular length scale must be introduced, i.e. $\rho = \rho_{2D}\Delta y$ and $I = I_{2D}\Delta y$. In both of these variables the one dimensional version depends on the arbitrary choice of Δy, however, it has already been shown that in the interception of light the 1D absorption coefficient is also determined by the y-length scale ($\alpha = \frac{2r_0}{\Delta y}$) such that this arbitrary part cancels in the product of α with particle number (or density), i.e. $\alpha\rho = \frac{2r_0}{\Delta y}\rho_{2D}\Delta y$. The arbitrary choice of y-length scale in the one dimensional light intensity also cancels with the dependence of thermal properties of the system on the y-length scale: Although the thermal *diffusivity*, κ, of the fluid is independent of the number of spatial dimensions ($[\kappa] = \frac{L^2}{T}$), the thermal *conductivity* is dimension dependent. The thermal conductivity is the coefficient in the relation of heat flux to temperature gradient ($\vec{q} = -k\nabla T$), and since the heat flux is the flow of energy per cross-sectional surface area, the dimensions of heat flux depend on the dimensions of the surface area, i.e. in n spatial dimensions $[\vec{q}] = \frac{E}{T\ L^{n-1}}$. The dimensions of the thermal conductivity must also depend on the number of spatial dimensions, i.e. $[k] = \frac{E}{T\ \Theta\ L^{n-2}}$, where the symbol Θ is used for temperature so that T is used for time. In particular, the thermal conductivity is related to the thermal diffusivity by the product with the volumetric heat capacity, $k = c\rho_f\kappa$, so the one dimensional thermal conductivity depends on the arbitrary y-length scale in the same way as the one dimensional fluid density does, $\rho_f = \rho_{f2D}\Delta y \Rightarrow k = k_{2D}\Delta y$. As can be seen from equation (2.5) relating heating to radiation divergence, the radiation intensity appears in equations in concert with the volumetric heat capacity (or equivalently with thermal conductivity, multiplying by κ), so that the dependence on y-length scale of the light intensity (an energy flux) is cancelled by the dependence on y-length scale of the thermal conductivity (a constant related to another energy flux). In other words, one expects to see the ratio $\frac{I}{k}$ or $\frac{I}{c\rho_f}$ in all analytical results and never to see these quantities expressed separately. This can be seen in equation (2.13): in the argument of the hyperbolic cosine there are products of αN and $\alpha\rho$, and in the prefactor to the hyperbolic cosine there is the product of $\alpha\rho$ and the ratio of $\frac{\sqrt{I_\infty I_{-\infty}}}{c\rho_f}$, as well as the product αN in the exponent.

2.3.3 Equations of Motion in 1D

Finally, incorporating equations (2.3), (2.4), and (2.13), leads to the one dimensional equations of motion,

$$\begin{cases} \frac{\partial T}{\partial t} = \kappa \frac{\partial^2 T}{\partial x^2} + \frac{2\alpha}{c\rho_f}\sqrt{I_\infty I_{-\infty}} e^{-\alpha N/2} \rho(x,t) \cosh\left[\alpha \int_x^{x_b} \rho dx' - \frac{\alpha N}{2} - \frac{1}{2}\log\frac{I_\infty}{I_{-\infty}}\right] \\ \frac{\partial \rho}{\partial t} = D\frac{\partial^2 \rho}{\partial x^2} - D_T \frac{\partial}{\partial x}\left(\rho \frac{\partial T}{\partial x}\right) \end{cases} \tag{2.14}$$

with boundary conditions $T(\pm x_b) = 0$, $D\frac{\partial \rho}{\partial x}|_{\pm x_b} = D_T \rho(\pm x_b)\frac{\partial T}{\partial x}|_{\pm x_b}$, and the condition $N = \int_{-x_b}^{x_b} \rho dx$.

To scale these equations to a dimensionless form introduce the length scale, λ, and let $x = \lambda\xi$, $\rho = \frac{N}{\lambda}\bar{\rho}$, $t = \frac{\lambda^2}{\kappa}\tau$, and $T = \frac{D}{D_T}\bar{T}$; then ξ, $\bar{\rho}$, τ, and $\bar{T}$ are the dimensionless length, density, time and temperature respectively. The boundaries in the dimensionless system are at $\xi = \pm\xi_b$, and the dimensionless density is normalised, i.e. $N = \int_{-x_b}^{x_b} \rho dx = \int_{-\xi_b}^{\xi_b} \frac{N}{\lambda}\bar{\rho}\lambda d\xi \to \int_{-\xi_b}^{\xi_b} \bar{\rho} d\xi = 1$. The differential operators are $\frac{\partial}{\partial x} = \frac{1}{\lambda}\frac{\partial}{\partial \xi}$, and $\frac{\partial}{\partial t} = \frac{\kappa}{\lambda^2}\frac{\partial}{\partial \tau}$, substituting this into equations (2.14),

$$\begin{cases} \frac{\kappa}{\lambda^2}\frac{D}{D_T}\frac{\partial \bar{T}}{\partial \tau} = \kappa\frac{D}{\lambda^2 D_T}\frac{\partial^2 \bar{T}}{\partial \xi^2} + \frac{2\alpha}{c\rho_f}\sqrt{I_\infty I_{-\infty}} e^{-\alpha N/2}\frac{N}{\lambda}\bar{\rho}\cosh\left[\alpha N \int_\xi^{\xi_b} \bar{\rho} d\xi' - \frac{\alpha N}{2} - \frac{1}{2}\ln\frac{I_\infty}{I_{-\infty}}\right] \\ \frac{\kappa N}{\lambda^3}\frac{\partial \bar{\rho}}{\partial \tau} = D\frac{N}{\lambda^3}\frac{\partial^2 \bar{\rho}}{\partial \xi^2} - D_T\frac{ND}{\lambda^3 D_T}\frac{\partial}{\partial \xi}\left(\bar{\rho}\frac{\partial \bar{T}}{\partial \xi}\right) \end{cases} \tag{2.15}$$

$$\Rightarrow \begin{cases} \frac{\partial \bar{T}}{\partial \tau} = \frac{\partial^2 \bar{T}}{\partial \xi^2} + \lambda\frac{2D_T\sqrt{I_\infty I_{-\infty}}}{c\rho_f \kappa D} e^{-\alpha N/2}\alpha N \bar{\rho}\cosh\left[\alpha N\left(\int_\xi^{\xi_b}\bar{\rho}d\xi' - \frac{1}{2}\right) - \frac{1}{2}\ln\frac{I_\infty}{I_{-\infty}}\right] \\ \frac{\kappa}{D}\frac{\partial \bar{\rho}}{\partial \tau} = \frac{\partial^2 \bar{\rho}}{\partial \xi^2} - \frac{\partial}{\partial \xi}\left(\bar{\rho}\frac{\partial \bar{T}}{\partial \xi}\right) \end{cases} \tag{2.16}$$

Choosing the length scale $\lambda = \frac{c\rho_f \kappa D}{2D_T\sqrt{I_\infty I_{-\infty}}}$ and defining the dimensionless parameter $a = \alpha N$, the dimensionless 1D equations of motion are,

$$\begin{cases} \frac{\partial \bar{T}}{\partial \tau} = \frac{\partial^2 \bar{T}}{\partial \xi^2} + a e^{-a/2}\bar{\rho}\cosh\left[a\left(\int_\xi^{\xi_b}\bar{\rho}d\xi' - \frac{1}{2}\right) - \frac{1}{2}\ln\frac{I_\infty}{I_{-\infty}}\right] \\ \frac{\kappa}{D}\frac{\partial \bar{\rho}}{\partial \tau} = \frac{\partial^2 \bar{\rho}}{\partial \xi^2} - \frac{\partial}{\partial \xi}\left(\bar{\rho}\frac{\partial \bar{T}}{\partial \xi}\right) \end{cases} \tag{2.17}$$

The boundary conditions on these equations are: $\bar{T}(\pm\xi_b) = 0$, $\frac{\partial \bar{\rho}}{\partial \xi}|_{\pm\xi_b} = \bar{\rho}(\pm\xi_b)\frac{\partial \bar{T}}{\partial \xi}|_{\pm\xi_b}$,

and the normalisation condition, $\int_{-\xi_b}^{\xi_b} \bar{\rho} d\xi = 1$. Notice that the parameter a is precisely the product of the absorption coefficient and the particle number, as discussed previously, and also the length scale, λ, involves the ratio of light intensity to thermal conductivity, as discussed above.

2.4 Stationary Solutions

We seek the stationary distribution that occurs when the system is under symmetric illumination ($I_\infty = I_{-\infty}$). From equation (2.2) a stationary distribution implies the particle current is divergence-less which occurs in three scenarios: the current is zero everywhere; the current is a non-zero, uniform vector field (hence all spatial derivatives are zero); the current is a non-zero, spatially varying vector field which can be expressed as the curl of a potential vector field (hence has zero divergence). The latter of these cannot occur in a one dimensional system, although it could happen in a two or three dimensional system with rectangular symmetry in the experimental set up but symmetry breaking in the particle distribution. This could potentially be realised if there were circulating currents in directions perpendicular to the radiation field, in which case there would be no balance between diffusion and thermophoresis, but rather in every location one of these processes is dominant in such a way as to loop the particle current. In the present work only 1D distributions are considered. A uniform current would require that particles are injected into the system at one side and removed at the other, which cannot happen with impermeable boundaries and conservation of particle number. A zero current state is equivalent to the balance of thermophoresis and diffusion. In this state: the absorption of energy into the system, by the colloids intercepting light radiation and conducting this as heat into the fluid, is balanced by the loss of energy as this heat is conducted into the heat bath at the boundaries of the system; and the diffusion of colloids is balanced by the thermophoretic drift of colloids up temperature gradients. The balance between diffusion and thermophoresis is the state of zero particle current, i.e. setting both sides of equation (2.1) to zero, the balance between diffusion and thermophoresis is described by $\nabla\rho = \frac{D_T}{D}\rho\nabla T$ in general, which means the relationship between density and temperature in a stationary state is

$$\rho\left(\vec{x}\right) = \rho\left(\vec{x}_b\right) e^{\frac{D_T}{D}\left(T(\vec{x})-T(\vec{x}_b)\right)} \tag{2.18}$$

with $\vec{x}_b$ being any point on the boundary. This is true in general whenever diffusion-thermophoresis balance occurs, i.e. in an arbitrary number of spatial dimensions, with arbitrary geometry (as long as the boundary is all the same temperature), the temperature field is effectively a (negative) potential for the particles which are distributed as a Boltzmann-like distribution (a similar Boltzmann form for thermophobic thermophoretic colloids has been observed experimentally [131]).

In a stationary state, there must be a balance between energy absorption in the

bulk of the system, and energy lost at the boundary. The total rate of energy absorption in the bulk of the system is the integral of the heating function over the entire volume of the system, i.e. $\dot{Q} = c\rho_f \int_V \Gamma(\vec{x})\, dV$. The energy conducted to the heat bath at the boundary is the integral over the surface of the outward temperature gradient (multiplied by thermal conductivity), i.e. $-c\rho_f \kappa \oint_S \nabla T.d\vec{S}$. Since the source of energy for the system is the light radiation passing through it, the total energy absorbed by the system is the difference between the energy in the incident radiation as it enters the system and energy that remains as the radiation leaves the system. In one dimension, where the radiation is directed along the x-axis, the total rate of energy absorption is $\dot{Q} = I_\infty - I_+(-x_b) + I_{-\infty} - I_-(x_b)$. Using equation (2.7), this is

$$\begin{aligned}
\dot{Q} &= I_\infty \left(1 - e^{-\alpha \int_{-x_b}^{x_b} \rho dx}\right) + I_{-\infty} \left(1 - e^{-\alpha \int_{-x_b}^{x_b} \rho dx}\right) && (2.19)\\
\Rightarrow \dot{Q} &= I_\infty \left(1 - e^{-\alpha N}\right) + I_{-\infty} \left(1 - e^{-\alpha N}\right) && (2.20)\\
\Rightarrow \dot{Q} &= \left(I_\infty + I_{-\infty}\right) \left(1 - e^{-\alpha N}\right) && (2.21)\\
&= \left(I_\infty + I_{-\infty}\right) \left(1 - e^{-a}\right) && (2.22)\\
&= c\rho_f \int_{-x_b}^{x_b} \Gamma(x)\, dx && (2.23)
\end{aligned}$$

Notice that the amount of energy absorbed in the system depends only on fixed system parameters, in particular the total number of particles in the system, and not on the functional form of the density, $\rho(x)$. This is because the probability that a light ray passes through the system without being intercepted depends on the number of particles on average along the light ray's path, and not on how those particles are distributed along the path. In a system with one dimensional symmetry, the number of particles along the path is independent of the form of the density distribution. In higher dimensional systems the particles can be distributed in different ways such that the number of particles seen on average along a typical light ray trajectory can vary.

The dimensionless heating functional in 1D, from equation (2.17), is

$$\bar{\Gamma}(\xi) = a e^{-a/2} \bar{\rho} \cosh\left[a\left(\int_\xi^{\xi_b} \bar{\rho} d\xi' - \frac{1}{2}\right) - \frac{1}{2} \ln \frac{I_\infty}{I_{-\infty}}\right]$$

This is related to the physical heating functional by $\bar{\Gamma} = \frac{\lambda^2 D_T}{\kappa D}\Gamma$, where λ is the length scale defined above, so the integral of the dimensionless heating functional

over the entire system can be computed as follows:

$$\dot{Q} = c\rho_f \int_{-x_b}^{x_b} \Gamma dx = c\rho_f \int_{-\xi_b}^{\xi_b} \frac{\kappa D}{\lambda^2 D_T} \bar{\Gamma} \lambda d\xi = \frac{c\rho_f \kappa D}{\lambda D_T} \int_{-\xi_b}^{\xi_b} \bar{\Gamma} d\xi \tag{2.24}$$

$$\Rightarrow \int_{-\xi_b}^{\xi_b} \bar{\Gamma} d\xi = \lambda \frac{D_T}{c\rho_f \kappa D} \dot{Q} = \frac{c\rho_f \kappa D}{2D_T \sqrt{I_\infty I_{-\infty}}} \frac{D_T}{c\rho_f \kappa D} \dot{Q} \tag{2.25}$$

$$= \frac{\dot{Q}}{2\sqrt{I_\infty I_{-\infty}}} = \frac{(I_\infty + I_{-\infty})(1 - e^{-a})}{2\sqrt{I_\infty I_{-\infty}}} \tag{2.26}$$

2.4.1 Stationary Solution of the Heat Equation in One Dimension

Consider the heat equation in one dimension, $\frac{\partial T}{\partial t} = \kappa \frac{\partial^2 T}{\partial x^2} + \Gamma(x)$, in a stationary state this is

$$\kappa \frac{d^2 T}{dx^2} = -\Gamma(x) \tag{2.27}$$

subject to the boundary conditions $T(\pm x_b) = 0$. We adopt a Green's function approach to solving this equation: consider the equation

$$\kappa \frac{d^2}{dx^2} G(x; x_0) = -\delta(x - x_0) \tag{2.28}$$

which describes the temperature profile corresponding to a single heat source at x_0. The temperature profile from an arbitrary distribution of heat sources can be calculated as the convolution of the Green's function with the heat source function. To see this, convolve both side of this equation with the heating function,

$$\int_{x_0=-x_b}^{x_b} \Gamma(x_0) \kappa \frac{d^2}{dx^2} G(x; x_0) dx_0 = -\int_{-xb}^{x_b} \Gamma(x_0) \delta(x - x_0) dx_0 \tag{2.29}$$

$$\kappa \frac{d^2}{dx^2} \int_{-x_b}^{x_b} \Gamma(x_0) G(x; x_0) dx_0 = -\Gamma(x) \tag{2.30}$$

$$\Rightarrow T(x) = \int_{-x_b}^{x_b} \Gamma(x_0) G(x; x_0) dx_0 \tag{2.31}$$

To solve for the Green's function, first consider the region $x > x_0$, there $\frac{d^2 G}{dx^2} = 0$. Integrating twice from x to x_b, and using the boundary condition $G(\pm x_b; x_0) = 0$, the solution to this is clearly linear, in particular $G(x; x_0) = -\frac{dG}{dx}|_{x_b} (x_b - x)$. Integrating twice from $-x_b$ to x in the region $x < x_0$ one also obtains a linear

function, $G(x;x_0) = \frac{dG}{dx}|_{-x_b}(x+x_b)$. So far the Green's function takes the form,

$$G(x;x_0) = \begin{cases} \frac{dG}{dx}|_{-x_b}(x+x_b) & , \ x < x_0 \\ -\frac{dG}{dx}|_{x_b}(x_b - x) & , \ x > x_0 \end{cases} \tag{2.32}$$

with unknown gradients at the boundaries. To determine the gradients at the boundaries, first integrate the differential equation for the Green's function over the point x_0,

$$\int_{x_0-\epsilon}^{x_0+\epsilon} \kappa \frac{d^2G}{dx^2} dx = -\int_{x_0-\epsilon}^{x_0+\epsilon} \delta(x - x_0)\, dx \tag{2.33}$$

$$\Rightarrow \kappa \left(\left.\frac{dG}{dx}\right|_{x_0+\epsilon} - \left.\frac{dG}{dx}\right|_{x_0-\epsilon} \right) = -1 \tag{2.34}$$

$$\Rightarrow \kappa \left(\left.\frac{dG}{dx}\right|_{x_b} - \left.\frac{dG}{dx}\right|_{-x_b} \right) = -1 \tag{2.35}$$

Second, assert continuity of the Green's function at the point x_0, i.e. $\lim_{x\to x_0^-} G(x;x_0) = \lim_{x\to x_0^+} G(x;x_0)$, that is

$$\left.\frac{dG}{dx}\right|_{-x_b}(x_0 + x_b) = -\left.\frac{dG}{dx}\right|_{x_b}(x_b - x_0) \tag{2.36}$$

$$\Rightarrow \kappa \left(\left.\frac{dG}{dx}\right|_{x_b} + \left.\frac{dG}{dx}\right|_{-x_b} \right) = -\frac{x_0}{x_b} \tag{2.37}$$

The gradients at the boundaries are then determined by

$$\left.\begin{cases} \kappa\left(\frac{dG}{dx}|_{x_b} - \frac{dG}{dx}|_{-x_b}\right) = -1 \\ \kappa\left(\frac{dG}{dx}|_{x_b} + \frac{dG}{dx}|_{-x_b}\right) = -\frac{x_0}{x_b} \end{cases}\right\} \Rightarrow \begin{cases} \kappa\frac{dG}{dx}|_{x_b} = -\frac{1}{2}\left(1 + \frac{x_0}{x_b}\right) \\ \kappa\frac{dG}{dx}|_{-x_b} = \frac{1}{2}\left(1 - \frac{x_0}{x_b}\right) \end{cases} \tag{2.38}$$

Substituting these boundaries, the Green's function is

$$G(x;x_0) = \begin{cases} \frac{1}{2\kappa}\left(1 - \frac{x_0}{x_b}\right)(x + x_b) & , \ x < x_0 \\ \frac{1}{2\kappa}\left(1 + \frac{x_0}{x_b}\right)(x_b - x) & , \ x > x_0 \end{cases} \tag{2.39}$$

This is the temperature profile for a point heat source at x_0 subject to the temperature at the boundaries being zero. There are a number of features of this profile worth noting: mathematically speaking, the second derivative being zero everywhere except the point x_0 means the profile is a straight line, which means the temperature

profile must take on a triangular shape, and the effect of the Dirac delta function is that the sum of the magnitudes of the gradients at each end must be the same as the magnitude weighting the delta function (i.e. unity, in this case); physically speaking, the temperature profile has a constant gradient (everywhere except the point of heat source, x_0) because the heat flux is proportional to temperature gradient, and in one dimension there is no possibility of geometric spreading of heat flux, which means the flux of heat into an interval on one side must be the same as the flux out on the other side (assuming the interval does not contain any sources of heat), which means the temperature gradient on each side must be the same; physically speaking, the sum of the magnitudes of the gradients at each boundary matches the magnitude of the heat source simply because of the conservation of energy, i.e. the heat lost across the boundaries equals the heat added at the heat source. Two important consequences of this Green's function are: if all the heat sources are contained in a region around the origin, $[-x_r, x_r]$, then the temperature profile *outside* this region must have uniform gradient, with the gradients on each side summing in magnitude to the total heat source inside the interval; as the boundaries are extended to infinity, $x_b \to \infty$, the temperature diverges to infinity everywhere, however, the temperature *gradients* do not diverge. So, as long as the behaviour of the system depends only on temperature *gradients* and not the absolute value of the temperature, one can consider the idealised case of an infinite system.

The temperature field from a general distribution of heat sources, $\Gamma(x)$, is computed

from the convolution of this with the Green's function, i.e.

$$T(x) = \int_{-x_b}^{x_b} \Gamma(x_0)\, G(x; x_0)\, dx_0 \tag{2.40}$$

$$\begin{aligned} &= \int_{-x_b}^{x} \Gamma(x_0)\, \frac{1}{2\kappa}\left(1 + \frac{x_0}{x_b}\right)(x_b - x)\, dx_0 \\ &\quad + \int_{x}^{x_b} \Gamma(x_0)\, \frac{1}{2\kappa}\left(1 - \frac{x_0}{x_b}\right)(x + x_b)\, dx_0 \end{aligned} \tag{2.41}$$

$$\begin{aligned} \Rightarrow \kappa\, T(x) &= \frac{1}{2}(x_b - x)\left[\int_{-x_b}^{x} \Gamma(x_0)\, dx_0 + \frac{1}{x_b}\int_{-x_b}^{x} x_0 \Gamma(x_0)\, dx_0\right] \\ &\quad + \frac{1}{2}(x + x_b)\left[\int_{x}^{x_b} \Gamma(x_0)\, dx_0 - \frac{1}{x_b}\int_{x}^{x_b} x_0 \Gamma(x_0)\, dx_0\right] \end{aligned} \tag{2.42}$$

$$\begin{aligned} &= \frac{1}{2}(x_b - x)\int_{-x_b}^{x_b} \Gamma(x_0)\, dx_0 + \frac{1}{2}\left(1 - \frac{x}{x_b}\right)\int_{-x_b}^{x_b} x_0 \Gamma(x_0)\, dx_0 \\ &\quad - \int_{x}^{x_b} (x_0 - x)\, \Gamma(x_0)\, dx_0 \end{aligned} \tag{2.43}$$

$$= \frac{1}{2}\left(1 - \frac{x}{x_b}\right)\int_{-x_b}^{x_b} (x_b + y)\, \Gamma(y)\, dy - \int_{x}^{x_b} (y - x)\, \Gamma(y)\, dy \tag{2.44}$$

In equation (2.44) the first term is linear in x (the pre-factor to the integral is linear and the integral is definite), and the second term is curved but only if the region defined by the limits of the integral contains variable amounts heat sources, i.e. non-zero Γ which varies as the lower integral limit varies. So if the heating function, $\Gamma(x)$, is non-zero only in a region around the origin, $x \in [-x_r, x_r]$, then to the right of this region the second term in equation (2.44) is zero and the temperature variation for $x > x_r$ is linear, whereas to the left of this region the second term is constant and the temperature variation for $x < -x_r$ is linear, i.e. as above, the temperature variation outside the regions of heating are linearly variable. This also means, as can be seen in equation (2.43), that as the boundary is taken to infinity ($x_b \to \infty$) the temperature diverges. However, as discussed for the Green's function above, the temperature gradients do not diverge in the infinite domain limit. To see this, differentiating equation (2.44),

$$\kappa \frac{dT}{dx} = \int_{x}^{x_b} \Gamma(y)\, dy - \frac{1}{2x_b}\int_{-x_b}^{x_b} (x_b + y)\, \Gamma(y)\, dy \tag{2.45}$$

in the limit $x_b \to \infty$ the x_b's in the second term cancel leaving a finite temperature gradient. To compare with equations (2.38), evaluate the temperature gradient at

the boundaries:

$$\begin{cases} \kappa \frac{dT}{dx}\big|_{x_b} & = -\frac{1}{2x_b} \int_{-x_b}^{x_b} (x_b + y)\, \Gamma(y)\, dy \\ \kappa \frac{dT}{dx}\big|_{-x_b} & = \frac{1}{2x_b} \int_{-x_b}^{x_b} (x_b - y)\, \Gamma(y)\, dy \end{cases} \tag{2.46}$$

$$\Rightarrow \begin{cases} \kappa \left(\frac{dT}{dx}\big|_{-x_b} - \frac{dT}{dx}\big|_{x_b} \right) & = \int_{-x_b}^{x_b} \Gamma(y)\, dy \\ \kappa \left(\frac{dT}{dx}\big|_{-x_b} + \frac{dT}{dx}\big|_{x_b} \right) & = -\frac{1}{x_b} \int_{-x_b}^{x_b} y \Gamma(y)\, dy \end{cases} \tag{2.47}$$

Comparing equations (2.47) with equations (2.38) for the Green's function: the first equation in (2.47) matches the total flux of energy out of the system at the boundaries with total flux of energy into the system across the heat sources, and the second equation describes how the asymmetry in the distribution of heat sources links to the asymmetry in the temperature gradient at the boundary, i.e. if there are more sources of heat to the right closer to x_b, that is $\Gamma(x)$ is skewed to the right, then the temperature gradient on the right boundary will have a greater magnitude.

2.4.2 Exact Stationary Solutions

Recall the dimensionless heat equation in (2.17),

$$\frac{\partial \bar{T}}{\partial \tau} = \frac{\partial^2 \bar{T}}{\partial \xi^2} + ae^{-a/2}\bar{\rho}\cosh\left[a\left(\int_{\xi}^{\xi_b}\bar{\rho}d\xi' - \frac{1}{2}\right) - \frac{1}{2}\ln\frac{I_\infty}{I_{-\infty}}\right] \tag{2.48}$$

Under symmetric illumination, and in a stationary state this reduces to

$$\frac{d^2\bar{T}}{d\xi^2} = -ae^{-a/2}\bar{\rho}\cosh\left[a\left(\int_{\xi}^{\xi_b}\bar{\rho}d\xi' - \frac{1}{2}\right)\right] \tag{2.49}$$

To solve this integro-differential equation define the function $\psi(\xi) = a\left(\frac{1}{2} - \int_{\xi}^{\xi_b}\bar{\rho}d\xi'\right)$, which means the density is proportional to the gradient of ψ, $a\bar{\rho} = \frac{d\psi}{d\xi}$. Normalisation of the dimensionless density determines the boundary conditions on ψ, i.e. $\psi(\pm\xi_b) = \pm\frac{a}{2}$. In terms of ψ the heating functional is $\bar{\Gamma}(\xi) = e^{-a/2}\frac{d\psi}{d\xi}\cosh\psi$. From equation (2.44) the temperature is

$$\begin{aligned}\bar{T}(\xi) = \frac{1}{2}\xi_b\left(1 - \frac{\xi}{\xi_b}\right)\int_{-\xi_b}^{\xi_b}\bar{\Gamma}(y)\,dy + \frac{1}{2}\left(1 - \frac{\xi}{\xi_b}\right)\int_{-\xi_b}^{\xi_b} y\bar{\Gamma}(y)\,dy \\ - \int_{\xi}^{\xi_b}(y-\xi)\,\bar{\Gamma}(y)\,dy\end{aligned} \tag{2.50}$$

The components of this are as follows

$$\int_{-\xi_b}^{\xi_b} y\bar{\Gamma}(y)\,dy = e^{-a/2}\int_{-\xi_b}^{\xi_b} y\frac{d}{dy}\sinh\psi\,dy \tag{2.51}$$

$$= e^{-a/2}\left[y\sinh\psi\right]_{-\xi_b}^{\xi_b} - e^{-a/2}\int_{-\xi_b}^{\xi_b}\sinh\psi\,dy \tag{2.52}$$

$$= -e^{-a/2}\int_{-\xi_b}^{\xi_b}\sinh\psi\,dy \tag{2.53}$$

$$\equiv \sigma \tag{2.54}$$

$$\int_{\xi}^{\xi_b} y\bar{\Gamma}(y)\,dy = e^{-a/2}\left[y\sinh\psi\right]_{\xi}^{\xi_b} - e^{-a/2}\int_{\xi}^{\xi_b}\sinh\psi\,dy \tag{2.55}$$

$$= \xi_b\frac{1}{2}\left(1 - e^{-a}\right) - e^{-a/2}\xi\sinh\psi - e^{-a/2}\int_{\xi}^{\xi_b}\sinh\psi\,dy \tag{2.56}$$

$$\int_{\xi}^{\xi_b} \xi\bar{\Gamma}\left(y\right) dy = \xi e^{-a/2} \left[\sinh\psi\right]_{\xi}^{\xi_b} \tag{2.57}$$

$$= \xi\frac{1}{2}\left(1 - e^{-a}\right) - \xi e^{-a/2}\sinh\psi \tag{2.58}$$

and recall that $\int_{-\xi_b}^{\xi_b} \bar{\Gamma}\left(y\right) dy = \left(1 - e^{-a}\right)$. Substituting this in, the temperature is

$$\bar{T}\left(\xi\right) = \frac{1}{2}\left(1 - \frac{\xi}{\xi_b}\right)\sigma + e^{-a/2}\int_{\xi}^{\xi_b} \sinh\psi\, dy \tag{2.59}$$

$$\Rightarrow \frac{d\bar{T}}{d\xi} = -\frac{1}{2\xi_b}\sigma - e^{-a/2}\sinh\psi \tag{2.60}$$

The condition of zero particle current, satisfied when thermophoresis and diffusion are in balance, implies $\frac{d\bar{\rho}}{d\xi} = \bar{\rho}\frac{d\bar{T}}{d\xi}$. Substituting the temperature gradient in equation (2.60) into this,

$$\frac{d\bar{\rho}}{d\xi} = -\bar{\rho}\left(\frac{\sigma}{2\xi_b} + e^{-a/2}\sinh\psi\right) \tag{2.61}$$

$$\Rightarrow \frac{d^2\psi}{d\xi^2} = -\frac{d\psi}{d\xi}\left(\frac{\sigma}{2\xi_b} + e^{-a/2}\sinh\psi\right) \tag{2.62}$$

$$= -\frac{d}{d\xi}\left(\frac{\sigma}{2\xi_b}\psi + e^{-a/2}\cosh\psi\right) \tag{2.63}$$

Therefore the stationary state of the system is described by the ODE

$$\frac{d\psi}{d\xi} = c - \frac{\sigma}{2\xi_b}\psi - e^{-a/2}\cosh\psi \tag{2.64}$$

which must be solved subject to the boundary conditions $\psi\left(\pm\xi_b\right) = \pm\frac{a}{2}$. There are two unknown constants of integration in this equation, c and σ: the constant c is constrained by the fact that the density, and therefore the gradient of ψ, must be non-negative, so $c \geq \frac{1}{2}\left(1 + e^{-a}\right) + \frac{|\sigma|}{2\xi_b}\frac{a}{2}$; the constant σ is effectively a measure of the asymmetry of the distribution about the origin, recall that by definition $\sigma = -e^{-a/2}\int_{-\xi_b}^{\xi_b} \sinh\psi\left(\xi\right) d\xi$, so if the density is symmetrically distributed about the centre then the function ψ is anti-symmetric and the integral for σ is zero, whereas if the density is skewed to the right, say, then the integral will be positive. The constant, c, is determined by fixing the boundary conditions on ψ (or equivalently the normalisation of $\bar{\rho}$), whereas σ is determined self-consistently by the requirement that solutions to equation (2.64) must return σ when integrated. A numerical method for solving this could involve fixing σ, then numerically integrating equation

(2.64) with the right boundary condition, $\psi(\xi_b) = \frac{a}{2}$, for a given choice of c, checking the value of ψ on the left boundary, varying c until the boundary conditions are met and then checking the self-consistency condition for σ. Alternatively, integrate the ODE for ψ

$$\int_{\psi}^{\frac{a}{2}} \frac{d\psi}{c - \frac{\sigma}{2\xi_b}\psi - e^{-a/2}\cosh\psi} = \xi_b - \xi \tag{2.65}$$

Define the function $I_1(\sigma, c)$ to be the evaluation of this integral on the left boundary

$$I_1(\sigma, c) = \int_{-\frac{a}{2}}^{\frac{a}{2}} \frac{d\psi}{c - \frac{\sigma}{2\xi_b}\psi - e^{-a/2}\cosh\psi} \tag{2.66}$$

which is a definite integral over a dummy variable ψ. Also, observe the integral that defines σ which is, by definition, an integral over an unknown function, can be written as a definite integral over a dummy variable, i.e.

$$\int_{-\xi_b}^{\xi_b} \sinh\psi(\xi)\, d\xi = \int_{\psi(-\xi_b)}^{\psi(\xi_b)} \frac{\sinh\psi}{\frac{d\psi}{d\xi}} d\psi \tag{2.67}$$

Define the function $I_2(\sigma, c)$ by

$$I_2(\sigma, c) = -e^{-a/2} \int_{-\frac{a}{2}}^{\frac{a}{2}} \frac{\sinh\psi}{c - \frac{\sigma}{2\xi_b}\psi - e^{-a/2}\cosh\psi} d\psi \tag{2.68}$$

The constants of integration in equation (2.64) are then determined by the solutions to the simultaneous equations

$$\begin{cases} I_1(\sigma, c) = 2\xi_b \\ I_2(\sigma, c) = \sigma \end{cases} \tag{2.69}$$

Each equation defines a curve in the σ-c plane and the intersection of these curves determines the constants of integration, see figure (2.3) for an example of one such curve for I_1. Consider the integrand in I_2: if $\sigma = 0$ then the denominator of the integrand is symmetric so due to the anti-symmetric numerator the integral evaluates to zero; if σ is positive then the denominator is smaller at positive ψ than at $-\psi$, which means the magnitude of the integrand is *larger* for $\psi > 0$ than for $\psi < 0$, which means the integral is positive, which, when multiplied by $-e^{-a/2}$, makes the function I_2 negative, i.e. $\sigma > 0 \Rightarrow I_2(\sigma, c) < 0$ and $\sigma < 0 \Rightarrow I_2(\sigma, c) > 0$. However, we seek $\sigma = I_2(\sigma, c)$, so the only solutions are $\sigma = 0$. This can also be shown by

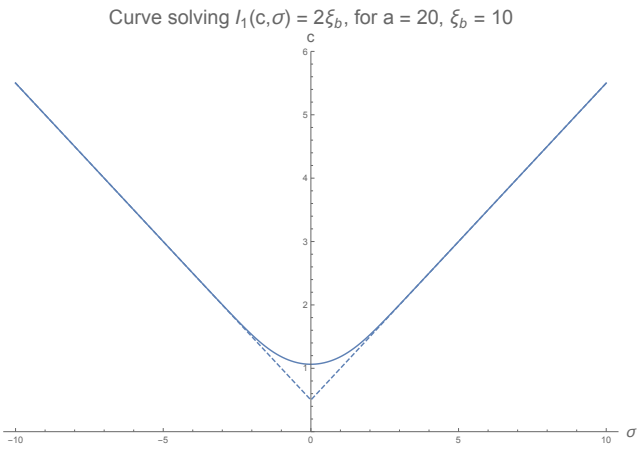

Figure 2.3: Curve in the c-σ plane that satisfies $I_1(\sigma, c) = 2\xi_b$ for $a = 20$ and $\xi_b = 10$. The dotted line is the lower bound on c, $c \geq \frac{1}{2}(1 + e^{-a}) + \frac{|\sigma|}{2\xi_b}\frac{a}{2}$.

taking a linear combination of I_1 and I_2:

$$I_2 - \frac{\sigma}{2\xi_b} I_1 = \int_{-\frac{a}{2}}^{\frac{a}{2}} \frac{-e^{-a/2}\sinh\psi - \frac{\sigma}{2\xi_b}}{c - e^{-a/2}\cosh\psi - \frac{\sigma}{2\xi_b}\psi} d\psi \tag{2.70}$$

which takes the form $\int_{-\frac{a}{2}}^{\frac{a}{2}} \frac{f'(\psi)}{f(\psi)} d\psi = [\ln f(\psi)]_{-\frac{a}{2}}^{\frac{a}{2}}$, so

$$I_2 - \frac{\sigma}{2\xi_b} I_1 = \ln\left[\frac{c - \frac{1}{2}(1 + e^{-a}) - \frac{\sigma}{2\xi_b}\frac{a}{2}}{c - \frac{1}{2}(1 + e^{-a}) + \frac{\sigma}{2\xi_b}\frac{a}{2}}\right] \tag{2.71}$$

Substituting $I_2 = \sigma$ and $I_1 = 2\xi_b$

$$0 = \ln\left[\frac{c - \frac{1}{2}(1 + e^{-a}) - \frac{\sigma}{2\xi_b}\frac{a}{2}}{c - \frac{1}{2}(1 + e^{-a}) + \frac{\sigma}{2\xi_b}\frac{a}{2}}\right] \tag{2.72}$$

$\Rightarrow \sigma = 0$.

Thus, the stationary states of the system under symmetric illumination must be symmetric about the centre (which implies $\psi(0) = 0$), and so the equation (2.64) reduces to

$$\frac{d\psi}{d\xi} = c - e^{-a/2}\cosh\psi \tag{2.73}$$

with $\psi(\pm\xi_b) = \pm\frac{a}{2}$. Integrating from the origin to an arbitrary point,

$$\int_0^{\psi} \frac{d\psi'}{c - e^{-a/2}\cosh\psi'} = \xi \tag{2.74}$$

Using the identities $\cosh\psi = 2\cosh^2\frac{\psi}{2} - 1$ and $\cosh^2\psi - \sinh^2\psi = 1$ one can show $c - e^{-a/2}\cosh\psi = \left(c - e^{-a/2}\right)\cosh^2\frac{\psi}{2} - \left(c + e^{-a/2}\right)\sinh^2\frac{\psi}{2}$. The integrand can be rewritten

$$\frac{1}{c - e^{-a/2}\cosh\psi} = \frac{1}{\sqrt{c^2 - e^{-a}}} \frac{\sqrt{\frac{c+e^{-a/2}}{c-e^{-a/2}}}\operatorname{sech}^2\frac{\psi}{2}}{\left(1 - \frac{c+e^{-a/2}}{c-e^{-a/2}}\tanh^2\frac{\psi}{2}\right)} \tag{2.75}$$

$$= \frac{1}{\sqrt{c^2 - e^{-a}}} \frac{2}{1 - F^2} \frac{dF}{d\psi} \tag{2.76}$$

$$= \frac{2}{\sqrt{c^2 - e^{-a}}} \frac{dF}{d\psi} \frac{d}{dF}\tanh^{-1} F \tag{2.77}$$

where $F(\psi) = \sqrt{\frac{c+e^{-a}}{c-e^{-a}}}\tanh\frac{\psi}{2}$. The integral then is

$$\int_0^{\psi} \frac{d\psi'}{c - e^{-a/2}\cosh\psi'} = \frac{2}{\sqrt{c^2 - e^{-a}}} \int_{F(0)}^{F(\psi)} \frac{d}{dF}\tanh^{-1} F\, dF \tag{2.78}$$

$$= \frac{2}{\sqrt{c^2 - e^{-a}}} \left[\tanh^{-1} F\right]_0^{\sqrt{\frac{c+e^{-1}}{c-e^{-a}}}\tanh\frac{\psi}{2}} \tag{2.79}$$

Therefore,

$$\xi = \frac{2}{\sqrt{c^2 - e^{-a}}}\tanh^{-1}\left[\sqrt{\frac{c + e^{-a/2}}{c - e^{-a/2}}}\tanh\frac{\psi}{2}\right] \tag{2.80}$$

This can be inverted to obtain an exact equation for ψ

$$\psi(\xi) = 2\tanh^{-1}\left[\sqrt{\frac{c - e^{-a/2}}{c + e^{-a/2}}}\tanh\left[\frac{\sqrt{c^2 - e^{-a}}}{2}\xi\right]\right] \tag{2.81}$$

However, to find the constant of integration one must solve the transcendental equation $\tanh\frac{a}{4} = \sqrt{\frac{c-e^{-a/2}}{c+e^{-a/2}}}\tanh\left[\sqrt{c^2 - e^{-a}}\frac{\xi_b}{2}\right]$ which cannot be achieved analytically. It is convenient to define a new unknown constant, a_o, by $c = e^{-a/2}\cosh\frac{a_o}{2}$, in which

case ψ is

$$\psi(\xi) = 2\tanh^{-1}\left[\tanh\frac{a_o}{4}\tanh\left[\frac{1}{2}e^{-a/2}\sinh\frac{a_o}{2}\,\xi\right]\right] \tag{2.82}$$

and the constant is determined by $\tanh\frac{a}{4} = \tanh\frac{a_o}{4}\tanh\left[\frac{1}{2}e^{-a/2}\sinh\frac{a_o}{2}\,\xi_b\right]$. The lower bound on the constant of integration, $c \geq \frac{1}{2}(1+e^{-a})$, translates to $a_o \geq a$. Using the identity $\cosh(2x) = \frac{1+\tanh^2 x}{1-\tanh^2 x}$, substituting the solution (2.82) into equation (2.73)

$$\frac{d\psi}{d\xi} = e^{-a/2}\frac{\left(\cosh\frac{a_o}{2}-1\right)-\left(\cosh\frac{a_o}{2}+1\right)\tanh^2\frac{a_o}{4}\tanh^2\left[\frac{1}{2}e^{-a/2}\sinh\frac{a_o}{2}\xi\right]}{1-\tanh^2\frac{a_o}{4}\tanh^2\left[\frac{1}{2}e^{-a/2}\sinh\frac{a_o}{2}\,\xi\right]} \tag{2.83}$$

$$= \frac{2e^{-a/2}\sinh^2\frac{a_o}{4}\left(1-\tanh^2\left[\frac{1}{2}e^{-a/2}\sinh\frac{a_o}{2}\xi\right]\right)}{1-\tanh^2\frac{a_o}{4}\tanh^2\left[\frac{1}{2}e^{-a/2}\sinh\frac{a_o}{2}\,\xi\right]} \tag{2.84}$$

$$= \frac{2e^{-a/2}\sinh^2\frac{a_o}{4}}{\cosh^2\left[\frac{1}{2}e^{-a/2}\sinh\frac{a_o}{2}\,\xi\right]-\tanh^2\frac{a_o}{4}\sinh^2\left[\frac{1}{2}e^{-a/2}\sinh\frac{a_o}{2}\,\xi\right]} \tag{2.85}$$

$$= \frac{2e^{-a/2}\sinh^2\frac{a_o}{4}}{1+\frac{\sinh^2\left[\frac{1}{2}e^{-a/2}\sinh\frac{a_o}{2}\,\xi\right]}{\cosh^2\frac{a_o}{4}}} \tag{2.86}$$

Thus, the exact solution for the density (up to an unknown constant, a_o) is

$$\bar{\rho}(\xi) = \frac{\frac{1}{a}2e^{-a/2}\sinh^2\frac{a_o}{4}}{1+\frac{\sinh^2\left[\frac{1}{2}e^{-a/2}\sinh\frac{a_o}{2}\,\xi\right]}{\cosh^2\frac{a_o}{4}}} \tag{2.87}$$

2.4.3 Solution on an Infinite Domain

Recall that on an infinite domain the temperature diverges though the temperature gradients do not. It is meaningful, then, to take $\xi_b \to \infty$ and analyse the solutions, as long as these do not depend on absolute temperature. This corresponds, physically, to a large system where the particles are far from the edges. Taking $\xi_b \to \infty$ in the transcendental equation that determines the constant of integration, it can be solved: $a_o = a$ (or $c = \frac{1}{2}(1+e^{-a})$), so the exact solutions are

$$\begin{cases} \psi(\xi) = 2\tanh^{-1}\left[\tanh\left[\frac{a}{4}\right]\tanh\left[\frac{\left(1-e^{-a}\right)}{4}\xi\right]\right] \\ \bar{\rho}(\xi) = \frac{\frac{1}{2a}\left(1-e^{-a/2}\right)^2}{1+\frac{\sinh^2\left[\frac{\left(1-e^{-a}\right)}{4}\xi\right]}{\cosh^2\left[\frac{a}{4}\right]}} \end{cases} \tag{2.88}$$

The relationship between temperature and density in a stationary state can be written in terms of the density at the origin as $\bar{\rho} = \bar{\rho}_o e^{\bar{T}(\xi)-T_o}$, where $\bar{\rho}_o$ and T_o are the density and temperature respectively at the origin, which means we can compute the temperature from the density by $\bar{T}(\xi) = T_o + \ln\left[\frac{\bar{\rho}(\xi)}{\rho_o}\right]$. Using the results in equation (2.88) the temperature field is

$$\overline{T}(\xi) = T_0 - \ln\left[1 + \frac{\sinh^2\left[\frac{\left(1-e^{-a}\right)}{4}\xi\right]}{\cosh^2\left(\frac{a}{4}\right)}\right] \tag{2.89}$$

The constant, T_o, diverges on an infinite domain, but this solution is a good approximation to a system where ξ_b is much larger than the characteristic width of the distribution, in which case the constant must be fixed to ensure the temperature at the edge matches that of the heat bath. See figure (2.6).

The light intensity is, in general, $I_{\pm}(\xi) = I_\infty e^{-a/2} e^{\pm\psi(\xi)}$. Using the solution for $\psi(\xi)$ and the identity $\tanh^{-1} x = \frac{1}{2}\ln\left(\frac{1+x}{1-x}\right)$, the light intensity can be computed (see figure (2.5))

$$I_+(\xi) = I_\infty e^{-a/2} \frac{1 + \tanh\left[\frac{a}{4}\right]\tanh\left[\frac{\left(1-e^{-a}\right)}{4}\xi\right]}{1 - \tanh\left[\frac{a}{4}\right]\tanh\left[\frac{\left(1-e^{-a}\right)}{4}\xi\right]} \tag{2.90}$$

The heating function, which is in general $\Gamma[\bar{\rho}] = ae^{-a/2}\overline{\rho}\cosh\psi$, can be computed explicitly as (see figure (2.5))

$$\Gamma(\xi) = \frac{\frac{1}{2}e^{-a/2}\left(1-e^{-a/2}\right)^2}{1 + \frac{\sinh^2\left[\frac{\left(1-e^{-a}\right)}{4}\xi\right]}{\cosh^2\left[\frac{a}{4}\right]}} \left(\frac{1 + \tanh^2\left[\frac{a}{4}\right]\tanh^2\left[\frac{\left(1-e^{-a}\right)}{4}\xi\right]}{1 - \tanh^2\left[\frac{a}{4}\right]\tanh^2\left[\frac{\left(1-e^{-a}\right)}{4}\xi\right]}\right) \tag{2.91}$$

Notice, also, that the heating function can be re-written as a *function* of the local density (i.e. not a *functional*): from equation (2.73) $\cosh\psi = \cosh\left(\frac{a}{2}\right) - ae^{a/2}\bar{\rho}$, so

$$\Gamma[\bar{\rho}] = a\bar{\rho}\left(\frac{1}{2}\left(1+e^{-a}\right) - a\bar{\rho}\right) \tag{2.92}$$

a remarkable identity. Discussion: a much simpler model might involve a heating term that is linearly dependent on the density, $\Gamma[\rho] = \alpha\rho$. Here the heating is proportional to the number of particles (i.e. sources of heat), with the heating per

particle taken to be the same for all particles [64]. This does not account for shading, as our analysis above does. The simplest non-linear model which could be argued accounts for shading might assume a heating term of the form $\Gamma[\rho] = \alpha\rho(\beta - \rho)$. The $\alpha\rho$ part captures the feature that the heating in some region is proportional to the number of heat sources in that region; and the $(\beta - \rho)$ part invokes the assumption that there is a linear dependence of heating contribution per particle on where the particle is in the swarm. More specifically, the argument here is that one expects the maximum density in the centre of the swarm, and the least density at the edge, whilst coincidentally the centre of the swarm should be the most shaded and the edge the least shaded; given that the energy for heating comes from external irradiation, the most shaded area should have the least heating per particle and vice versa. Hence, the effect of shading can be modelled by constructing a heating term that is proportional to density (heat sources per volume) modified by multiplying by a function of density that is large for small density and small for large density: a linear dependence is the simplest, hence $\Gamma[\rho] = \alpha\rho(\beta - \rho)$ is the simplest non-linear model accounting for the effect of shading. Our analysis above has accounted for shading explicitly, tracing the transfer of energy from radiation to heating without assuming correlation between where the heating per particle is maximal and where the density is lowest, and yet it turns out that when the system is in a stationary distribution, the heating term takes precisely this form.

There is only one system parameter in the stationary states on an infinite (or effectively infinite) domain: $a = \alpha N$ $(= 2r_0\rho_y = \pi r_0^2\rho_{yz})$ which determines the opacity of the system irrespective of the form the distribution takes. In the transparent case of $a \ll 1$, $\cosh\frac{a}{4} \approx 1$ so the denominator in $\bar{\rho}$ is approximately a squared hyperbolic cosine; whereas in the opaque case of $a \gg 1$, the hyperbolic cosine in the denominator dominates the hyperbolic sine until ξ is large enough at which point the hyperbolic sine dominates, thus in these limits the density can be approximated by

$$\bar{\rho}(\xi) \approx \begin{cases} \frac{a}{8}\mathrm{sech}^2\left(\frac{a}{4}\xi\right) & , \ a \ll 1 \\ \frac{1}{2a}\frac{1}{1+\exp\left[-\frac{1}{2}(a-|\xi|)\right]} & , \ a \gg 1 \end{cases} \tag{2.93}$$

Thus there are two phases: for small a - the case of low absorption (α) or low particle number (N), or less than one particle per particle diameter in perpendicular directions (e.g. $2r_0\rho_y < 1$) - there is a diffuse phase where the colloid distribution forms a wide bell shape; and for high a the colloids form a dense phase with uniform density up until the edge where the density tails of exponentially. The diffuse phase

corresponds to the low-shading, transparent limit in which light entering the swarm passes through with little absorption, meaning that each colloid particle sees almost the same intensity of light and therefore all particles contribute equally to heating, and so the heating of the fluid is proportional to colloid density. The compact phase corresponds to an opaque limit in which almost all the incident energy is absorbed in a narrow margin at the boundary of the swarm, and so these two margins at each end act as localised heat sources which means that colloids are free to diffuse throughout the bulk of the swarm but are contained by steep temperature gradients at the edge. See figure (2.5) which plots exact solutions for which the transition from transparent to opaque distributions are clear.

To analyse the density and heating functional in more detail, recall equation (2.62), setting $\sigma = 0$ this is $\frac{d^2\psi}{d\xi^2} = -e^{-a/2}\frac{d\psi}{d\xi}\sinh\psi$. This has been integrated to obtain $\frac{d\psi}{d\xi} = e^{-a/2}\left(\cosh\left[\frac{a}{2}\right] - \cosh\left[\psi\right]\right) = a\bar{\rho} \Rightarrow \cosh\left[\psi\right] = \cosh\left(\frac{a}{2}\right) - ae^{a/2}\overline{\rho}$ thus

$$\frac{d\bar{\rho}}{d\xi} = -ae^{-a/2}\bar{\rho}\sinh\psi = -ae^{-a/2}\bar{\rho}\sqrt{\cosh^2\psi - 1} \tag{2.94}$$

$$\Rightarrow \frac{d\bar{\rho}}{d\xi} = -\overline{\rho}\sqrt{\left(\frac{1+e^{-a}}{2} - a\,\overline{\rho}\right)^2 - e^{-a}} \tag{2.95}$$

This corresponds to the solution in $\xi > 0$. For the other half of the domain one must take the negative square root. This equation can actually be solved directly[4] though the integration described above on the variable ψ is much more straightforward. Observe figure (2.4): the solution that has been obtained corresponds to the region $[0, \rho_-]$, that is as the position coordinate is integrated from $\xi = 0$ to $\xi = \xi_b \to \infty$, the density is integrated from $\bar{\rho} = \rho_-$ to $\rho = 0$. This corresponds to a maximum density at the centre, where the density gradient is zero, and a decreasing density as the position coordinate extends outwards with density decaying to zero as $\xi \to \infty$, with zero density gradient in this limit. The interval $\bar{\rho} \in [0, \rho_-]$ is the only physically meaningful region: the left region ($\rho < 0$) is excluded because the density must be positive, and the right region is excluded because it corresponds to distributions that are unbounded with either a *minimum* density at the centre, with density increasing to infinity as $\xi \to \infty$, or a *finite* density at $\xi = \xi_b \to \infty$ and a diverging density at the centre. The maximum density at the centre can be computed by considering $\bar{\rho}' = 0$ in equation (2.95): then either $\bar{\rho} = 0$ (at $\xi \to \infty$) or $\overline{\rho}_\pm = \frac{1}{2a}\left(1 \pm e^{-a/2}\right)^2$. The lower of these is the density at the origin, which matches the solution in equation

[4] Separate the variables of ξ and $\bar{\rho}$ and the integral over $\bar{\rho}$ can be calculated by a sequence of substitutions: let $u = e^{-a/2}\cosh\frac{a}{2} - a\bar{\rho}$, then let $t = u + \sqrt{u^2 - e^{-a}}$, then let $\omega = \frac{t - e^{-a/2}\cosh\frac{a}{2}}{e^{-a/2}\sinh\frac{a}{2}}$ which leads to a standard integral.

(2.88).

Consider the gradient of the heating function: the heating function is $\Gamma[\overline{\rho}] = a\overline{\rho}\left(\frac{1}{2}\left(1+e^{-a}\right) - a\overline{\rho}\right)$, so the gradient is

$$\frac{d\Gamma}{d\xi} = a\overline{\rho}'\left(\frac{1}{2}\left(1+e^{-a}\right) - a\overline{\rho}\right) + a\overline{\rho}\left(-a\overline{\rho}'\right) \tag{2.96}$$

$$= a\overline{\rho}'\left(\frac{1}{2}\left(1+e^{-a}\right) - 2a\overline{\rho}\right) \tag{2.97}$$

Consider $\frac{d\Gamma}{d\xi} = 0$, then either $\frac{d\overline{\rho}}{d\xi} = 0$ which occurs at the peak of the density at the origin, or $\overline{\rho} = \frac{1}{4a}\left(1+e^{-a}\right)$. Seeking the position ξ_0 at which the latter is true,

$$\overline{\rho}\left(\xi_0\right) = \frac{1}{4a}\left(1+e^{-a}\right) = \frac{1}{2a}\left(1-e^{-a/2}\right)^2 \frac{1}{1+\frac{\sinh^2\left[\frac{\left(1-e^{-a}\right)}{4}\xi_0\right]}{\cosh^2\left(\frac{a}{4}\right)}} \tag{2.98}$$

$$\implies \xi_0 = \frac{4}{1-e^{-a}}\sinh^{-1}\left[\cosh\left(\frac{a}{4}\right)\sqrt{\frac{2\left(1-e^{-a/2}\right)^2}{1+e^{-a}} - 1}\right] \tag{2.99}$$

This exists only when the term under the root is non-negative, which requires $a > 2\ln\left(2+\sqrt{3}\right)$ (or $a < -2\ln\left(2+\sqrt{3}\right)$, but we must have $a > 0$ in general). This critical a corresponds to the transition to an opaque distribution, where the edge of the distribution shades the centre almost completely, so that the regions of maximal heating separate from the centre, moving, as a increases further, to the edge. For $a \gg 2\ln\left(2+\sqrt{3}\right)$ all the heating occurs in the edges with a flat temperature profile and a uniform density in the centre (see figure (2.5)). Typical realisations of the system can be seen in figures (2.7), (2.8), and (2.9) where the distinction between transparency and opacity is evident.

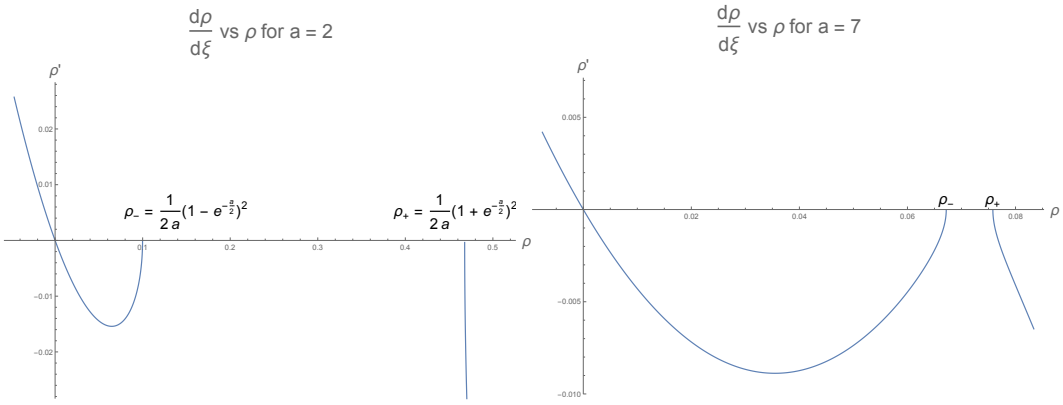

Figure 2.4: The plots show the gradient of density as a function of density, from equation (2.95). The point $\rho_- = \frac{1}{2a}\left(1 - e^{-a/2}\right)^2$ corresponds to the density at the origin, $\bar{\rho}\,(0)$, and as this curve is followed to the left $\rho \to 0$ corresponds to $\xi \to \infty$. To solve the problem we have integrated within the region $\rho \in [0, \rho_-]$

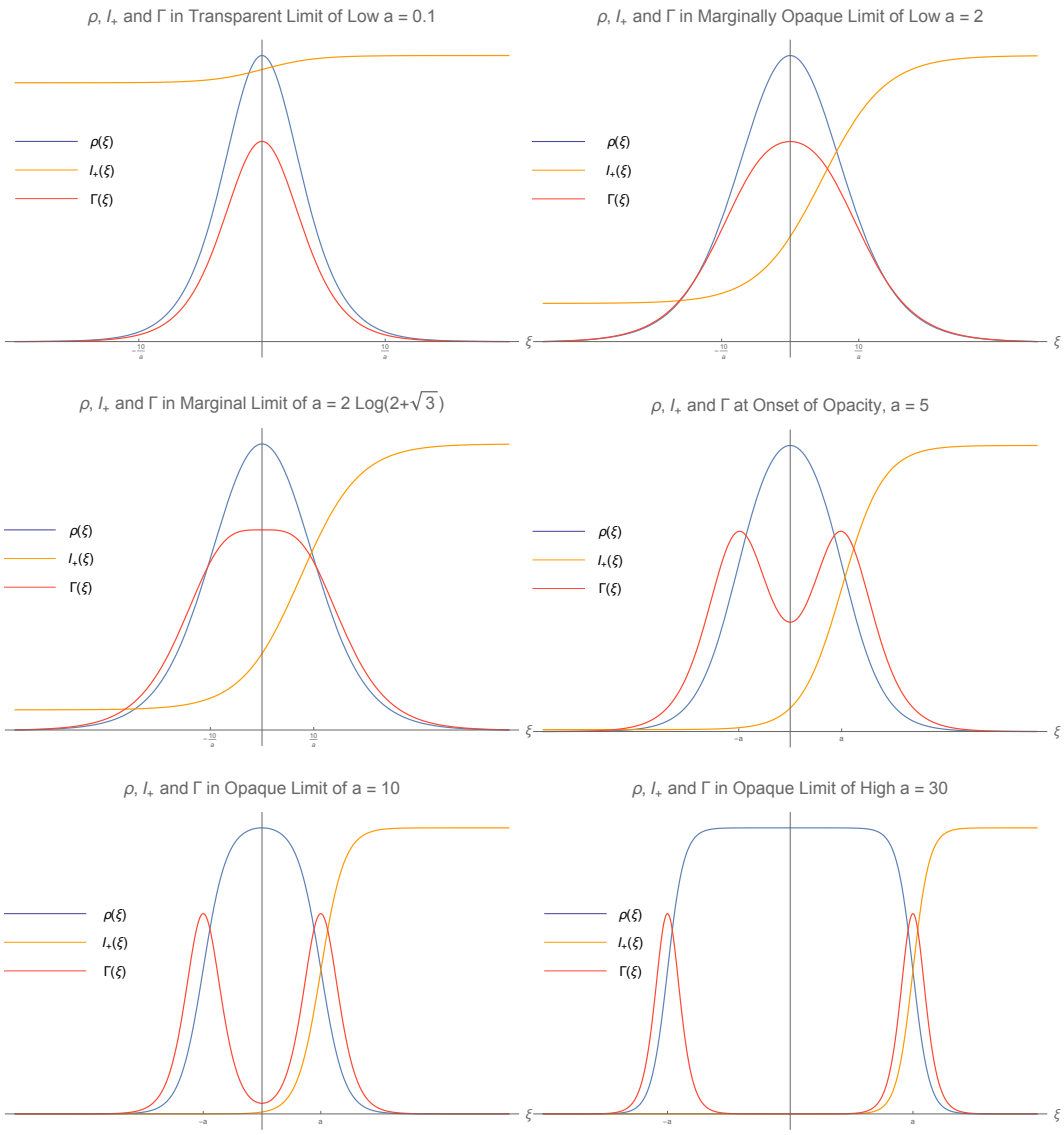

Figure 2.5: Plots show density, $\overline{\rho}(\xi)$ from equation (2.88), light intensity incident from the right (there will also be light from the left not shown here), $I_+(\xi)$ from equation (2.90), and heating, $\Gamma(\xi)$ from equation (2.91), though these have been vertically scaled to fit clearly on the same plot. One can see that in the transparent limit of low a the distribution is a wide bell shape (with width $\sim \frac{20}{a}$) and the heating term is proportional to the density, and as a is increased the density becomes more localised and the heating in the centre increases disproportionately little (no longer proportional to density) until at the critical $a = 2\ln\left(2+\sqrt{3}\right)$ the heating in the middle is reduced below that at the edges of the swarm. Essentially, the reason why the opaque distribution is uniform in the middle is because as all the energy is absorbed in a thin region at the edge of the swarm, all the heating is done in this edge region (in this case the width $\sim 2a$). Notice that in the transparent case a non-negligible fraction of light passes through the swarm, but as the system transitions to opaque the light intensity on the far side of the swarm is effectively zero.

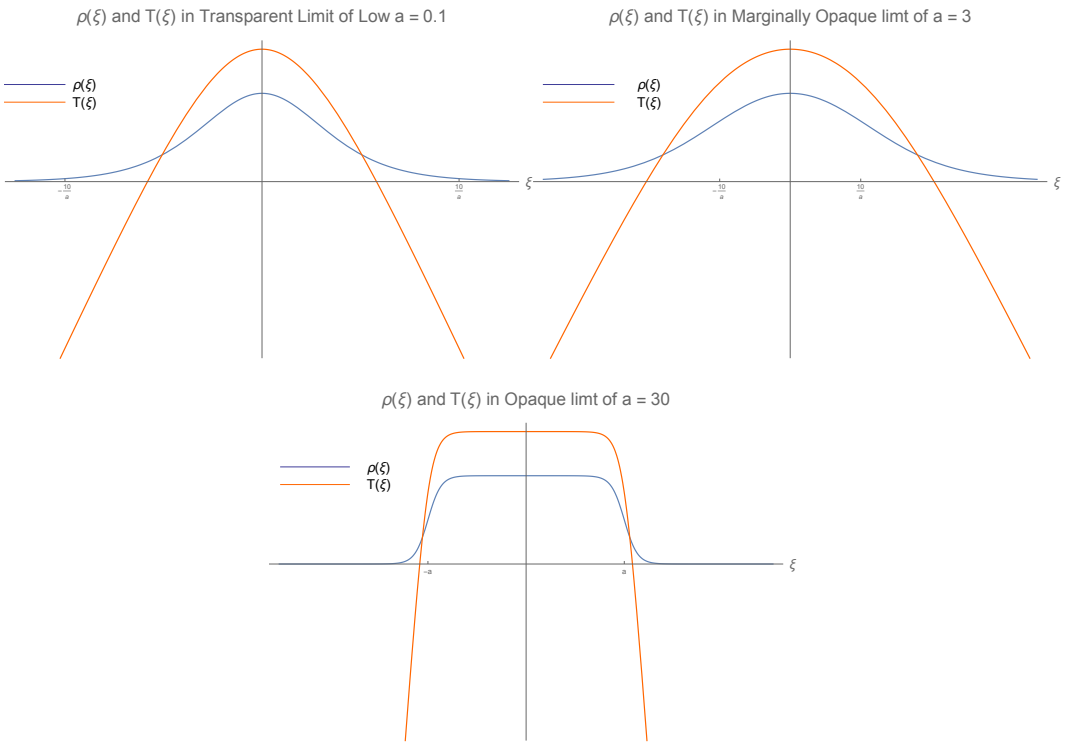

Figure 2.6: Plots show the temperature and density from equations (2.89) and (2.88) respectively. In the far field the temperature varies linearly. Note that the temperature has been scaled and the arbitrary constant chosen to fit clearly in the plot alongside density.

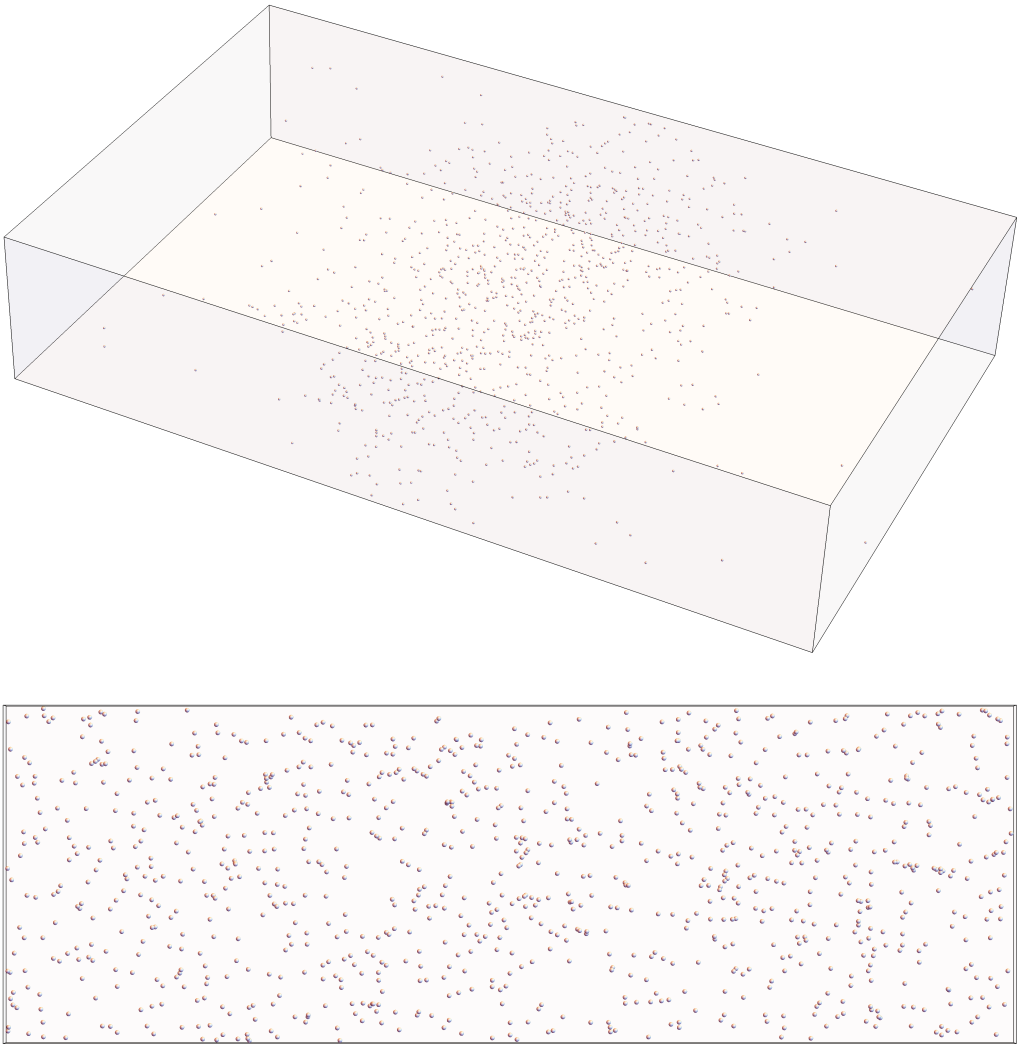

Figure 2.7: Illustration of the transparent phase with $a = 0.05$. The positions of the particles have been sampled independently from a 3D density $\rho_{3D}(x, y, z) = \rho_{yz}\rho(x)$ where $\rho(x)$ is the solution in equation (2.88), and the perpendicular density is a constant $\rho_{yz} = \frac{N}{\Delta y \Delta z}$. The radius of the particles is determined by $a = \pi r_o^2 \rho_{yz}$. The lower image is the view along the x direction demonstrating the transparency of the system.

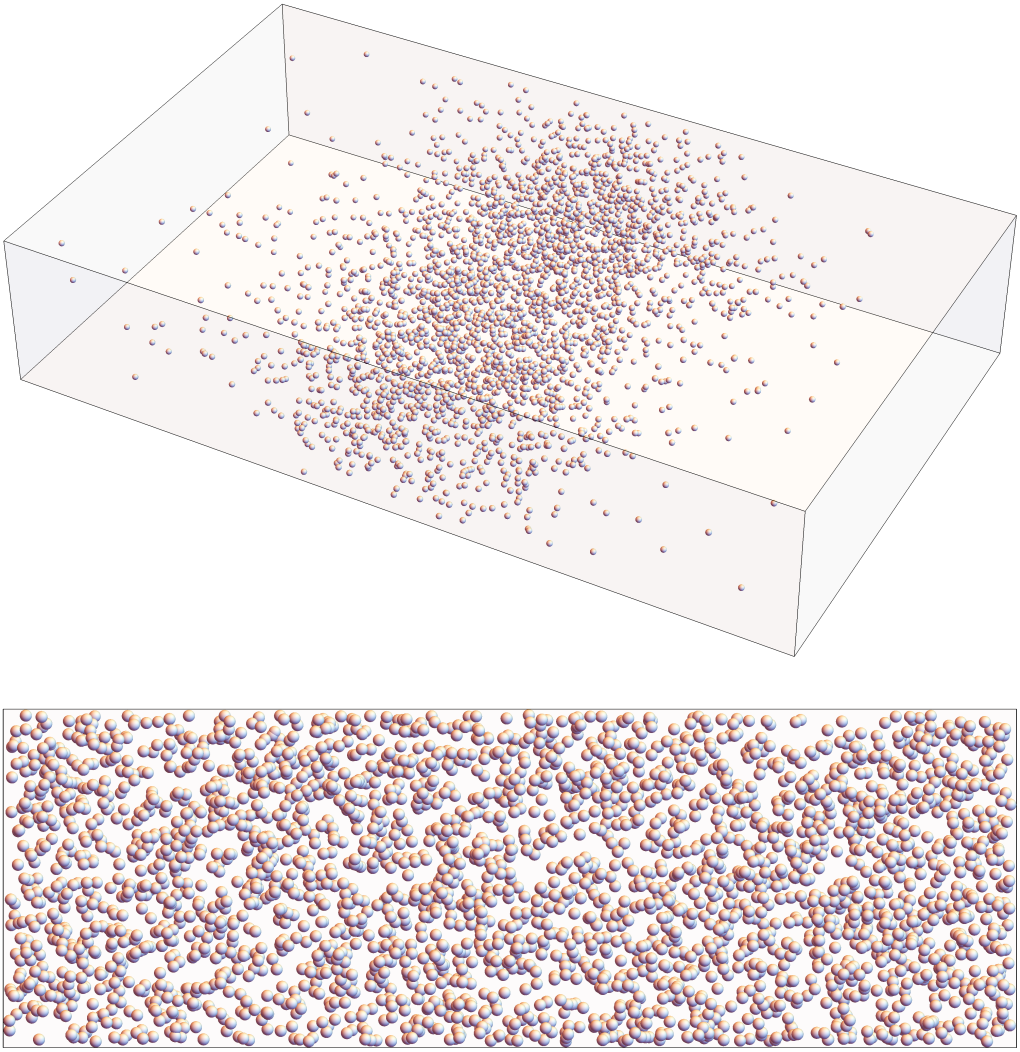

Figure 2.8: Illustration of the marginal phase with $a = 1$. The positions of the particles have been sampled independently from a 3D density $\rho_{3D}(x, y, z) = \rho_{yz}\rho(x)$ where $\rho(x)$ is the solution in equation (2.88), and the perpendicular density is a constant $\rho_{yz} = \frac{N}{\Delta y \Delta z}$. The radius of the particles is determined by $a = \pi r_o^2 \rho_{yz}$. The lower image is the view along the x direction demonstrating that the system is marginally opaque, i.e. when $a = 1$, on average a given line of sight will intercept of order one particle, but fluctuations mean that some lines of sight are clear and others intercept several particles. A significant fraction of the view is occluded but also a similar fraction is clear, hence the state is termed marginally opaque.

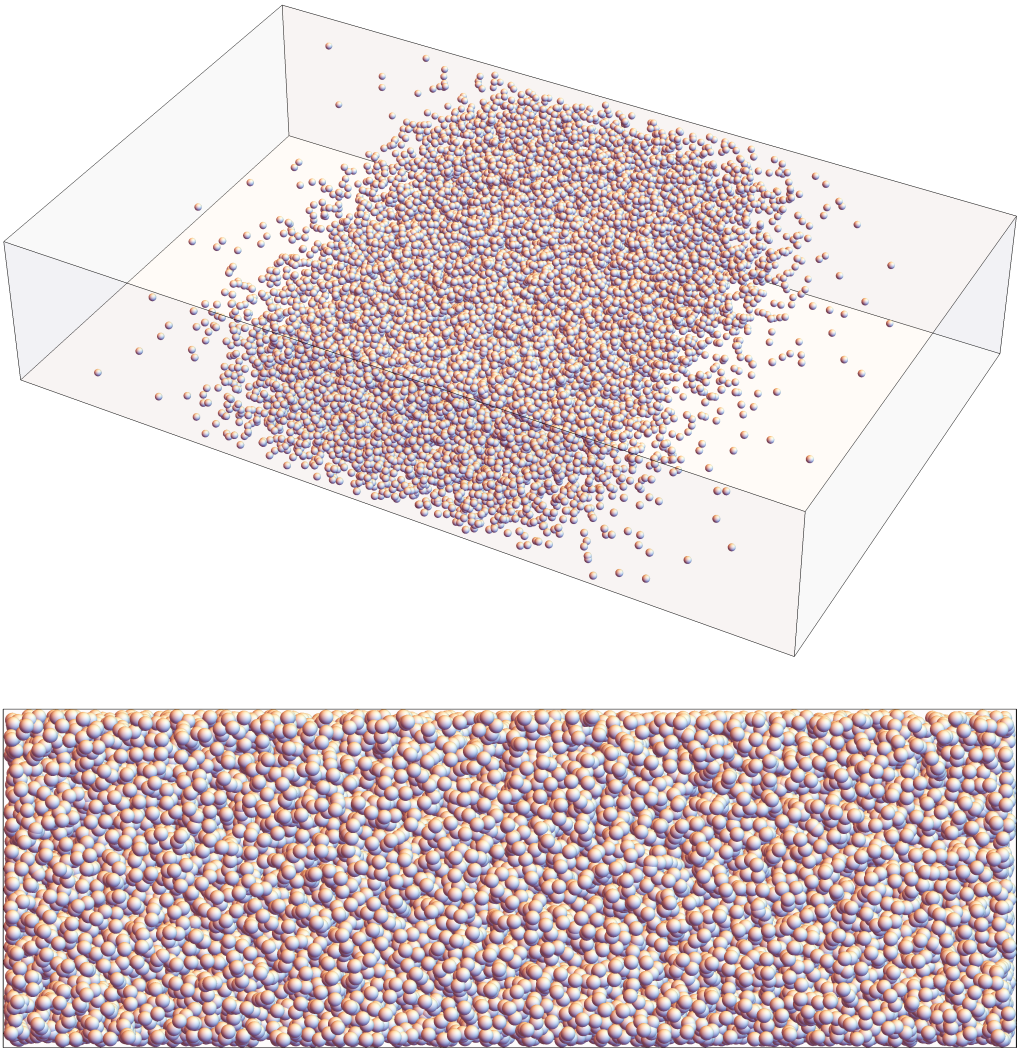

Figure 2.9: Illustration of the opaque phase with $a = 10$. The positions of the particles have been sampled independently from a 3D density $\rho_{3D}(x, y, z) = \rho_{yz}\rho(x)$ where $\rho(x)$ is the solution in equation (2.88), and the perpendicular density is a constant $\rho_{yz} = \frac{N}{\Delta y \Delta z}$. The radius of the particles is determined by $a = \pi r_o^2 \rho_{yz}$. The lower image is the view along the x direction demonstrating the opacity of the system.

3

Two Dimensional Model

3.1 The Model

Consider a system of N thermophoretic colloidal particles of radius r_o enclosed in a cylindrical container of radius R, which has a solid, transparent boundary impermeable to the colloids and in contact with a heat bath at some temperature (see figure (3.1)). The colloids are suspended in a fluid of specific heat capacity c and density ρ_f which conducts heat with thermal diffusivity κ; the colloids diffuse with diffusivity D and exhibit a net drift along temperature gradients, where the drift is linearly coupled to the temperature gradient, with thermophoretic mobility D_T. The system is illuminated from the outside by radiation directed radially through the system which, if it passes unobstructed through the full diameter of the cylinder, passes through the transparent boundary at the other side and leaves the system. Radiation intercepted by a colloid heats the colloid which heats the surrounding fluid, and this heat conducts through the fluid to the boundary whereupon it is transferred to the heat bath, which is maintained at a fixed temperature.

The model analysed in what follows applies correctly to isotropic thermophoretic colloids which potentially may collectively self-organise into moving swarms but which

are not individually self-propelling. However one might suppose that the particles are Janus particles [106] which create a local temperature gradient around themselves inducing directed motion along their own axis (self-thermophoresis). Such motion is a combination of diffusive (the Brownian motion of the colloid in the fluid) and ballistic motion on short time scales, however on longer time scales the Brownian rotation of the Janus colloids will result merely in an enhanced diffusivity. If this analysis is to be interpreted as a model of self-thermophoretic Janus colloids then the diffusivity must be replaced by the effective diffusivity of self-propelled particles, $D \to D_{eff}$. However, this can only be understood as a first approximation to such an analysis as the effective diffusivity should be spatially varying according to the effect of shading (see the discussion in the introduction to chapter 2).

The system is the same as in the one dimensional case considered in chapter 2, except for the cylindrical geometry which has important consequences for the behaviour of the particle distribution: the radially directed radiation is geometrically focussed as it passes near the symmetry axis so the light intensity changes with position, irrespective of whether it is absorbed. The opacity of the distribution depends on how the particles are distributed, which was not the case in one dimensional systems considered in chapter 2. The particles could be spread out throughout the system in a diffuse and transparent distribution, or localised near the centre in a dense and opaque distribution. Such a system could be experimentally realised with a single laser directed through the centre of a cylinder, which is rotated at a rate which is slow enough to avoid centrifugal effects but fast compared to the collective dynamics of the system, i.e. the time scale over which mean field quantities evolve. In detail, the laser would not be geometrically focused in such a set up, although as the cylinder rotates, the inner regions move at slower speeds so they will be under illumination for longer than outer regions (and, indeed, the centre will be under constant illumination), which has the same effect as geometric focussing.

The state of the system is characterised by a two dimensional mean field density, temperature, and light intensity distinguishing the incoming from outgoing radiation, I_{in} and I_{out} respectively. From the outset we shall seek radially symmetric distributions, $\rho(r)$, $T(r)$, $I_{in}(r)$, and $I_{out}(r)$, such that these quantities have dimensions: $[\rho] = \frac{1}{L^2}$, and $\left[I_{in/out}\right] = \frac{E}{T\,L}$. Although this model is purely 2D (i.e. a disc not a cylinder), an experimental realisation of the system would involve a three dimensional system with all mean field quantities invariant in the vertical direction ($\frac{\partial}{\partial z}\phi = 0$ where ϕ is any mean field quantity) with laser radiation directed radially. The particle distribution can be a 3D density ($[\rho_{3D}] = \frac{1}{L^3}$), and the radiation in-

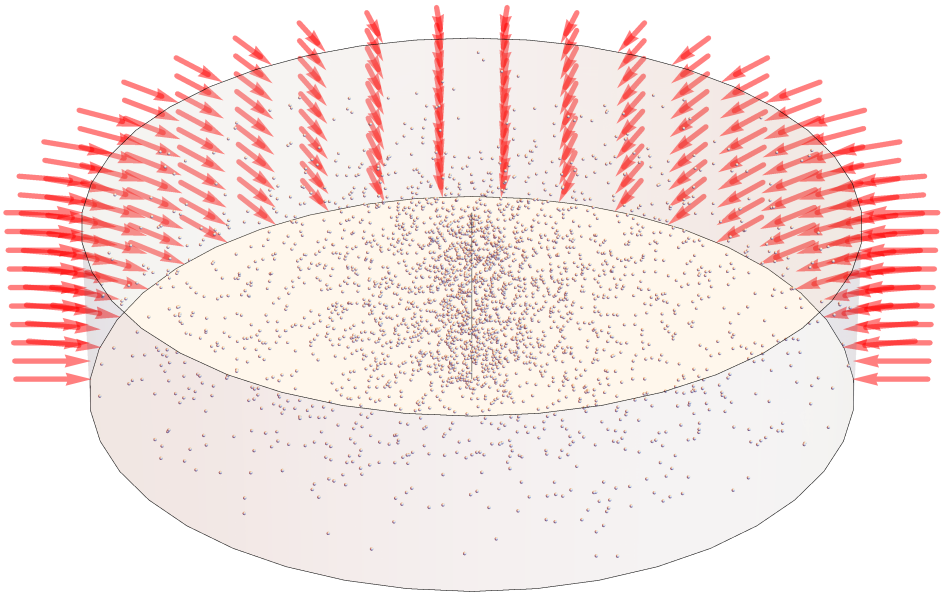

Figure 3.1: Schematic illustration of the system. Light rays are denoted by red arrows and a sketch of the colloid distribution is shown.

tensity can be a 3D variable ($[I_{3D}] = \frac{E}{T\ L^2}$). These are mapped to the purely 2D quantities by multiplying by a vertical length scale, $\rho = \rho_{3D}\Delta z$ and $I = I_{3D}\Delta z$. Similarly, though the temperature and thermal diffusivity are independent of the number of spatial dimensions, the thermal conductivity (or equivalently the fluid density) are not, that is the fluid density that appears in the purely 2D model is related to the actual fluid density by $\rho_f = \rho_{f3D}\Delta z$, so the thermal conductivity is $k = c\rho_f\kappa = c\rho_{f3D}\Delta z\kappa = k_{3D}\Delta z$, with dimensions $[k] = \frac{E}{T\ \Theta}$.

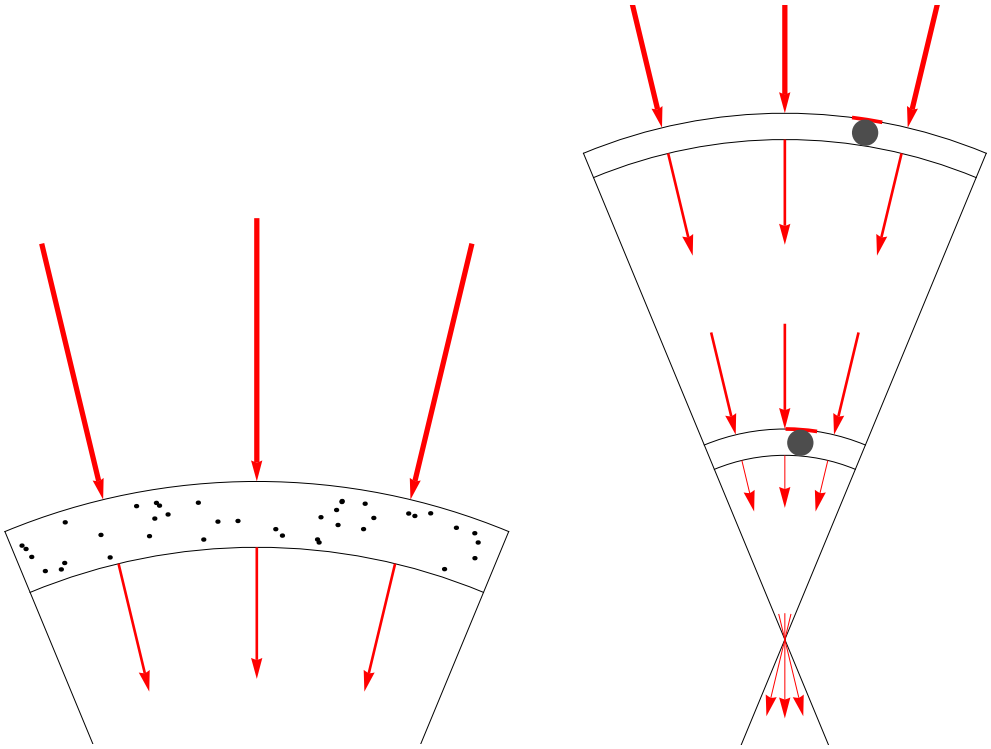

Figure 3.2: Schematic illustration of shading in 2D. Left: The energy absorbed in an annulus is proportional to the number of particles in the annulus. Right: The energy absorbed per particle is the ratio of the particle cross-section to circumference at that radius. The particles closer to the centre occlude a greater proportion of the circumference. Also note the radiation not absorbed on the way in passes through the centre and becomes outgoing radiation on the other side.

3.2 2D Equations of Motion

The dynamic variables in 2D are density, $\rho(r,t)$, temperature, $T(r,t)$, and incoming/outgoing light intensity, $I_{in/out}(r,t)$. The boundary conditions are: fixed temperature at the radius R which we take to be zero without loss of generality, $T(R)=0$; fixed total laser power, P, at the boundary $I_{in}(R)=\frac{P}{2\pi R}$; zero particle current on the boundary, $\frac{\partial\rho}{\partial r}|_R=\frac{D_T}{D}\rho(R)\frac{\partial T}{\partial r}|_R$.

3.2.1 Light Interception

Consider an annulus at radius r, the rate of incoming radiation energy (power) entering this annulus at $r+\Delta r$ is $\dot{E}_{in}=I_{in}(r+\Delta r)\,2\pi(r+\Delta r)$, and the rate of energy leaving at r is $\dot{E}_{out}=I_{in}(r)\,2\pi r$ (the outgoing radiation shall be considered

next). The rate of energy absorption in the annulus must therefore be $\dot{E}_{in} - \dot{E}_{out} = 2\pi \left(I_{in} \left(r + \Delta r \right) \left(r + \Delta r \right) - I_{in} \left(r \right) r \right)$. The fraction of the light passing through the annulus that is absorbed is the fraction of the surface of the annulus occluded by the particles it contains. This is the number of particles, $\rho 2\pi r \Delta r$, multiplied by the fraction of the annulus surface occluded per particle, $\frac{2r_o}{2\pi r}$, see figure (3.2). So,

$$\frac{2\pi \left(I_{in} \left(r + \Delta r \right) \left(r + \Delta r \right) - I_{in} \left(r \right) r \right)}{2\pi I_{in} \left(r + \Delta r \right) \left(r + \Delta r \right)} = \rho 2\pi r \Delta r \frac{2r_o}{2\pi r} \tag{3.1}$$

and taking the infinitesimal limit,

$$\frac{d}{dr} \left[r I_{in} \right] = 2 r_o \rho r I_{in} \tag{3.2}$$

$$\Rightarrow r I_{in} \left(r \right) = \frac{P}{2\pi} e^{-2r_o \int_r^R \rho dr'} \tag{3.3}$$

Notice that the intensity scales like $\frac{1}{r}$, this is the geometric focusing, modified by a term that accounts for the reduction of energy in the light field due to absorption from the colloid distribution. The outgoing radiation is modelled similarly,

$$\frac{d}{dr} \left[r I_{out} \right] = -2 r_o \rho r I_{out} \Rightarrow \int_0^r \frac{d \left(r I_{out} \right)}{r I_{out}} = -2 r_o \int_0^r \rho dr' \tag{3.4}$$

The source of energy in the outgoing radiation that passes through the symmetry axis at $r = 0$ is the energy of the incoming radiation that was not absorbed, i.e. $\lim_{r \to 0} \left\{ r I_{in} \right\} = \lim_{r \to 0} \left\{ r I_{out} \right\} = \frac{P}{2\pi} e^{-2r_o \int_0^R \rho dr}$, thus

$$r I_{out} \left(r \right) = \frac{P}{2\pi} e^{-2r_o \int_0^R \rho dr'} e^{-2r_o \int_0^r \rho dr'} \tag{3.5}$$

This analysis so far applies to a purely two dimensional model. Consider the three dimensional system with cylindrical symmetry as illustrated in figure (3.1). The density is a 3D density with 3D dimensions of number per volume ($[\rho_{3D}] = \frac{1}{L^3}$) and the light intensity has dimensions of energy per time per area ($[I_{3D}] = \frac{E}{T\ L^2}$). The fraction of this energy absorbed as it passes through a cylindrical annulus is the fraction of the surface of the annulus occluded by all the particles, which is the number of particles ($\rho_{3D} 2\pi r \Delta r \Delta z$) multiplied by the fraction of the surface

occluded per particle ($\frac{\pi r_o^2}{2\pi r \Delta z}$), see figure (3.3).

$$\frac{I_{3D}\left(r+\Delta r\right)2\pi\left(r+\Delta r\right)\Delta z - I_{3D}\left(r\right)2\pi r\Delta z}{I_{3D}\left(r+\Delta r\right)2\pi\left(r+\Delta r\right)\Delta z} = \rho_{3D}2\pi r\Delta r\Delta z\frac{\pi r_o^2}{2\pi r\Delta z} \tag{3.6}$$

$$\implies \frac{d}{dr}\left(I_{3D}r\right) = \pi r_o^2\rho_{3D}rI_{3D} \tag{3.7}$$

Equation (3.7) has the same form as equation (3.2) but with 3D quantities instead of 2D quantities. To relate the 3D variables to 2D variables multiply them by a vertical length scale, $\rho = \rho_{3D}\Delta z$ and $I = I_{3D}\Delta z$, then

$$\Rightarrow \frac{d}{dr}\left(Ir\right) = \frac{\pi r_0^2}{\Delta z}\rho rI \tag{3.8}$$

If this equation is to correspond precisely to equation (3.2) of the purely 2D model then one must have $\frac{\pi r_o^2}{\Delta z} = 2r_o$ which means the vertical length scale used to map 3D quantities onto 2D quantities must be $\Delta z = \frac{\pi r_o}{2}$. If the vertical scale is anything else then this introduces an absorption coefficient into the purely 2D model without actually generalising the model or providing insight. It is somewhat interesting that the vertical length scale that maps 3D→2D is not entirely arbitrary in cylindrical geometry, where it was completely arbitrary in mapping 3D/2D→1D in systems with linear symmetry, however this does not affect the phenomenology of the system.

Consider the mapping from 3D cylindrical symmetry to purely 2D with regards to particle number: in a purely 2D model the total number of particles, $N = 2\pi\int_0^R \rho r dr$, is a fixed system parameter; in a 3D cylindrical model the total number of particles is not a fixed parameter, rather the vertical density, $\rho_z = 2\pi\int_0^R \rho_{3D} r dr$, is the fixed parameter. Relating these using $\rho = \rho_{3D}\Delta z$, $N = 2\pi\int_0^R \rho_{3D}\Delta z r dr = \Delta z\rho_z$. With the value of the vertical length scale determined above, the 2D parameter of the particle number is $N = \frac{\pi}{4}2r_o\rho_z$; if the 2D parameter N is large then this means that in 3D there are many particles per particle diameter in the vertical direction (which does not mean that they overlap since they can be laterally dispersed). This is reminiscent of the 1D case where the 1D parameters are related to higher dimensional parameters by (for the 2D example) $\alpha N = 2r_o\rho_y$. In rectangular symmetry the parameter $a = \alpha N$ can be thought of as the perpendicular density in units of particles diameter, and in cylindrical symmetry the parameter N can similarly be thought of as the vertical density in units of particle diameter (up to a factor of $\frac{\pi}{4}$).

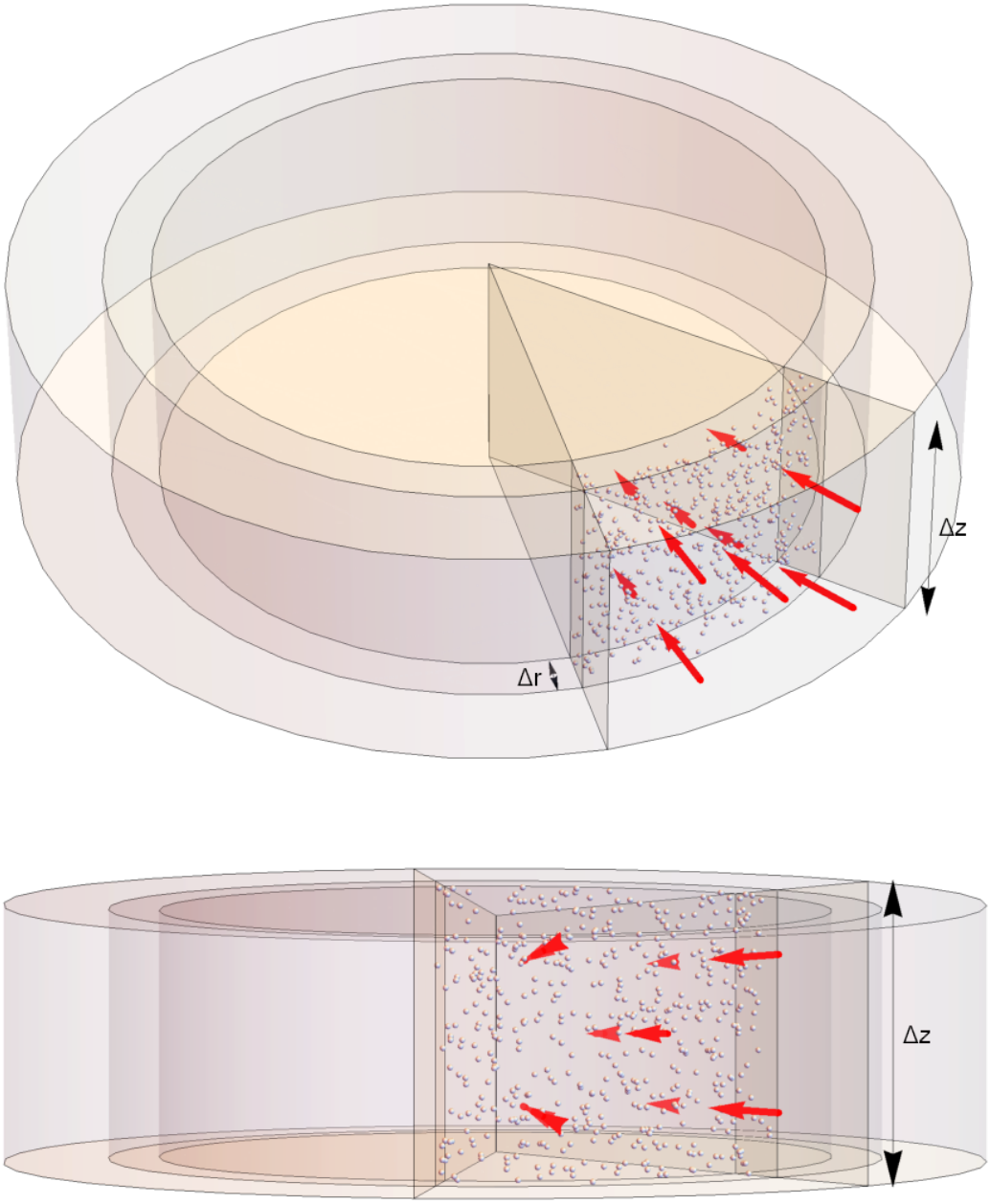

Figure 3.3: Schematic illustration of shading in three dimensions with cylindrical symmetry. The fraction of radiation absorbed passing through the cylindrical annulus is the fraction of the surface occluded, which is the number of particles in the section multiplied by the fraction of the surface occluded per particle.

3.2.2 Conversion of Intercepted Energy to Heating

The conversion of intercepted radiation to heating is governed generally by equation (2.5) which is

$$\Gamma[\rho] = -\frac{1}{c\rho_f}\nabla.\left(\vec{I}_{in} + \vec{I}_{out}\right)$$

In the case of cylindrically symmetric radiation we have $\vec{I}_{in} = -I_{in}\hat{r}$ and $\vec{I}_{out} = I_{out}\hat{r}$, so the heating functional is

$$\Gamma(r) = \frac{1}{c\rho_f r}\left(\frac{d}{dr}(rI_{in}) - \frac{d}{dr}(rI_{out})\right) \tag{3.9}$$

$$= \frac{1}{c\rho_f r}(2r_o\rho r I_{in} + 2r_o\rho r I_{out}) \tag{3.10}$$

Substituting the solutions from equations (3.3) and (3.5) this is

$$\Gamma(r) = \frac{2r_o P}{2\pi c\rho_f}\frac{\rho}{r}\left(e^{-2r_o\int_r^R \rho dr'} + e^{-2r_o\int_0^R \rho dr'}e^{-2r_o\int_0^r \rho dr'}\right) \tag{3.11}$$

The exponentials in this equation can be combined, similarly to the 1D heating functional, which gives the result

$$\Gamma(r) = \frac{2r_o P}{\pi c\rho_f}e^{-2r_o\int_0^R \rho dr}\frac{\rho}{r}\cosh\left[2r_o\int_0^r \rho dr'\right] \tag{3.12}$$

Observe the features of this heating functional: it is proportional to the density, i.e. the heating per volume is proportional to the number of heat sources per volume; it is inversely proportional to radius, thus accounting for geometric focusing of the light radiation which is the source of heat energy; and it is modified by a functional of the density, which accounts for shading of light radiation.

In the purely 2D model the parameter, $P = 2\pi R I_{in}(R)$, is the total laser power which is a fixed parameter of the system defined in terms of the purely 2D light intensity. However the 2D light intensity is really determined by the 3D light intensity multiplied by a vertical length scale, $I = I_{3D}\Delta z$, thus the parameter $P = 2\pi R I_{in\,3D}(R)\Delta z = P_{3D}\Delta z$, where P_{3D}, the total laser power per vertical length, is the fixed parameter of the system. Similar to the one dimensional analysis, the dependence of the 2D parameter, P, on vertical length scale should cancel with that of thermal conductivity, $k = k_{3D}\Delta z$, in all results.

3.2.3 Equations of Motion in 2D

Incorporating equations (2.3), (2.4) and (3.12), the equations of motion for a cylindrically symmetric system are

$$\begin{cases} \frac{\partial T}{\partial t} = \frac{\kappa}{r}\frac{\partial}{\partial r}\left(r\frac{\partial T}{\partial r}\right) + \frac{2r_oP}{\pi c\rho_f}e^{-2r_o\int_0^R \rho dr}\frac{\rho}{r}\cosh\left[2r_o\int_0^r \rho dr'\right] \\ \frac{\partial \rho}{\partial t} = \frac{D}{r}\frac{\partial}{\partial r}\left(r\frac{\partial \rho}{\partial r}\right) - \frac{D_T}{r}\frac{\partial}{\partial r}\left(r\rho\frac{\partial T}{\partial r}\right) \end{cases} \tag{3.13}$$

with boundary conditions $T(R) = 0$, $\frac{\partial \rho}{\partial r}\big|_R = \frac{D_T}{D}\rho(R)\frac{\partial T}{\partial r}\big|_R$, and the condition $N = 2\pi\int_0^R \rho r dr$. The temperature of the heat bath has been taken to be zero, without loss of generality; to compare with an experiment where the heat bath is at temperature T_0, this should be added, i.e. $T(r) \to T(r) + T_0$.

Recast these equations in dimensionless form by scaling $r = \lambda\bar{r}$, $t = \frac{\lambda^2}{\kappa}\tau$, $T = \frac{D}{D_T}\bar{T}$, and $\rho(r,t) = \frac{N}{\lambda^2}\bar{\rho}(\bar{r},\tau)$, where we now have dimensionless radius $(\bar{r})$, time (τ), temperature $(\bar{T})$ and density $(\bar{\rho})$, and the dimensionless density is normalised so that $1 = 2\pi\int_0^{\bar{R}} \bar{\rho}\,\bar{r}d\bar{r}$. The equations of motion then become

$$\begin{cases} \frac{\kappa}{\lambda^2}\frac{D}{D_T}\frac{\partial \bar{T}}{\partial \tau} = \frac{\kappa}{\lambda^2}\frac{D}{D_T}\frac{1}{\bar{r}}\frac{\partial}{\partial \bar{r}}\left(\bar{r}\frac{\partial \bar{T}}{\partial \bar{r}}\right) + \frac{2r_oP}{\pi c\rho_f}e^{-2r_o\int_0^{\bar{R}}\frac{N}{\lambda^2}\bar{\rho}\lambda d\bar{r}}\frac{N}{\lambda^3}\frac{\bar{\rho}}{\bar{r}}\cosh\left[2r_o\int_0^{\bar{r}}\frac{N}{\lambda^2}\bar{\rho}\lambda d\bar{r}'\right] \\ \frac{\kappa}{\lambda^2}\frac{N}{\lambda^2}\frac{\partial \bar{\rho}}{\partial \tau} = \frac{D}{\lambda^2}\frac{N}{\lambda^2}\frac{1}{\bar{r}}\frac{\partial}{\partial \bar{r}}\left(\bar{r}\frac{\partial \bar{\rho}}{\partial \bar{r}}\right) - \frac{D_T}{\lambda^2}\frac{N}{\lambda^2}\frac{D}{D_T}\frac{1}{\bar{r}}\frac{\partial}{\partial \bar{r}}\left(\bar{r}\bar{\rho}\frac{\partial \bar{T}}{\partial \bar{r}}\right) \end{cases} \tag{3.14}$$

$$\Rightarrow \begin{cases} \frac{\partial \bar{T}}{\partial \tau} = \frac{1}{\bar{r}}\frac{\partial}{\partial \bar{r}}\left(\bar{r}\frac{\partial \bar{T}}{\partial \bar{r}}\right) + \frac{D_TP}{\pi c\rho_f\kappa D}\frac{2r_oN}{\lambda}e^{-\frac{2r_oN}{\lambda}\int_0^{\bar{R}}\rho d\bar{r}}\frac{\bar{\rho}}{\bar{r}}\cosh\left[\frac{2r_oN}{\lambda}\int_0^{\bar{r}}\bar{\rho}d\bar{r}'\right] \\ \frac{\kappa}{D}\frac{\partial \bar{\rho}}{\partial \tau} = \frac{1}{\bar{r}}\frac{\partial}{\partial \bar{r}}\left(\bar{r}\frac{\partial \bar{\rho}}{\partial \bar{r}}\right) - \frac{1}{\bar{r}}\frac{\partial}{\partial \bar{r}}\left(\bar{r}\bar{\rho}\frac{\partial \bar{T}}{\partial \bar{r}}\right) \end{cases} \tag{3.15}$$

Choosing the length scale $\lambda = 2r_oN$, which means the dimensionless system radius is $\bar{R} = \frac{R}{2r_oN}$, and defining a new dimensionless parameter $\gamma = \frac{D_TP}{\pi c\rho_f\kappa D}$, the dimensionless equations of motion are

$$\begin{cases} \frac{\partial \bar{T}}{\partial \tau} = \frac{1}{\bar{r}}\frac{\partial}{\partial \bar{r}}\left(\bar{r}\frac{\partial \bar{T}}{\partial \bar{r}}\right) + \gamma e^{-\int_0^{\bar{R}}\bar{\rho}d\bar{r}}\frac{\bar{\rho}}{\bar{r}}\cosh\left[\int_0^{\bar{r}}\bar{\rho}d\bar{r}'\right] \\ \frac{\kappa}{D}\frac{\partial \bar{\rho}}{\partial \tau} = \frac{1}{\bar{r}}\frac{\partial}{\partial \bar{r}}\left(\bar{r}\frac{\partial \bar{\rho}}{\partial \bar{r}}\right) - \frac{1}{\bar{r}}\frac{\partial}{\partial \bar{r}}\left(\bar{r}\,\bar{\rho}\frac{\partial \bar{T}}{\partial \bar{r}}\right) \end{cases} \tag{3.16}$$

The boundary conditions are $\bar{T}(\bar{R}) = 0$, $\frac{\partial \bar{\rho}}{\partial \bar{r}}\big|_{\bar{R}} = \bar{\rho}(\bar{R})\frac{\partial \bar{T}}{\partial \bar{r}}\big|_{\bar{R}}$, and the normalisation condition $1 = 2\pi\int_0^{\bar{R}}\bar{\rho}\bar{r}d\bar{r}$. The length scale has a clear physical interpretation, $\lambda = 2r_oN$, which is the sum of the particle diameters. The dimensionless parameter, γ, is determined by various physical parameters including the ratio of total radiation power to thermal conductivity (thus cancelling the dependence of each on the vertical

length scale in mapping from 3D→2D). In particular the most readily tuned physical parameter in γ is the total radiation power, so it is useful and insightful to interpret γ as a dimensionless radiation power. It is interesting to notice that these combinations of physical parameters determined the length scale in the one dimensional model while the particle number determined the opacity, whereas here the particle number determines the length scale, while these parameters (ratio of radiation power to thermal conductivity and thermophoretic mobility to diffusivity) determine γ (which in part determines the opacity, see below).

Interpretation of $\bar{R}$

A key parameter in the scaled system is the dimensionless radius, $\bar{R}$, which is the ratio of the system radius to length scale, more specifically

$$\bar{R} = \frac{R}{2r_o N} \tag{3.17}$$

To interpret this, suppose first that $\bar{R} \gg 1$. In this case a uniform distribution of particles will be transparent, i.e. most lines of sight through the centre of the system will not intercept a particle. If $\bar{R} \ll 1$ then a uniform distribution of particles will be opaque, i.e. almost every line of sight through the centre will intercept at least one particle. Finally, $\bar{R} \sim 1$ corresponds to the case in which a uniform distribution of such particles would be marginally opaque: some lines of sight through the centre intercept at least one particle, and some do not, but on average the every line of sight intercepts of order one particle (see figure (3.4)). Note that the case of $\bar{R} \ll 1$ must always be opaque no matter how the particles are distributed (assuming radially symmetric distributions), whereas a system with $\bar{R} \gg 1$ would be transparent for a *uniform* distribution but could be opaque if the particles are localised near the centre. In what follows we shall be primarily interested in the case $\bar{R} \gg 1$.

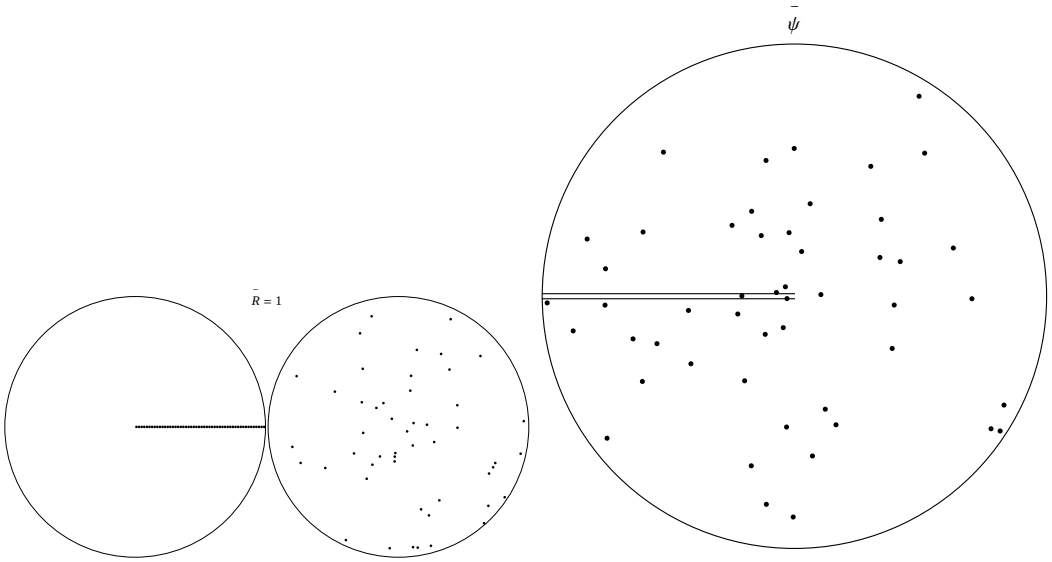

Figure 3.4: Schematic Illustrating the meaning of $\bar{R}$ and $\bar{\psi}$. $\bar{R} = 1$ means the particles can be lined from centre to edge (left image), in which case a uniform distribution is marginally opaque, such that, on average, one particle is seen through to the centre of the system (right image). $\bar{\psi}$ is the number of particles intercepted by such a line of width the particle diameter.

3.3 Stationary Solutions

We seek stationary solutions to equations (3.16). In such a state the absorption of energy from the light radiation throughout the system balances the energy conducted into the heat bath at the boundary, and the distribution and temperature field are such that the diffusion of the colloids is balanced by their thermophoretic drift up the temperature gradient. In this case, as discussed in the chapter on the one dimensional case, the diffusion-thermophoresis balance is described by the equation $\nabla\rho = \frac{D_T}{D}\rho\nabla T$, and the density distribution is $\rho(\vec{x}) = \rho(\vec{x}_b)\, e^{\frac{D_T}{D}(T(\vec{x})-T(\vec{x}_b))}$. The total energy absorption rate in the system is the integral of the heating function over the entire volume, $\dot{Q} = c\rho_f \int_V \Gamma(\vec{x})\, dV$, which must balance the energy lost at the boundary conducted into the heat bath, thus $\kappa R \frac{dT}{dr}\big|_R = -\int_0^R \Gamma(r)\, r\, dr$. Also, the total heating rate is the difference between the power of incident radiation and

the power of outgoing radiation as it leaves the system, i.e.

$$\dot{Q} = P - 2\pi R I_{out}(R) \tag{3.18}$$

$$= P - Pe^{-2r_o \int_0^R \rho dr'} e^{-2r_o \int_0^R \rho dr'} \tag{3.19}$$

$$= P\left(1 - e^{-2\ 2r_o \int_0^R \rho dr'}\right) \tag{3.20}$$

$$= c\rho_f 2\pi \int_0^R \Gamma(r)\, r dr \tag{3.21}$$

By contrast with the one dimensional case, the total energy absorption rate is not determined uniquely by fixed system parameters, but rather can vary depending on the form of the distribution, $\rho(r)$.

In scaling the equations to dimensionless form the total laser power maps to the dimensionless laser power, $P \to \gamma$, so it is meaningful to consider the dimensionless heating rate in terms of γ. The dimensionless heating function is $\bar{\Gamma} = \frac{\lambda^2 D_T}{\kappa D}\Gamma$, so it follows that $2\pi \int_0^{\bar{R}} \bar{\Gamma}\bar{r}d\bar{r} = \frac{\dot{Q}D_T}{c\rho_f \kappa D}$. Defining the total dimensionless absorption rate $\gamma_{abs} = 2\int_0^{\bar{R}} \bar{\Gamma}\bar{r}d\bar{r}$, this is

$$\gamma_{abs} = \left(1 - e^{-2\int_0^{\bar{R}} \bar{\rho} d\bar{r}}\right)\gamma \tag{3.22}$$

The boundary condition on the dimensionless temperature gradient becomes

$$\bar{R}\frac{d\bar{T}}{d\bar{r}}\Big|_{\bar{R}} = -\int_0^{\bar{R}} \bar{\Gamma}\,\bar{r}d\bar{r} = -\frac{\gamma_{abs}}{2} \tag{3.23}$$

3.3.1 Stationary Solution to the Heat Equation in Cylindrical Geometry

The two dimensional heat equation with cylindrical symmetry is $\frac{\partial \bar{T}}{\partial \tau} = \frac{1}{\bar{r}}\frac{\partial}{\partial \bar{r}}\left(\bar{r}\frac{\partial \bar{T}}{\partial \bar{r}}\right) + \Gamma(\bar{r})$. In a stationary state this is

$$\frac{1}{\bar{r}}\frac{d}{d\bar{r}}\left(\bar{r}\frac{d\bar{T}}{d\bar{r}}\right) = -\Gamma(\bar{r}) \tag{3.24}$$

with $\bar{T}\left(\bar{R}\right) = 0$. We shall adopt a Green's function approach to solving this. Consider the function $G(r; r')$ satisfying the equation

$$\frac{1}{r}\frac{d}{dr}\left(r\frac{dG}{dr}\right) = -\delta\left(r - r'\right) \tag{3.25}$$

subject to the boundary conditions $G\left(\bar{R};r'\right)=0$, and $\bar{R}\frac{dG}{dr}\Big|_{\bar{R}}=-\int_0^{\bar{R}}\delta\left(r-r'\right)r\,dr=-r'$. Then

$$\Gamma\left(r'\right)\frac{1}{r}\frac{d}{dr}\left(r\frac{dG\left(r;r'\right)}{dr}\right)=-\Gamma\left(r'\right)\delta\left(r-r'\right) \tag{3.26}$$

$$\Rightarrow\int_0^{\bar{R}}\Gamma\left(r'\right)\frac{1}{r}\frac{d}{dr}\left(r\frac{dG\left(r;r'\right)}{dr}\right)dr'=-\int_0^{\bar{R}}\Gamma\left(r'\right)\delta\left(r-r'\right)dr' \tag{3.27}$$

$$\Rightarrow\frac{1}{r}\frac{d}{dr}\left(r\frac{d}{dr}\int_0^{\bar{R}}G\left(r;r'\right)\Gamma\left(r'\right)dr'\right)=-\Gamma\left(r\right) \tag{3.28}$$

$$\Rightarrow T\left(r\right)=\int_0^{\bar{R}}G\left(r;r'\right)\Gamma\left(r'\right)dr' \tag{3.29}$$

Consider the region $r>r'$ in equation (3.25), then

$$\frac{d}{dr}\left(r\frac{dG}{dr}\right)=0\Rightarrow\frac{dG}{dr}=\frac{C}{r}\Rightarrow G\left(r;r'\right)=C\ln r+\alpha \tag{3.30}$$

Similarly in the region $r<r'$,

$$\frac{d}{dr}\left(r\frac{dG}{dr}\right)=0\Rightarrow\frac{dG}{dr}=\frac{C'}{r}\Rightarrow G\left(r;r'\right)=C'\ln r+\alpha' \tag{3.31}$$

Integrating equation (3.25) in a small interval around r',

$$\int_{r'-\epsilon}^{r'+\epsilon}\frac{d}{dr}\left(r\frac{dG}{dr}\right)dr=-\int_{r'-\epsilon}^{r'+\epsilon}r\delta\left(r-r'\right)dr=-r' \tag{3.32}$$

$$\Rightarrow\left[r\frac{dG}{dr}\right]_{r'-\epsilon}^{r'+\epsilon}=\left(r'+\epsilon\right)\frac{C}{r'+\epsilon}-\left(r'-\epsilon\right)\frac{C'}{r'-\epsilon} \tag{3.33}$$

$$=C-C' \tag{3.34}$$

$$\Rightarrow C'=C+r' \tag{3.35}$$

The balance of energy absorbed in the system and energy lost at the boundary requires, $\bar{R}\frac{dG}{dr}\Big|_{\bar{R}}=-r'\Rightarrow\bar{R}\frac{C}{\bar{R}}=-r'\Rightarrow C=-r'\Rightarrow C'=0$. So far,

$$G\left(r;r'\right)=\begin{cases}-r'\ln r+\alpha & ,\,r>r'\\ \alpha' & ,\,r<r'\end{cases} \tag{3.36}$$

The constants of integration can be constrained further by imposing continuity at the radius r', so $\alpha'=\alpha-r'\ln r'$, and finally the boundary condition that the temperature at the boundary must be the temperature of the heat bath, $G\left(\bar{R};r'\right)=$

$0 \Rightarrow \alpha = r' \ln \bar{R}$.

$$\therefore G\left(r; r'\right) = \begin{cases} r' \ln \bar{R} - r' \ln r & , r > r' \\ r' \ln \bar{R} - r' \ln r' & , r < r' \end{cases} \tag{3.37}$$

The temperature for an arbitrary radially symmetric distribution of heat sources can then be computed,

$$T\left(r\right) = \int_0^r G\left(r; r'\right) \Gamma\left(r'\right) dr' + \int_r^{\bar{R}} G\left(r; r'\right) \Gamma\left(r'\right) dr' \tag{3.38}$$

Substituting the Green's function for $r > r'$ into the first integral and for $r < r'$ into the second,

$$T\left(r\right) = \int_0^r \left(r' \ln \bar{R} - r' \ln r\right) \Gamma\left(r'\right) dr' + \int_r^{\bar{R}} \left(r' \ln \bar{R} - r' \ln r'\right) \Gamma\left(r'\right) dr' \tag{3.39}$$

$$\begin{aligned} &= \ln \bar{R} \int_0^r \Gamma\left(r'\right) r' dr' - \ln r \int_0^r \Gamma\left(r'\right) r' dr' \\ &\quad + \ln \bar{R} \int_r^{\bar{R}} \Gamma\left(r'\right) r' dr' - \int_r^{\bar{R}} \ln r' \Gamma\left(r'\right) r' dr' \end{aligned} \tag{3.40}$$

$$= \ln \bar{R} \int_0^{\bar{R}} \Gamma\left(r'\right) r' dr' - \ln r \int_0^r \Gamma\left(r'\right) r' dr' - \int_r^{\bar{R}} \ln r' \Gamma\left(r'\right) r' dr' \tag{3.41}$$

The temperature gradient for a cylindrically symmetric distribution of heat sources is then,

$$\frac{dT}{dr} = -\frac{1}{r} \int_0^r \Gamma\left(r'\right) r' dr' \tag{3.42}$$

The stationary temperature gradient at a particular radius, described by this equation, is the total heating rate below that radius modified by a factor of $\frac{1}{r}$ to account for geometric spreading of the heat flux.

3.3.2 Stationary Density

The dimensionless incoming light intensity at radius $\bar{r}$ is the portion of the incident light radiation not absorbed by that point, i.e. $\gamma_{in}(\bar{r}) = e^{-\int_{\bar{r}}^{\bar{R}} \bar{\rho} d\bar{r}'} \gamma$. Of this radiation, the remainder that has not been absorbed after passing through the centre of the system and out again is $\gamma_{out}(\bar{r}) = \gamma_{in}(\bar{r}) e^{-2\int_0^{\bar{r}} \bar{\rho} d\bar{r}'}$. The energy absorption rate below the radius $\bar{r}$ is the difference of these, i.e.

$$2\int_0^{\bar{r}} \bar{\Gamma}(\bar{r}) \bar{r}' d\bar{r}' = \gamma_{in}(\bar{r}) - \gamma_{out}(\bar{r}) = 2\gamma e^{-\int_0^{\bar{R}} \bar{\rho} d\bar{r}} \sinh\left[\int_0^{\bar{r}} \bar{\rho} d\bar{r}'\right] \tag{3.43}$$

Therefore, the stationary temperature variation of the colloid distribution is

$$\bar{r}\frac{d\bar{T}}{d\bar{r}} = -\gamma e^{-\int_0^{\bar{R}} \bar{\rho} d\bar{r}} \sinh\left[\int_0^{\bar{r}} \bar{\rho} d\bar{r}'\right] \tag{3.44}$$

The balance of diffusion and thermophoresis of the stationary colloid distribution for this temperature field requires $\frac{d\bar{\rho}}{d\bar{r}} = \bar{\rho}\frac{d\bar{T}}{d\bar{r}}$, hence

$$\frac{d\bar{\rho}}{d\bar{r}} = -\gamma e^{-\int_0^{\bar{R}} \bar{\rho} d\bar{r}} \frac{\bar{\rho}}{\bar{r}} \sinh\left[\int_0^{\bar{r}} \bar{\rho} d\bar{r}'\right] \tag{3.45}$$

Following the analysis of the one dimensional model, we convert this integro-differential equation into a pure ODE by defining the new variable $\psi(\bar{r}) \equiv \int_0^{\bar{r}} \bar{\rho} d\bar{r}'$. This quantity remains dimensionless when expressed in terms of physical variables, specifically $\psi(r) = 2r_o \int_0^r \rho dr$ in 2D or $\psi(r) = \pi r_o^2 \int_0^r \rho_{3D} dr$ in terms of 3D variables. The interpretation of ψ is thus straight forward: it is the number of particles intercepted, on average, along a line of sight from the origin outwards to radius r, and, in particular, evaluating ψ on the boundary introduces a new and important metric of the system

$$\bar{\psi} \equiv \psi\left(\bar{R}\right) \tag{3.46}$$

$$= \int_0^{\bar{R}} \bar{\rho} d\bar{r} \tag{3.47}$$

$$= 2r_o \int_0^R \rho dr \tag{3.48}$$

This is the integral of a two dimensional density along a radial line multiplied by a small width, $2r_0$, the diameter of a particle (or the integral of a 3D density multiplied by a small surface area, πr_o^2, the cross-sectional surface area of a particle), and thus is the number of particles of that diameter encountered along this line. Therefore, if $\bar{\psi} \gg 1$ then a line of sight through the centre of the system will, on average, intersect

many particles so almost all light rays will be intercepted, so the system is opaque. Whereas, if $\bar{\psi} \ll 1$, then almost all light rays through the system go through without interception and the system is transparent. When $\bar{\psi} \sim 1$ the system is marginally opaque, see figure (3.4). Substituting ψ in equation (3.45),

$$\bar{r}\frac{d^2\psi}{d\bar{r}^2} = -\gamma e^{-\overline{\psi}}\frac{d\psi}{d\bar{r}}\sinh\psi \tag{3.49}$$

Integrating by parts the LHS, i.e. $r\frac{d^2\psi}{dr^2} = \frac{d}{dr}\left(r\frac{d\psi}{dr}\right) - \frac{d\psi}{dr}$, then

$$\bar{r}\frac{d\psi}{d\bar{r}} = c + \psi - \gamma e^{-\overline{\psi}}\cosh\psi \tag{3.50}$$

The constant of integration can be determined by considering the asymptotics of the density, $\bar{\rho} = \frac{d\psi}{d\bar{r}}$, near the origin: if the density is finite then $\lim_{\bar{r}\to 0}\left\{\bar{r}\frac{d\psi}{d\bar{r}}\right\} = 0$ so, since $\psi(0) = 0$, the constant of integration is $c = \gamma e^{-\overline{\psi}}$; if the density is infinite at the origin then it may scale as $\bar{\rho} \sim \bar{r}^{-\zeta}$, but the integrated density must nevertheless be finite, so $\zeta < 2$. In this case in the limit of $\bar{r} \to 0$ the LHS may be zero ($\zeta < 1$), infinite ($\zeta > 1$), or finite ($\zeta = 1$). However, the parameter $\overline{\psi} = \int_0^{\bar{R}} \bar{\rho} d\bar{r}$ and, indeed, the variable $\psi(\bar{r})$, will be infinite for all radii unless $\zeta < 1$. In this case $\lim_{\bar{r}\to 0}\left\{\bar{r}\frac{d\psi}{d\bar{r}}\right\} = 0$, so the constant of integration must be[1] $c = \gamma e^{-\overline{\psi}}$, thus

$$\bar{r}\frac{d\psi}{d\bar{r}} = \psi - 2\gamma e^{-\overline{\psi}}\sinh^2\frac{\psi}{2} \tag{3.51}$$

As with the analysis of the one dimensional model where the variable ψ was defined as the integral of the density for which it was necessary to impose a boundary condi-

[1]This argument implicitly assumes without proof that the function $\psi(\bar{r}) \equiv \int_0^{\bar{r}} \rho d\bar{r}' < \infty$. This assumption was implicitly made not only at the definition of ψ and the recasting of equations in terms of ψ, but even earlier at equation (3.12) where the two exponential terms in the heating functional were combined into the hyperbolic cosine of the integral of density from the origin, which does not exist if the density diverges at the origin faster than or as fast as $1/r$. Consider equation (3.3) for the incoming light intensity: no assumptions have been made in the derivation of this equation about the behaviour of the density at the origin, and one can take this result arbitrarily close to the origin. The product of the radius with intensity is the total power in the radiation field (up to a factor of 2π), so if the integral of density down to the origin diverges such that the RHS of equation (3.3) is zero, then the power in the radiation field is zero. Thus the assumption of a diverging density at least as fast as $1/r$ is equivalent to the assumption of complete absorption, hence there is no outgoing radiation in this case. If one follows through with this analysis without outgoing radiation and defines the function $\phi(\bar{r}) \equiv -\int_{\bar{r}}^{\bar{R}} \rho d\bar{r}'$, for which $\phi(\bar{R}) = 0$ and the assumption of complete absorption $\Rightarrow \phi(\bar{r}\to 0) \to -\infty$, then the equation for this function is $\bar{r}\frac{d\phi}{d\bar{r}} = c + \phi + \frac{\gamma}{2}e^{\phi}$ with $c \geq \frac{\gamma}{2}$ to ensure positive density. However, the RHS of this equation is zero at finite ϕ, thus $\phi(0) > -\infty$. This, then, is a proof by contradiction: assume ρ diverges at least as fast as $1/r \Rightarrow$ complete absorption $\Rightarrow$ an equation for ϕ which $\Rightarrow \phi$ is finite at the origin $\Rightarrow$ incomplete absorption, which is a contradiction. Thus, the density does not diverge as fast as $1/r$.

tion on ψ that ensured the normalisation of the density (in that case $\psi(\pm\xi_b) = \pm\frac{a}{2}$), so it is here, except that in this case the condition that guarantees normalisation is

$$2\pi\int_0^{\bar{R}}\bar{r}\frac{d\psi}{d\bar{r}}d\bar{r} = 1 = 2\pi\left(\bar{R}\,\overline{\psi} - \int_0^{\bar{R}}\psi(\bar{r})\,d\bar{r}\right) \tag{3.52}$$

Thus

$$\begin{cases}\bar{r}\frac{d\psi}{d\bar{r}} = \psi - 2\gamma e^{-\overline{\psi}}\sinh^2\frac{\psi}{2} & ,\ \psi\left(\bar{R}\right) = \overline{\psi} \\ \overline{\psi} = \frac{1}{2\pi\bar{R}} + \frac{1}{\bar{R}}\int_0^{\bar{R}}\psi(\bar{r})\,d\bar{r}\end{cases} \tag{3.53}$$

The second equation is a non-local boundary condition on the first equation: the constant $\overline{\psi}$ is the boundary condition in the differential equation (but also modifies the form of the ODE) determining the function that solves it, but $\overline{\psi}$ must itself be determined by the definite integral over that function, and hence is a *non-local* boundary condition. This can be thought of as a self-consistency condition in the definition of ψ. The dimensionless parameters, $\bar{R}$ and γ, are fixed system parameters and for some choice of these parameters only a restricted set of values of $\overline{\psi}$ will satisfy the self-consistency condition. Essentially this is a root finding problem: define the function $F\left(\overline{\psi}\right) = \frac{1}{2\pi\bar{R}} + \frac{1}{\bar{R}}\int_0^{\bar{R}}\psi(r)\,dr$, where ψ is the function that solves the ODE in (3.53) for this $\overline{\psi}$. Then the problem is to find the roots of $F\left(\overline{\psi}\right) - \overline{\psi} = 0$. A constraint on this can be found by observing that the density must always be positive, which means the gradient of ψ must always be positive, and this is minimal at the system radius, so $\bar{R}\,\psi'|_{\bar{R}} = \overline{\psi} - \frac{\gamma}{2}\left(1 - e^{-\overline{\psi}}\right)^2 \geq 0 \Rightarrow \gamma \leq \frac{2\overline{\psi}}{\left(1-e^{-\overline{\psi}}\right)^2}$. In the γ-$\overline{\psi}$ plane there is an excluded region defined by this equation, in particular the smallest γ in this excluded region is $\gamma_{min} = \frac{4}{1-\left(1+\frac{1}{W_{-1}\left(-\frac{1}{2}\exp\left(-\frac{1}{2}\right)\right)}\right)^2} \approx 4.91081$, for which $\overline{\psi} = -\left(\frac{1}{2} + W_{-1}\left(-\frac{1}{2}e^{-\frac{1}{2}}\right)\right)$, where W_{-1} is the second real branch of the Lambert function [132]. In the limit of large or small $\overline{\psi}$ this constraint is $\gamma \leq 2\overline{\psi}$ and $\gamma \leq \frac{2}{\overline{\psi}}$ respectively.

Solving the self-consistency condition

Consider the function

$$F\left(\overline{\psi}\right) = \frac{1}{2\pi\bar{R}} + \frac{1}{\bar{R}}\int_0^{\bar{R}}\psi(r)\,dr \tag{3.54}$$

where the function $\psi(r)$ solves the ODE in equation (3.53). This can be recast as an explicit function of the variable $\overline{\psi}$: separate the variables in the ODE and integrate from some radius to the boundary

$$\int_{\psi}^{\overline{\psi}} \frac{d\psi'}{\psi' - 2\gamma e^{-\overline{\psi}} \sinh^2 \frac{\psi'}{2}} = \int_{\bar{r}}^{\overline{R}} \frac{dr'}{r'} = -\ln \frac{\bar{r}}{\overline{R}} \tag{3.55}$$

This can be re-arranged for the radius as a function of ψ written in terms of an unknown integral,

$$\bar{r}(\psi) = \overline{R} e^{-\int_{\psi}^{\overline{\psi}} \frac{d\psi'}{\psi' - 2\gamma e^{-\overline{\psi}} \sinh^2 \frac{\psi'}{2}}} \tag{3.56}$$

Consider the integral of the function ψ over radius in the function F, this can be converted into an integral over ψ itself

$$\int_0^{\overline{R}} \psi(\bar{r})\, d\bar{r} = \int_0^{\overline{\psi}} \frac{\psi}{\frac{d\psi}{d\bar{r}}} d\psi \tag{3.57}$$

$$= \int_0^{\overline{\psi}} \frac{\psi\, \bar{r}(\psi)}{\psi - 2\gamma e^{-\overline{\psi}} \sinh^2 \frac{\psi}{2}} d\psi \tag{3.58}$$

$$= \overline{R} \int_0^{\overline{\psi}} \frac{\psi \exp\left[-\int_{\psi}^{\overline{\psi}} \frac{d\psi'}{\psi' - 2\gamma e^{-\overline{\psi}} \sinh^2 \frac{\psi'}{2}}\right]}{\psi - 2\gamma e^{-\overline{\psi}} \sinh^2 \frac{\psi}{2}} d\psi \tag{3.59}$$

Therefore the self-consistency function expressed explicitly in terms of $\overline{\psi}$ is

$$F(\overline{\psi}) = \frac{1}{2\pi \bar{R}} + \int_0^{\overline{\psi}} \frac{\psi \exp\left[-\int_{\psi}^{\overline{\psi}} \frac{d\psi'}{\psi' - 2\gamma e^{-\overline{\psi}} \sinh^2 \frac{\psi'}{2}}\right]}{\psi - 2\gamma e^{-\overline{\psi}} \sinh^2 \frac{\psi}{2}} d\psi \tag{3.60}$$

Notice that the dependence on system radius has entirely factored out of the second term in the function, which can be written as $F(\overline{\psi}) = \frac{1}{2\pi \bar{R}} + g(\overline{\psi}; \gamma)$, so the dependence on $\bar{R}$ in the function is a vertical translation, this can be seen in figure (3.6). The self-consistency function is plotted for various parameters in figures (3.5) and (3.6). As can be seen, when $\gamma > \gamma_{min} \approx 4.91$ there is an interval in which the function does not exist, and on either side of this interval the function gradient is $\pm\infty$, (though the function is finite). It can be shown, by differentiating equation (3.60), that its derivative is of the form $F'(\overline{\psi}) = \frac{\overline{\psi}}{\overline{\psi} - 2\gamma e^{-\overline{\psi}} \sinh^2 \frac{\overline{\psi}}{2}} + \ldots$ where the additional terms are integrals that do not diverge at $\overline{\psi}$, thus for $\gamma > \gamma_{min}$, as $\overline{\psi}$ approaches the limits of the existence region (where $\overline{\psi} = 2\gamma e^{-\overline{\psi}} \sinh^2 \frac{\overline{\psi}}{2}$) the gradi-

ent in F approaches infinity. As can be seen from the figures, when γ is small the self-consistency function intersects the straight line, $\overline{\psi}$, only once. Above a critical point, γ_c, the curve bends enough to intersect the straight line three times, and then continues to bend (and splits around the non-existence region) such that the lower part bends above the straight line and there is only one intersection at higher $\overline{\psi}$. As the parameter $\bar{R}$ is increased for *fixed* γ, the effect is to lower the curve of the self-consistency function (that is vertically translate $g\left(\overline{\psi}\right)$ by differing amounts), thus changing the intersects with the straight line, so that if the curve is bent enough then over some interval in $\bar{R}$ there will be multiple intersections. More specifically, if the gradient of the function is greater than unity somewhere then it must be possible to vertically translate the curve $g\left(\overline{\psi}\right)$ such that there are multiple intersections around this point; otherwise, for $g'\left(\overline{\psi}\right) < 1 \; \forall \, \overline{\psi}$, there can only be one intersection. Therefore, the critical point, γ_c, is the smallest γ for which the gradient is unity at least somewhere.

Although the self-consistency function can be written explicitly in terms of $\overline{\psi}$, as per equation (3.60), it is somewhat unwieldy; so a simpler and quicker approach is to evaluate the function $F\left(\overline{\psi}\right)$ point-wise by numerically solving the differential equation in (3.53) subject to the boundary condition $\overline{\psi}$, and then numerically integrate the result. The differential equation in (3.53) is a first order one dimensional ODE, solutions of which exist and are finite and continuous- as long as the parameters $(\gamma, \overline{\psi})$ are not in the non-existence region of parameter space, the boundaries for which are precisely known in advance- and so can be straight-forwardly solved and the solution also integrated using standard numerical methods[2]. To find the intersections of the self-consistency function with the straight line, $\overline{\psi}$, i.e. to find those $\overline{\psi}$ that satisfy the self-consistency condition for a given pair of parameters $\bar{R}$ and γ, one can employ a standard root finding algorithm such as the Newton-Raphson method[3]. The results are displayed in figure (3.7).

As can be seen there is a cusp bifurcation in the existence of stationary distributions: For low $\bar{R}$ there is only one possible $\overline{\psi}$ for any given γ, and $\overline{\psi}$ monotonically increases with γ; above a critical $\bar{R}$ hysteresis occurs, that is for γ small enough or large enough only one possible value of $\overline{\psi}$ exists, which monotonically increases with γ. However, between two critical values of γ three values of $\overline{\psi}$ are possible. We anticipate that the lower and upper branches are stable and the intermediate branch unstable, but we have not proven this. Recall that when $\bar{R} < 1$ so many particles are confined

[2]Using, for example, Mathematica's in-built algorithms for ODE analysis, and numerical integration

[3]Or a variation on this, such as the secant method or false position method.

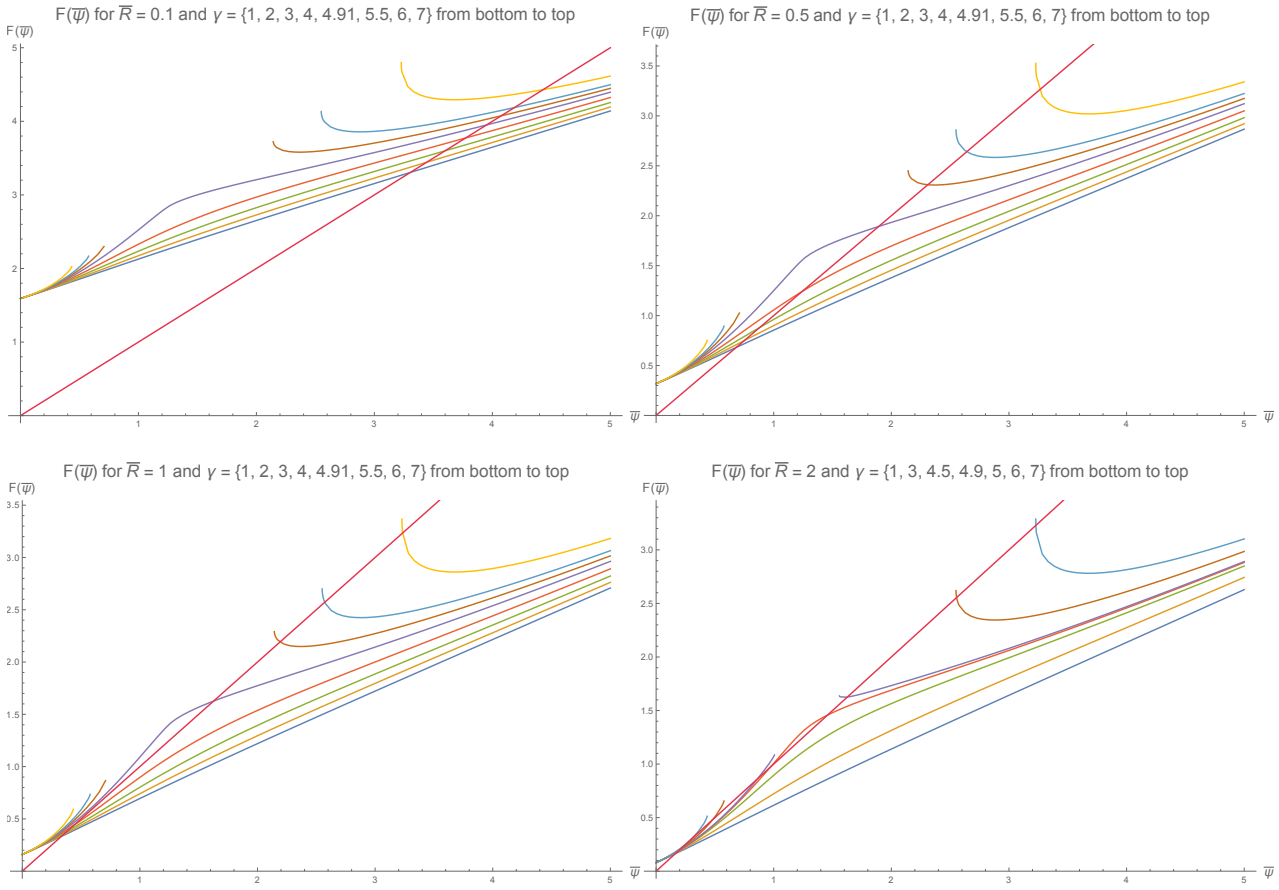

Figure 3.5: The self-consistency function, $F\left(\overline{\psi}\right)$ in equation (3.60) is shown. Each image corresponds to a particular $\bar{R}$, and each curve within an image corresponds to a particular γ. When $\gamma > \dfrac{4}{1-\left(1+\dfrac{1}{W_{-1}\left(-\frac{1}{2}\exp\left(-\frac{1}{2}\right)\right)^1}\right)^2} \approx 4.91081$ there is a zone where the function does not exist. The intersections of these curves with the straight line correspond to solutions of the self-consistency condition.

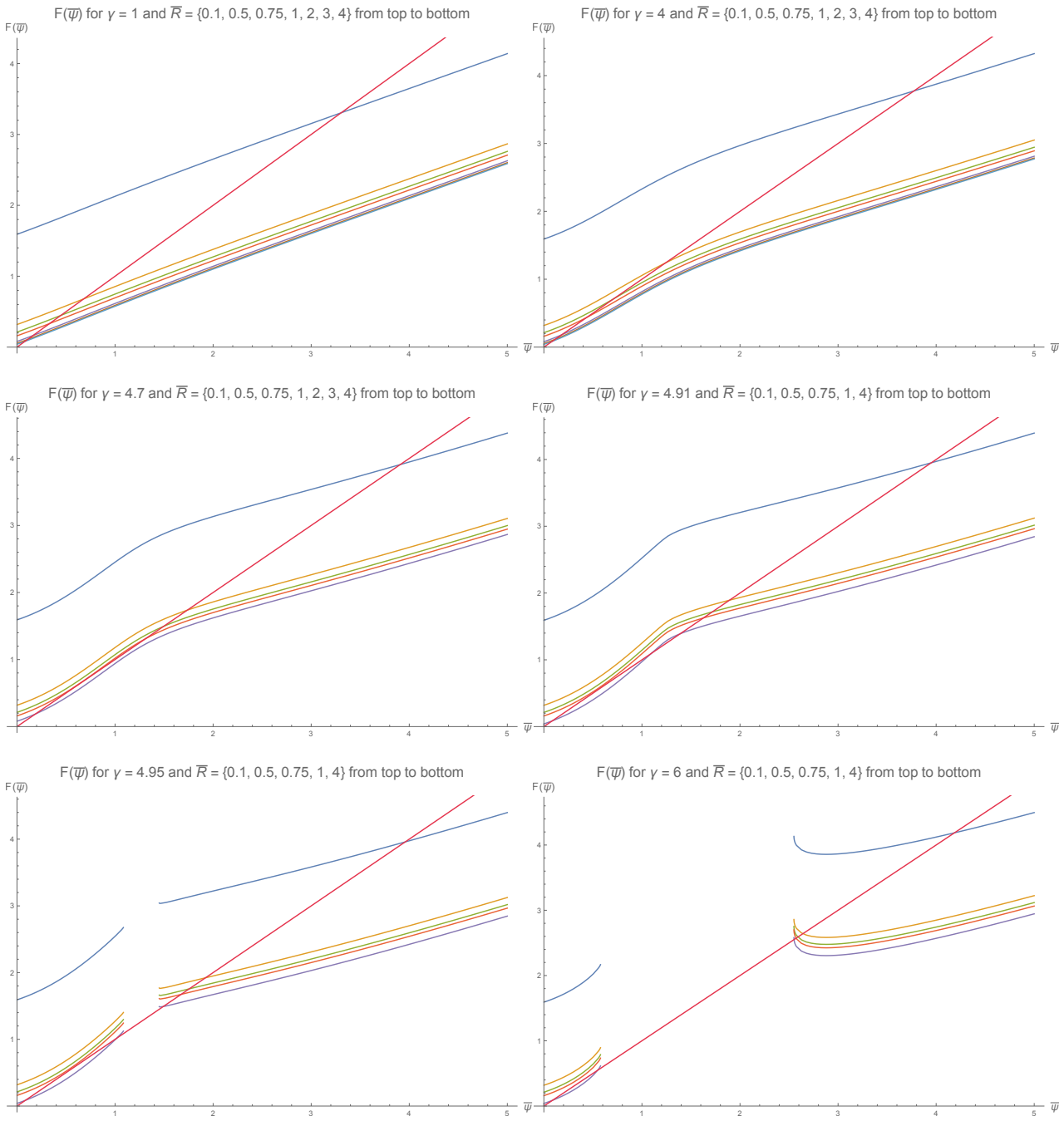

Figure 3.6: The self-consistency function, $F\left(\overline{\psi}\right)$ in equation (3.60) is shown. Each image corresponds to a particular γ and each curve within an image corresponds to a particular $\bar{R}$. Within an image, each curve is the same function, $g\left(\overline{\psi}\right) = \int_0^{\overline{\psi}} \frac{\psi \exp\left[-\int_{\psi}^{\overline{\psi}} \frac{d\psi'}{\psi' - 2\gamma e^{-\overline{\psi}} \sinh^2 \frac{\psi'}{2}}\right]}{\psi - 2\gamma e^{-\overline{\psi}} \sinh^2 \frac{\psi}{2}} d\psi$, translated vertically by $\frac{1}{2\pi\bar{R}}$. The intersections of the curves with the straight line correspond to solutions to the self-consistency condition.

in a small enough radius that the system is always opaque no matter how diffuse, whereas when $\bar{R} > 1$ the particles could be widely dispersed so that the distribution is transparent, or they could be localised near the centre so that they form an opaque distribution. Recall also that $\overline{\psi}$ measures the number of particles on average intercepting a line of sight from the centre to the edge so that $\overline{\psi} \geq 1 \Rightarrow$ the system is opaque, $\overline{\psi} \leq 1 \Rightarrow$ the system is transparent, and $\overline{\psi} \sim 1 \Rightarrow$ the system is marginally opaque. On the hysteresis curves, shown in figure (3.7), the lower branch has small $\overline{\psi}$ over a broad range of $\gamma \in [0, \gamma_{max}]$; all these curves intercept the y-axis at $\frac{1}{\pi \bar{R}}$, corresponding to a uniform density, and the lower branches of the hysteresis stay close to this value up until their second bifurcation point at the maximum $\gamma = \gamma_{max}$ of the lower branch. The upper branches, which exist on the range $\gamma \in [\gamma_{min}, \infty)$, all have $\overline{\psi} > 1$ which increases as γ increases (approximately linearly, $\overline{\psi} \sim \frac{1}{2}\gamma$, in the limit of large γ). The intermediate branches of the hysteresis curves exist between $\gamma \in [\gamma_{min}, \gamma_{max}]$, and correspond to intermediate magnitudes of $\overline{\psi} \lesssim 1$. So, the lower branches of the hysteresis curves are transparent, the upper branches opaque, and the intermediate branches marginally opaque. Observe, also, that the cusp bifurcation occurs when $\bar{R} \sim 1$ and $\overline{\psi} \sim 1$. That is the onset of bistability of transparent and opaque states occurs when the radius of the system is large enough that the particles could be distributed so as to form transparent distributions, or they could be localised, forming opaque distributions. At system radii lower than this this bistability cannot occur. Also, *all* of the upper branches begin, at their lower bound, with $\overline{\psi} \sim 1$. This means that in the hysteresis cycle, as the parameter γ is tuned downwards the upper branches cease to exist at marginal opacity.

Discussion of Hysteresis Phenomenon

The dimensionless parameter, $\gamma = \frac{D_T P}{\pi c \rho_f \kappa D}$, is determined by several physical parameters, but the most easily controlled is the total radiation power, P, so it is convenient to interpret γ as a dimensionless power. Therefore, γ determines the total energy absorption rate that is available to the system, but the fraction of that energy that is actually absorbed is determined by the opacity of the distribution which can vary depending on whether the particles are spread out or condensed near the origin. In particular, the (dimensionless) rate of energy absorption is $\gamma_{abs} = \left(1 - e^{-2\overline{\psi}}\right)\gamma$, which must balance the energy lost by the system to the heat bath at the boundary. In a stationary state the distribution of particles is determined by the balance between diffusion, which tends to spread the particles out, and thermophoresis, which tends to condense the particles in the hottest region, i.e. near the centre. The

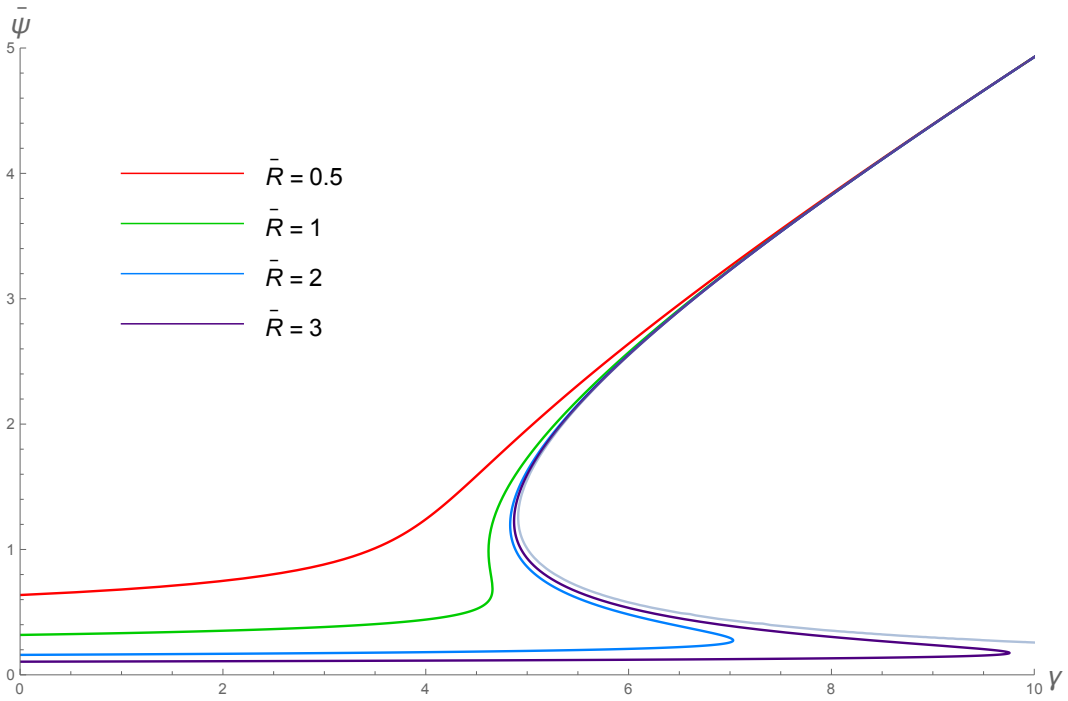

Figure 3.7: The solutions to the self-consistency condition in equation (3.53). Each curve corresponds to a particular dimensionless system size $\bar{R}$, and indicates for each γ which value(s) of $\overline{\psi}$ correspond to functions $\psi(\bar{r})$ which solve the first equation in (3.53) and whose derivative, $\bar{\rho} = \frac{d\psi}{d\bar{r}}$, is a normalised function. These curves intercept the $\overline{\psi}$ axis at $\overline{\psi}|_{\gamma=0} = \frac{1}{\pi \bar{R}}$ corresponding to a uniform distribution. The limit of these curves as $\bar{R} \to \infty$ is the curve $\gamma = \frac{2\bar{\psi}}{\left(1-e^{-\bar{\psi}}\right)^2}$ which is the boundary of the existence zone. For $\bar{R} < 1$, corresponding to systems which are always opaque, the curves are monotonically increasing, approaching the asymptotic curve as $\gamma \to \infty$. For $\bar{R} > 1$, corresponding to systems which could either be transparent or opaque, the curves have a fold. Observe that the lower critical γ, where the localised states of the upper branch cease to exist, occurs where $\bar{\psi} \sim 1$ corresponding to marginal opacity. The cusp bifurcation point is the triple of parameters: $\bar{R}_c = 0.94455$, $\gamma_c = 4.5702$, and $\overline{\psi}_c = 0.8484$.

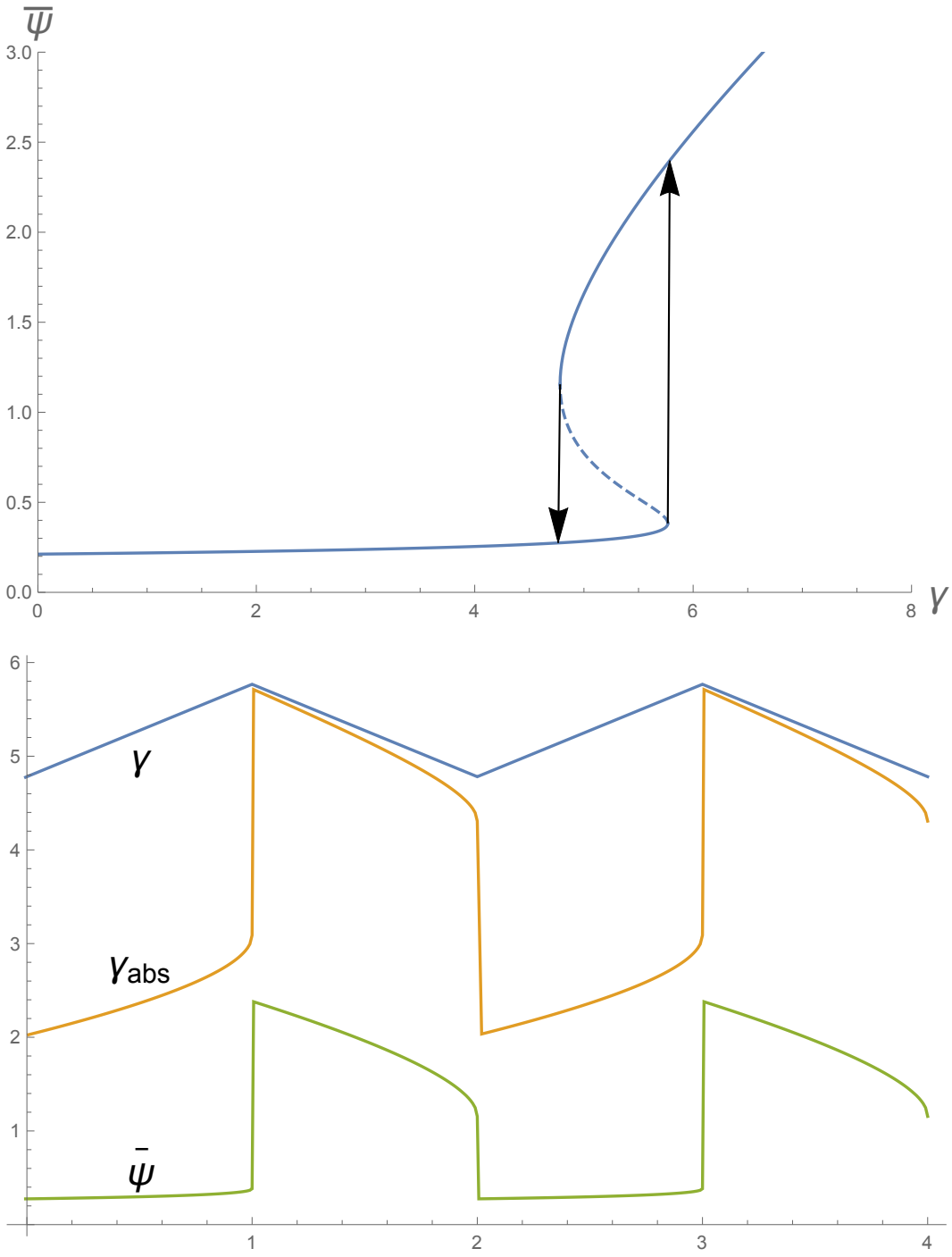

Figure 3.8: Illustration of the hysteresis phenomenon. The top image shows the solutions to the self-consistency condition for $\overline{R} = 1.5$. As γ is tuned beyond the critical points the system transitions from one phase to the other. The lower image is an illustration of this: the $x-$axis is time-like but it is assumed that the system is in a stationary state at all times; as γ (the top line) is tuned up the rate of energy absorption, γ_{abs} (the middle line), increases, though $\overline{\psi}$ does not change appreciably until close to the critical point.

strength of the thermophoresis effect determines how condensed the colloid distribution is and is itself determined by the magnitude of the temperature gradient, which is caused by the flow of heat energy conducting through the fluid; the overall flow of energy through the system is determined by γ_{abs}, which is determined by the available power (i.e. γ) and opacity of the system (i.e. determined by $\bar{\psi}$) which is larger when the system is more condensed. If the system is *not* in a stationary state then either: i) the system has a high energy absorption rate despite having a relatively diffuse distribution, in which case thermophoresis will dominate and the particles will condense towards the origin until balance with diffusion is attained, or ii) the system has a low energy absorption rate despite having a relatively dense distribution, in which case diffusion will dominate and the particles will spread out.

In a stationary state the diffusion - thermophoresis balance is determined by energy flow. The possible states are limited by the maximum available energy flow (γ, a non-dynamic parameter), and the limits on opacity ($\bar{\psi}$ which is dynamically variable), i.e. the system can never be perfectly transparent. The hysteresis phenomenon is determined as follows: i) if the maximum available energy flow (and therefore temperature gradient) is too small to overcome diffusion so as to create a significantly localised distribution, then thermophoresis is too weak and the only stationary distribution possible is diffuse; ii) the system has a minimum possible absorption of available energy corresponding to the most transparent state (that of a uniform distribution), so if the available energy flow is large enough then even the least absorption of this is enough to overcome diffusion from the diffuse state, so diffuse states cannot be stationary and the only stationary distributions are localised (and therefore opaque); iii) for γ too small the system cannot absorb enough energy to overcome diffusion, and when γ is too large the system cannot avoid absorbing enough of it to condense, so there must be an intermediate range of γ within which there are multiple possibilities: a diffuse distribution which is transparent and so absorbs only a small fraction of available energy, so little that it remains diffuse and transparent; or a localised distribution which is opaque enough to absorb a large enough fraction of the available energy to establish steep enough temperature gradients to maintain the localised distribution. This explains the hysteresis. The cusp bifurcation exists because there is no dependence of the energy absorption rate on the form of the distribution whenever the system is always opaque no matter how diffuse. i.e. if a large enough number of particles are placed in a small enough disk (corresponding to low $\bar{R}$) then even a uniform distribution is opaque, in which case almost all the radiation will be absorbed by the system, so as the laser power is increased, the system will transition continuously from diffuse to localised. The

hysteresis phenomenon is illustrated in figure (3.8). If the dimensionless radiation power, γ, is tuned up while the system is in the transparent state ($\overline{\psi} < 1$) the distribution of particles is not significantly affected and so the system remains transparent with little change to $\overline{\psi}$, but the dimensionless absorption rate, γ_{abs}, does increase. This is because a system with (almost) unchanging $\overline{\psi}$ will continue to absorb the same *proportion* of available energy, so as the available power increases so does the absorbed power. At the critical point, the absorption rate is high enough to overcome diffusion from the diffuse state: as the system becomes more compacted it becomes more opaque, increasing the proportion of available energy that is absorbed,thus, via this positive feedback, the system collapses to the localised, opaque state where $\overline{\psi} > 1$. In this state almost all the available energy is absorbed, as shown in the figure. Tuning γ back down again does not change the fact that the system is absorbing almost all available energy, so the energy absorption rate remains close to γ, though it decreases as the available energy decreases. As γ_{abs} decreases the system gradually spreads out becoming incrementally less opaque until $\overline{\psi}$ approaches ~ 1 at which point the system is marginally opaque, thus absorbing a significantly smaller proportion of available energy. This results in the distribution spreading out and thus becoming more transparent with an even smaller energy absorption rate. Via this positive feedback the system disperses to the diffuse, transparent state with $\overline{\psi} < 1$. This can be seen in figure (3.8). Illustrations of typical realisations of the system are shown in figures (3.10),(3.11), and (3.12), where the opacity and transparency can be seen.

3.3.3 Tail Asymptotics and the Existence of a Localised Swarm

In this section the localised, opaque distributions shall be analysed in the far field. This shall be approached with two methods: the first is a more "physics" based approach and the second is more mathematical, so to speak (though of course, both methods are in fact mathematical physics). The first method is a self-consistency argument that assumes the existence of a localised distribution close to the origin containing most of the particles where most of the heating is taking place, and then analyses the variation of density in the far field, hence the asymptotics of the density field. For the argument to be self-consistent this density variation in the far field must contain only a small fraction of the particles in the system, and must generate a temperature profile that is dominated by that due to the central swarm. At first this argument is followed with a simplifying assumption concerning the heating due to the far field density, which leads to a neat argument that places constraints

on the possible existence of a localised distribution, which provides insight into the first bifurcation point in the hysteresis phenomenon. This argument is then developed in a slightly more complicated way that does not make the unreasonable assumption concerning heating due to the far field density. The analysis is a little more complicated, though the conclusion is the same. The second method follows from the exact mathematical theory developed above: the RHS of equation (3.53) is Taylor expanded about $\overline{\psi}$ and then solved finding a power law in the asymptotic density in accordance with the first method.

A Physical Approach to Density Asymptotics

Consider a distribution of thermophoretic colloids that is localised in the sense that most of the particles are in a swarm confined to a small region near the origin with few in a cloud in the rest of the system. We shall analyse the asymptotics of the tails of this distribution (i.e. the density variation of the cloud) and analyse the existence of this localised swarm by a self-consistency argument. To begin with, assume that the particles in the far field make negligible contribution to the heating and are therefore enslaved by the temperature field due to the heating from the localised swarm, and then find the variation of the cloud density in this case. Then, given this variation of the cloud density, compute the number of particles in the cloud and the cloud's contribution to the temperature field, so that if this is of lower order than that due to the swarm, and if the number of particles in the cloud can be small, then the assumption that the swarm exists and enslaves a cloud is consistent with its implications, and the argument is thus self-consistent.

First assume that the total heating rate for $r < r_s$ is P_s with no heating outside this region. Then at radii greater than r_s the temperature satisfies Laplace's equation, $\nabla^2 T = 0$, which means $\frac{dT}{dr} = -\frac{\alpha}{r}$ (note these are physical variables, not dimensionless variables). The heat flux is proportional to the temperature gradient, $\vec{q} = -k\frac{dT}{dr} = -c\,\rho_f\,\kappa\frac{dT}{dr}$. The heat flux at r_s will therefore be $\frac{P_s}{2\pi r_s}$, thus $-c\rho_f\kappa\frac{dT}{dr}\big|_{r_s} = \frac{P_s}{2\pi r_s}$,

$$\Rightarrow \frac{dT}{dr}\Big|_{r_s} = -\frac{P_s}{2\pi c\rho_f\kappa r_s} = -\frac{\alpha}{r_s} \tag{3.61}$$

$$\Rightarrow \alpha = \frac{P_s}{2\pi c\rho_f\kappa} \tag{3.62}$$

$$\therefore \frac{dT}{dr} = -\frac{P_s}{2\pi c\rho_f\kappa}\frac{1}{r}\ \forall r > r_s \tag{3.63}$$

Which corresponds to a logarithmic temperature field, $T(r) = -\frac{P_s}{2\pi c\rho_f \kappa} \ln \frac{r}{R}$. We have merely described the variation of temperature in the far field due to a heat source near the origin. Next we analyse the distribution of thermophoretic particles in the far field induced by the sources near the origin. The balance of thermophoresis with diffusion requires $\frac{d\rho}{dr} = \frac{D_T}{D}\rho\frac{dT}{dr}$, and so

$$\frac{d\rho}{dr} = -\frac{D_T P_s}{2\pi c\rho_f \kappa D}\frac{\rho}{r} \tag{3.64}$$

By analogy with the definition of the parameter γ, define $\gamma_s = \frac{D_T P_s}{\pi c\rho_f \kappa D}$, then

$$\frac{d}{dr}\ln\rho = -\frac{\gamma_s}{2}\frac{1}{r} \tag{3.65}$$

$$\Rightarrow \rho = B\, r^{-\frac{\gamma_s}{2}} \tag{3.66}$$

for some constant of integration, B (if there are few particles in the cloud then B is small).

Second, the self-consistency check shows two things: i) there can be negligibly few particles in the cloud, ii) the dominant contribution to the far field temperature is from the central swarm and not the cloud. The material in the cloud is computed from the integral

$$\int_{r_s}^{R} \rho r dr \sim \frac{1}{2\left(\frac{\gamma_s}{4}-1\right)}\left(r_s^{-2\left(\frac{\gamma_s}{4}-1\right)} - R^{-2\left(\frac{\gamma_s}{4}-1\right)}\right) \tag{3.67}$$

For this to be small the power needs to be negative so that the power law is decaying and there can be few particles in the cloud even for large system radius. Therefore the fraction of the distribution in the cloud is small only if $\gamma_s > 4$.

Consider now the temperature contribution from the heating of the cloud: let the temperature outside of the localised swarm ($r > r_s$) be $T(r) = T_s(r) + \delta T(r)$, where $T_s(r)$ is the temperature due to the centralised swarm and $\delta T(r)$ is the correction from the cloud. The temperature from the central swarm is the logarithmic function $-\frac{\gamma_s}{2}\ln r + const.$ In general, solutions to the Poisson equation, $\nabla^2\Phi(r) = -\phi(r)$, where the source term, $\phi(r)$, is cylindrically symmetrically distributed about an interior region, are such that the interior sources contribute a logarithmically decaying field to the exterior region, and the exterior region contributes a constant term to the interior region, and this is true for any choice of radius that defines the interior region. In the case of localised swarm and dispersed cloud, the overall heating from the cloud makes no difference to the variation of temperature in the central

swarm (below the radius r_s) except to add a constant; but since thermophoresis is a response to temperature *gradients* this makes no difference to the central swarm. The central swarm affects the cloud with a logarithmic temperature field, and the interior parts of the cloud affect the exterior parts according to Poisson's equation, $\nabla^2 \delta T = -\eta\rho$, (where the coefficient η accounts for thermal properties and also the heating rate per particle) i.e.

$$\frac{1}{r}\frac{d}{dr}\left(r\frac{d\delta T}{dr}\right) = -\eta B r^{-\frac{\gamma_s}{2}} \Rightarrow \frac{d}{dr}\left(r\frac{d\delta T}{dr}\right) = -\eta B r^{1-\frac{\gamma_s}{2}} \tag{3.68}$$

$$\Rightarrow r\frac{d\delta T}{dr} = C - \frac{\eta B}{2-\frac{\gamma_s}{2}} r^{2-\frac{\gamma_s}{2}} \Rightarrow \frac{d\delta T}{dr} = \frac{C}{r} - \frac{\eta B}{2-\frac{\gamma_s}{2}} r^{1-\frac{\gamma_s}{2}} \tag{3.69}$$

$$\therefore \delta T\left(r\right) = C\ln r - \frac{\eta B}{\left(2-\frac{\gamma_s}{2}\right)^2} r^{-2\left(\frac{\gamma_s}{4}-1\right)} \tag{3.70}$$

As a first approximation, suppose the constant of integration, C, is zero. Then the correction to the temperature field from the cloud is $\delta T\left(r\right) = -\frac{\eta B}{\left(2-\frac{\gamma_s}{2}\right)^2} r^{-2\left(\frac{\gamma_s}{4}-1\right)}$ which decays faster than the logarithmic variation from the central swarm, hence there must be a radius large enough that only the temperature from the swarm matters, and in this case the cloud can be enslaved to the central swarm. This is only possible if $\gamma_s > 4$.

Therefore, if there is a central, localised swarm surrounded by a diffuse cloud, where most of the particles are in the swarm and the (dimensionless) heating rate of the central swarm is γ_s, then the cloud can be entrained by the temperature field generated by the swarm only when $\gamma_s > 4$, and in this case the density profile of the cloud is (i.e. the far field tails of the colloid distribution are asymptotically) a power law with a power that depends on the heating rate in the swarm, $\rho\left(r\right) \sim r^{-\frac{\gamma_s}{2}}$.

In general, the total (dimensionless) absorption/heating rate of the system is $\gamma_{abs} = \left(1-e^{-2\overline{\psi}}\right)\gamma$. If we assume that all of this is absorbed in the localised swarm, then $\gamma_s = \left(1-e^{-2\overline{\psi}}\right)\gamma$. Consider the critical case of $\gamma_s = 4$: at the critical point where the opaque swarm ceases to exist one expects the swarm to be marginally opaque with $\overline{\psi} \sim 1$, rearranging one obtains $\gamma = \frac{4}{1-e^{-2}} \approx 4.63$. This is a good estimate of the lower bifurcation on the hysteresis curve for the onset of the localised, opaque state: the cusp bifurcation occurs at $\gamma_c = 4.57$ and all the lower bifurcation points occur between $\gamma \in [4.57, 4.91]$.

If the constant of integration in equation (3.70) is non-zero, that is if the temperature due to the cloud is $\delta T\left(r\right) = C\ln r - \frac{\eta B}{\left(2-\frac{\gamma_s}{2}\right)^2} r^{-2\left(\frac{\gamma_s}{4}-1\right)}$ with $C \neq 0$, then the heating

from the cloud is not negligible, and in this case the temperature field is

$$T(r) = \left(C - \frac{\gamma_s}{2}\right) \ln r - \frac{\eta B}{\left(2 - \frac{\gamma_s}{2}\right)^2} r^{-2\left(\frac{\gamma_s}{4} - 1\right)} \tag{3.71}$$

The second term is small compared to the first term for sufficiently large radius, and so the effect of the heating from the cloud is to modify the coefficient of the logarithm. This temperature field was derived by assuming that only the heating from the central swarm determines the density distribution of the cloud (hence the power in the density distribution is determined by γ_s), however this leads to the conclusion that not only the central swarm, but also the cloud determines the far field temperature and therefore the cloud distribution. To make this argument self-consistent, let the temperature be the logarithm $T(r) = -\frac{\alpha}{2} \ln r$, with unkown coefficient α. Then the density distribution entrained by this is, $\rho(r) = Be^{T(r)} = Br^{-\frac{\alpha}{2}}$. The contribution to temperature from this distribution is $\delta T(r) = C' \ln r - \frac{\eta B}{4\left(\frac{\alpha}{4} - 1\right)^2} r^{-2\left(\frac{\alpha}{4} - 1\right)}$, so the total temperature field is

$$T(r) = -\frac{1}{2}\left(\gamma_s - 2C'\right) \ln r - \frac{\eta B}{4\left(\frac{\alpha}{4} - 1\right)^2} r^{-2\left(\frac{\alpha}{4} - 1\right)} \tag{3.72}$$

For this to be self-consistent the coefficient of the logarithm must be the same coefficient that was assumed, that is $\alpha = \gamma_s - 2C'$. If the constant of integration, C', is non-zero then the cloud *does* have an effect on itself and is not entirely enslaved to the central swarm. Although the effect it has is to change the exponent in the power law, not to change the fact that the dominant form of the temperature field is logarithmic, causing a power law in density. It remains to be proven that the contribution that the cloud makes to the far field temperature is small compared to the temperature due to the central swarm.

As an intermediate integration in the analysis of the temperature contribution from the cloud, the equation

$$r\frac{d\delta T}{dr} = C - \frac{\eta B}{2 - \frac{\alpha}{2}} r^{2 - \frac{\alpha}{2}} = C + \frac{\eta B}{2\left(\frac{\alpha}{4} - 1\right)} r^{-2\left(\frac{\alpha}{4} - 1\right)} \tag{3.73}$$

was considered. Notice that the coefficient of the power law term must be positive if $\alpha > 4$, but the temperature must be a decreasing function of radius, so the constant of integration must be non-zero. The power law term is most positive at the smallest radius where the cloud exists, that is at the radius of the swarm, r_s, so to ensure

the temperature from the cloud is a decreasing function of r, the constant must be

$$C \leq -\frac{\eta B}{2\left(\frac{\alpha}{4}-1\right)} r_s^{-2\left(\frac{\alpha}{4}-1\right)} \tag{3.74}$$

Moreover, the heat flux from the cloud at r_s should be zero since the cloud does not heat for $r < r_s$, so $C = -\frac{\eta B}{2\left(\frac{\alpha}{4}-1\right)} r_s^{-2\left(\frac{\alpha}{4}-1\right)}$. In this case the temperature field is

$$T(r) = -\frac{1}{2}\left(\gamma_s + \frac{\eta B}{\frac{\alpha}{4}-1} r_s^{-2\left(\frac{\alpha}{4}-1\right)}\right) \ln r + \frac{\eta B}{4\left(\frac{\alpha}{4}-1\right)^2} r^{-2\left(\frac{\alpha}{4}-1\right)} \tag{3.75}$$

and the self-consistency condition on the exponent is $\alpha = \gamma_s + \frac{\eta B}{\frac{\alpha}{4}-1} r_s^{-2\left(\frac{\alpha}{4}-1\right)}$ which can be re-written $y\left(y - 2\left(\frac{\gamma_s}{4}-1\right)\right) r_s^y = \eta B$ for $y = 2\left(\frac{\alpha}{4}-1\right)$. Localised distributions exist only when solutions to this transcendental equation exist for $y > 0$, which requires $\gamma_s > 4$ (reconfirming the above analysis on the existence of the localised state). Since the cloud contains few particles, the constant B must be small, so the solutions to the transcendental equation will occur slightly above the axis intercept, $y \gtrsim 2\left(\frac{\gamma_s}{4}-1\right) \Rightarrow \alpha \gtrsim \gamma_s$. In particular, a linear expansion around this point gives $y \approx 2\left(\frac{\gamma_s}{4} - 1 + \frac{\eta B}{2\left(\frac{\gamma_s}{4}-1\right)} r_s^{-2\left(\frac{\gamma_s}{4}-1\right)}\right)$ which means

$$\alpha \approx \gamma_s + \frac{\eta B}{\left(\frac{\gamma_s}{4}-1\right)} r_s^{-2\left(\frac{\gamma_s}{4}-1\right)} \tag{3.76}$$

Consider the coefficient of the logarithm in the temperature in equation (3.75): it contains a contribution from the localised swarm, γ_s, and a contribution from the cloud which is the remainder, and is stated in that equation in terms of the exponent α. Using the relationship between α and γ_s in equation (3.76) and substituting this into the coefficient of the logarithm in equation (3.75), the contribution to heating from the cloud is,

$$\frac{\eta B}{\frac{\alpha}{4}-1} r_s^{-2\left(\frac{\alpha}{4}-1\right)} = \frac{\eta B\left(\gamma_s - 4\right)}{4\left(\frac{\gamma_s}{4}-1\right)^2 + r_s^{-2\left(\frac{\gamma_s}{4}-1\right)}} r_s^{-2\left[\frac{\gamma_s}{4}-1+\frac{\eta B}{\gamma_s-4} r_s^{-2\left(\frac{\gamma_s}{4}-1\right)}\right]} \tag{3.77}$$

If the dimensionless swarm radius is greater than unity, $r_s > 1$ (only possible if $\bar{R} > 1$), then the cloud temperature contribution is always smaller than that from the core, i.e. $\frac{\eta B}{\frac{\alpha}{4}-1} r_s^{-2\left(\frac{\alpha}{4}-1\right)} < \gamma_s$, and so the heating from the core dominates. If $r_s < 1$ then the exponent, $r_s^{-2\left(\frac{\gamma_s}{4}-1\right)} = e^{-2\left(\frac{\gamma_s}{4}-1\right)\ln r_s} = e^{2\left(\frac{\gamma_s}{4}-1\right)\ln\frac{1}{r_s}}$, is growing in γ_s and eventually dominates, for γ_s large enough, so the heating from the cloud may

be the dominant contribution to temperature in the far field. However, this can be mitigated if the fraction of the particles in the cloud (controlled by the parameter B) decreases exponentially.

This more precise analysis does not refine the estimate on the critical γ_c that determines the onset of the localised states. The conclusion of this asymptotic analysis is that the system can be structured as a localised, central swarm consisting of the majority of the particles surrounded by a diffuse cloud of colloids only when the energy absorption rate of the system (central swarm plus cloud) is large enough, which corresponds to the radiation power being large enough ($\gamma_c \sim 4.63$). In this state the density of the cloud varies as a power law with an exponent that depends on the rate of energy absorption of the system, and the onset of the localised state corresponds to this exponent being large enough that the number of particles in the cloud does not diverge as system radius grows. The majority of this energy is absorbed in the central swarm, thus determining the behaviour of the cloud, however the cloud is not entirely enslaved to the swarm as the heating from the cloud does modify the exponent in the power law somewhat, although it remains the case that the dominant contribution comes from the swarm.

A Mathematical Approach to Density Asymptotics

Moreover, a similar analysis can be performed by asymptotic analysis of equation (3.53) directly. Considering the equation $r\frac{d\psi}{dr} = F(\psi)$, with $F(\psi) = \psi - 2\gamma e^{-\overline{\psi}} \sinh^2 \frac{\psi}{2}$. If $\gamma e^{-\overline{\psi}}$ is large then the hyperbolic function dominates the linear function immediately, which means the function dips down whilst ψ is small $\implies \sinh^2 \frac{\psi}{2} \approx \frac{1}{4}\psi^2$ so F is roughly quadratic. If $\gamma e^{-\overline{\psi}}$ is small then the hyperbolic function is suppressed and the linear function dominates until ψ is large enough that the hyperbolic function can dominate at which point there is a very rapid drop off. This region where $F'(\psi) \ll 0$ could reasonably be approximated by a straight line over a narrow interval in ψ. Taylor expand the function F at $\overline{\psi}$, then $F(\psi) = \alpha + \omega\psi$ with $\alpha = F\left(\overline{\psi}\right) - \overline{\psi}F'\left(\overline{\psi}\right) = \left(\frac{1}{2}\left(1+\overline{\psi}\right)\left(1-e^{-2\overline{\psi}}\right) - \left(1-e^{-\overline{\psi}}\right)\right)\gamma$, and $\omega = F'\left(\overline{\psi}\right) = 1 - \frac{1}{2}\left(1-e^{-2\overline{\psi}}\right)\gamma = 1 - \frac{1}{2}\gamma_{abs}$. For ψ in the vicinity of $\overline{\psi}$ (and for a transparent cloud all of the region $r \in \left[r_s, \bar{R}\right]$ corresponds to $\psi \lesssim \overline{\psi}$)

$$r\frac{d\psi}{dr} = \alpha + \omega\psi \tag{3.78}$$

$$\Rightarrow \psi = \frac{1}{\omega}\left(\left(\frac{r}{k}\right)^{\omega} - \alpha\right) \tag{3.79}$$

for some constant of integration, k. From $\frac{d\psi}{dr} = \rho$, the density is

$$\rho(r) = \left(\frac{r}{k}\right)^{\omega-1} = \left(\frac{r}{k}\right)^{-\frac{1}{2}\gamma_{abs}} \tag{3.80}$$

This result matches that of equation (3.66) with the equality of γ_s with the dimensionless absorption rate $\gamma_{abs} = \left(1 - e^{-2\overline{\psi}}\right)\gamma$. This asymptotic analysis is *always* valid precisely on the boundary, that is in the limit $\psi \to \overline{\psi}$, i.e. for $r_s \to \bar{R}$. The equality of the system absorption rate and the swarm absorption rate is because it really is true that all the energy being absorbed below the radius considered is all the energy absorbed by the system when the radius considered is the system radius, i.e. when $r_s \to \bar{R}$, that is when $\psi \to \overline{\psi}$ the Taylor expansion is exact. The localised distributions exist when this analysis is also valid far from the boundary, which occurs when a large interval in radius corresponds to a small change in ψ. In the bulk of the cloud (i.e. not precisely on the boundary) an improved estimate of the far field density can be obtained by including additional terms in the Taylor expansion: approximate the function as $F(\psi) \approx F\left(\overline{\psi}\right) + F'\left(\overline{\psi}\right)\left(\psi - \overline{\psi}\right) + \frac{1}{2}F''\left(\overline{\psi}\right)\left(\psi - \overline{\psi}\right)^2$, and defining $\hat{\psi} = \psi - \overline{\psi}$ then the ODE becomes

$$r\frac{d\hat{\psi}}{dr} = \alpha - \omega\hat{\psi} - \eta\hat{\psi}^2 \tag{3.81}$$

Completing the square and gathering terms this can be written

$$\int \frac{d\left(\frac{\hat{\psi}+\frac{\omega}{2\eta}}{\sqrt{\frac{\omega^2}{4\eta^2}+\frac{\alpha}{\eta}}}\right)}{1 - \left(\frac{\hat{\psi}+\frac{\omega}{2\eta}}{\sqrt{\frac{\omega^2}{4\eta^2}+\frac{\alpha}{\eta}}}\right)^2} = \eta\sqrt{\frac{\omega^2}{4\eta^2} + \frac{\alpha}{\eta}} \int \frac{dr}{r} \tag{3.82}$$

$$\Rightarrow \tanh^{-1}\left[\frac{\hat{\psi} + \frac{\omega}{2\eta}}{\sqrt{\frac{\omega^2}{4\eta^2} + \frac{\alpha}{\eta}}}\right] = \eta\sqrt{\frac{\omega^2}{4\eta^2} + \frac{\alpha}{\eta}} \ln\left(\frac{r}{k}\right) \tag{3.83}$$

$$\Rightarrow \hat{\psi} = \frac{1}{\eta}\sqrt{\frac{\omega^2}{4} + \alpha\eta}\, \tanh\left[\sqrt{\frac{\omega^2}{4} + \alpha\eta} \ln\left(\frac{r}{k}\right)\right] - \frac{\omega}{2\eta} \tag{3.84}$$

where k is a constant of integration. Differentiating this to obtain the density,

$$\rho(r) = \frac{1}{\eta}\left(\frac{\omega^2}{4} + \alpha\eta\right) \operatorname{sech}^2\left[\sqrt{\frac{\omega^2}{4} + \alpha\eta}\ln\left(\frac{r}{k}\right)\right] r^{-1} \tag{3.85}$$

$$\Rightarrow \rho(r) = \frac{1}{\eta}\left(\omega^2 + 4\alpha\eta\right) \frac{r^{-1}}{\left(\left(\frac{r}{k}\right)^{\frac{1}{2}\sqrt{\omega^2+4\alpha\eta}} + \left(\frac{r}{k}\right)^{-\frac{1}{2}\sqrt{\omega^2+4\alpha\eta}}\right)^2} \tag{3.86}$$

In the limit of large radius, the positive exponent in the denominator dominates and the density can be approximated as

$$\rho(r) = \frac{1}{\eta}\left(\omega^2 + 4\alpha\eta\right) k^{\sqrt{\omega^2+4\alpha\eta}} r^{-\left(1+\sqrt{\omega^2+4\alpha\eta}\right)} \tag{3.87}$$

which is a power law with a new exponent. With the quadratic expansion: $\alpha = F\left(\overline{\psi}\right) = \overline{\psi} - 2\gamma e^{-\overline{\psi}} \sinh^2\frac{\overline{\psi}}{2}$ which must be positive, since $\frac{d\psi}{dr} \geq 0$, and small if $\frac{d\psi}{dr}|_{\bar{R}}$ is small; $\omega = -F'\left(\overline{\psi}\right) = \gamma e^{-\overline{\psi}} \sinh\overline{\psi} - 1 > 0$ which is of the order of γ; and $\eta = -\frac{1}{2}F''\left(\overline{\psi}\right) = \frac{\gamma e^{-\overline{\psi}}}{2}\cosh\overline{\psi} > 0$, which is of the order of γ. The total energy absorption rate of the system is $\gamma_{abs} = \left(1 - e^{-2\overline{\psi}}\right)\gamma$, so the terms in the square root in the exponent are

$$\omega^2 = \left(\frac{1}{2}\gamma_{abs} - 1\right)^2 \tag{3.88}$$

$$4\alpha\eta = 2\left(\overline{\psi} - 2\gamma e^{-\overline{\psi}} \sinh^2\frac{\overline{\psi}}{2}\right)\gamma e^{-\overline{\psi}}\cosh\overline{\psi} \tag{3.89}$$

If $\alpha\eta$ is zero then this is the same exponent as in the analysis of the linear expansion, and if $\alpha\eta$ is small (and one expects α to be small) then this is a small modification to the exponent. This asymptotic analysis of the ODE, equation (3.53), reconfirms the asymptotic analysis discussed above.

3.3.4 Low ψ Approximation

We shall analyse equation (3.53) in the limit of low ψ, which corresponds to transparent distributions. For $\psi \ll 1$, $\sinh\psi \approx \psi \Rightarrow \psi - 2\gamma e^{-\overline{\psi}} \sinh^2\left[\frac{\psi}{2}\right] \approx \psi - \frac{\gamma}{2}e^{-\overline{\psi}}\psi^2$. Defining a new parameter $a^2 = \frac{\gamma}{2}e^{-\overline{\psi}}$, the ODE for ψ is

$$r\frac{d\psi}{dr} = \psi - a^2\psi^2 \tag{3.90}$$

with $\psi\left(\bar{R}\right) = \overline{\psi}$. This can be readily solved as follows

$$\int \frac{d\psi}{\psi\left(1 - a^2\psi\right)} = \int \frac{dr}{r} = \ln\left(r\right) + \ln\left(\frac{A}{a^2}\right) \tag{3.91}$$

for some constant of integration, A. Then $\frac{\psi}{1-a^2\psi} = \frac{A}{a^2}r$, which means the constant of integration satisfies $A\bar{R} = \frac{a^2\overline{\psi}}{1-a^2\overline{\psi}}$, and the approximate solution is

$$\psi\left(r\right) = \frac{\frac{A}{a^2}r}{1 + Ar} \tag{3.92}$$

This corresponds to a density of

$$\rho\left(r\right) = \frac{A}{a^2}\frac{1}{\left(1 + A\,r\right)^2} \tag{3.93}$$

With this approximation the self-consistency condition can be integrated, though not solved explicitly,

$$\overline{\psi} = \frac{1}{2\pi\overline{R}} + \frac{1}{a^2} + \frac{1 - a^2\overline{\psi}}{a^4\overline{\psi}}\ln\left(1 - a^2\overline{\psi}\right) \tag{3.94}$$

As can be seen from figure (3.9) this is a reasonable approximation when $\overline{\psi} < 0.4$.

The functional form of equation (3.92) is valid close to the origin in general, not just for $\overline{\psi} \ll 1$, but anywhere that $\psi \ll 1$. Notice that the gradient of density, the second derivative of ψ, is non-zero at the origin. This could also be shown with a Taylor expansion: taking $\psi\left(r\right) \approx \rho_0 r + \frac{1}{2}\rho_0' r^2 + cr^3$ one can show that $\rho_0' = -\gamma e^{-\overline{\psi}}\rho_0^2$. This is somewhat unnatural for a mean field theory because it means that there is a discontinuity in density gradient moving through the centre of the swarm. This is an artefact of the singularity in the heating functional at the origin.

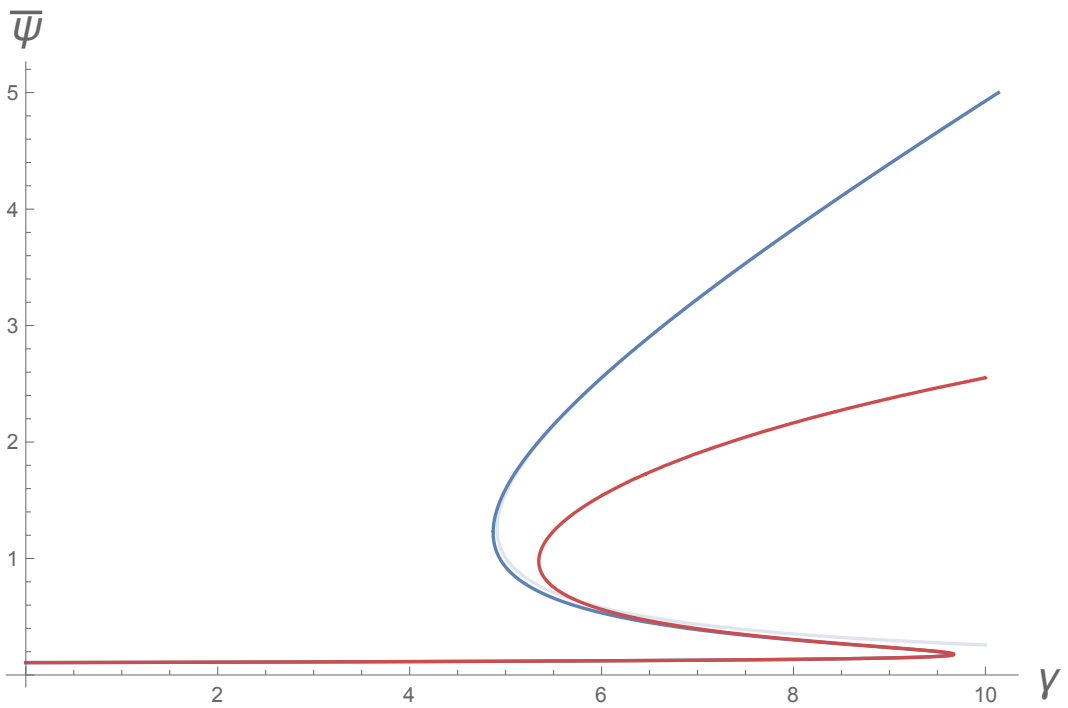

Figure 3.9: The implicit self-consistency condition from equation (3.94) is shown in red in comparison with the numerical solution in blue, for $\bar{R} = 3$.

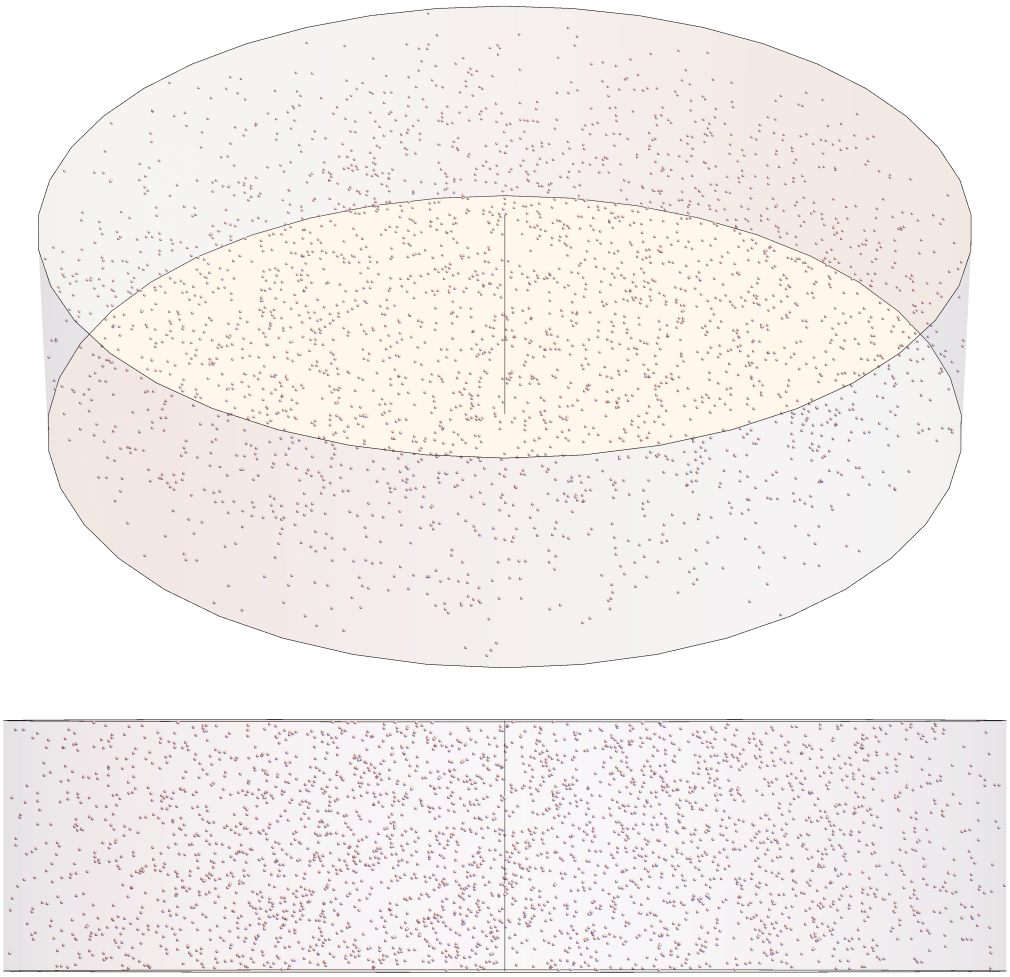

Figure 3.10: Illustration of the transparent phase with parameters: $\bar{R} = 5$, $\gamma = 6$, and $\overline{\psi} = 0.0685$. The positions of the particles have been sampled independently from a 3D density $\rho_{3D}(x, y, z) = \rho_z \rho(r)$, where $\rho(r)$ is the solution determined by $\rho = \frac{d\psi}{dr}$ in equations (3.53), and the vertical density is a constant $\rho_z = \frac{N}{\Delta z}$. The dimensionless radius is related to these 3D quantities by $\bar{R} = \frac{R}{\pi r_o^2 \rho_z}$, and the radius of the particles is determined by $r_o = \sqrt{\frac{R}{\pi \bar{R} \rho_z}}$. The lower image is the view along the horizontal direction demonstrating the transparency of the system. Notice that the distribution is diffuse, filling the available space.

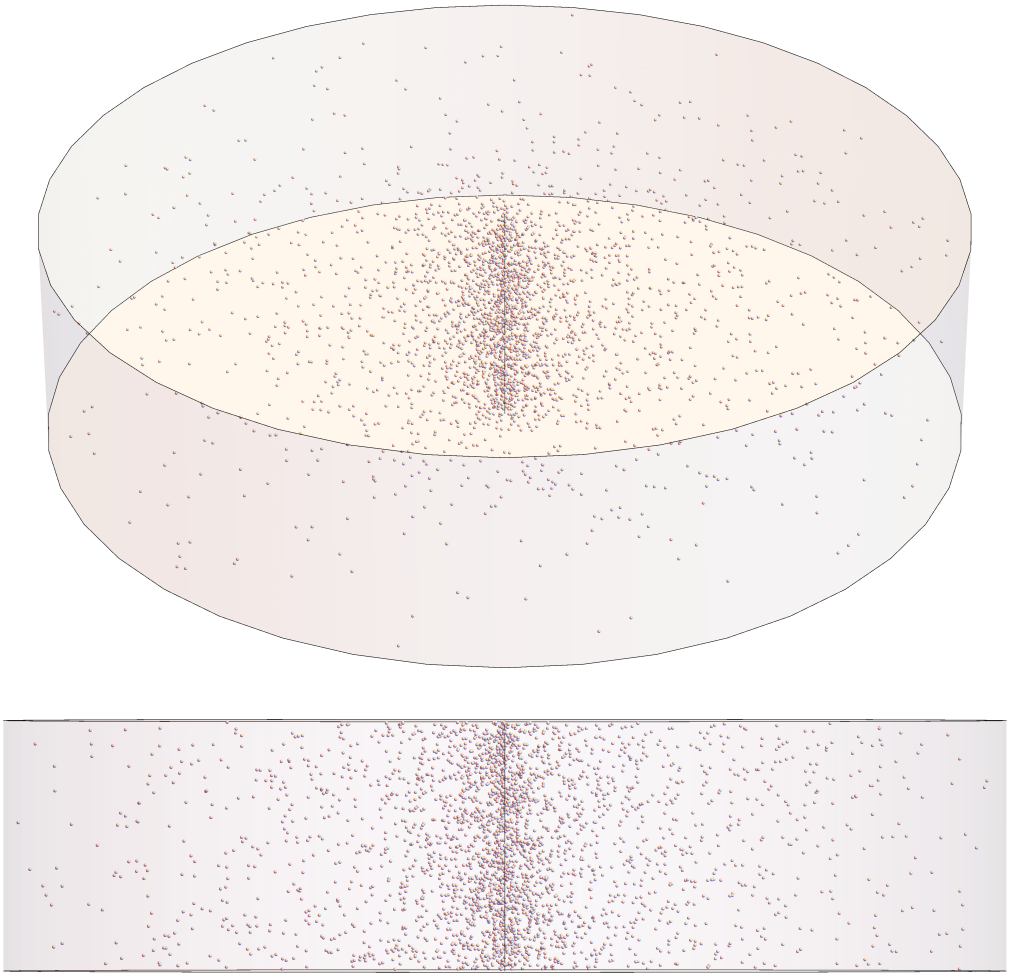

Figure 3.11: Illustration of the marginally opaque phase with parameters: $\bar{R} = 5$, $\gamma = 6$, and $\overline{\psi} = 0.567$. The positions of the particles have been sampled independently from a 3D density $\rho_{3D}(x, y, z) = \rho_z \rho(r)$, where $\rho(r)$ is the solution determined by $\rho = \frac{d\psi}{dr}$ in equations (3.53), and the vertical density is a constant $\rho_z = \frac{N}{\Delta z}$. The dimensionless radius is related to these 3D quantities by $\bar{R} = \frac{R}{\pi r_o^2 \rho_z}$, and the radius of the particles is determined by $r_o = \sqrt{\frac{R}{\pi \bar{R} \rho_z}}$. The lower image is the view along the horizontal direction demonstrating the marginal opacity of the system: a substantial fraction of the lines of sight through the centre are occluded, but also a similar fraction are clear.

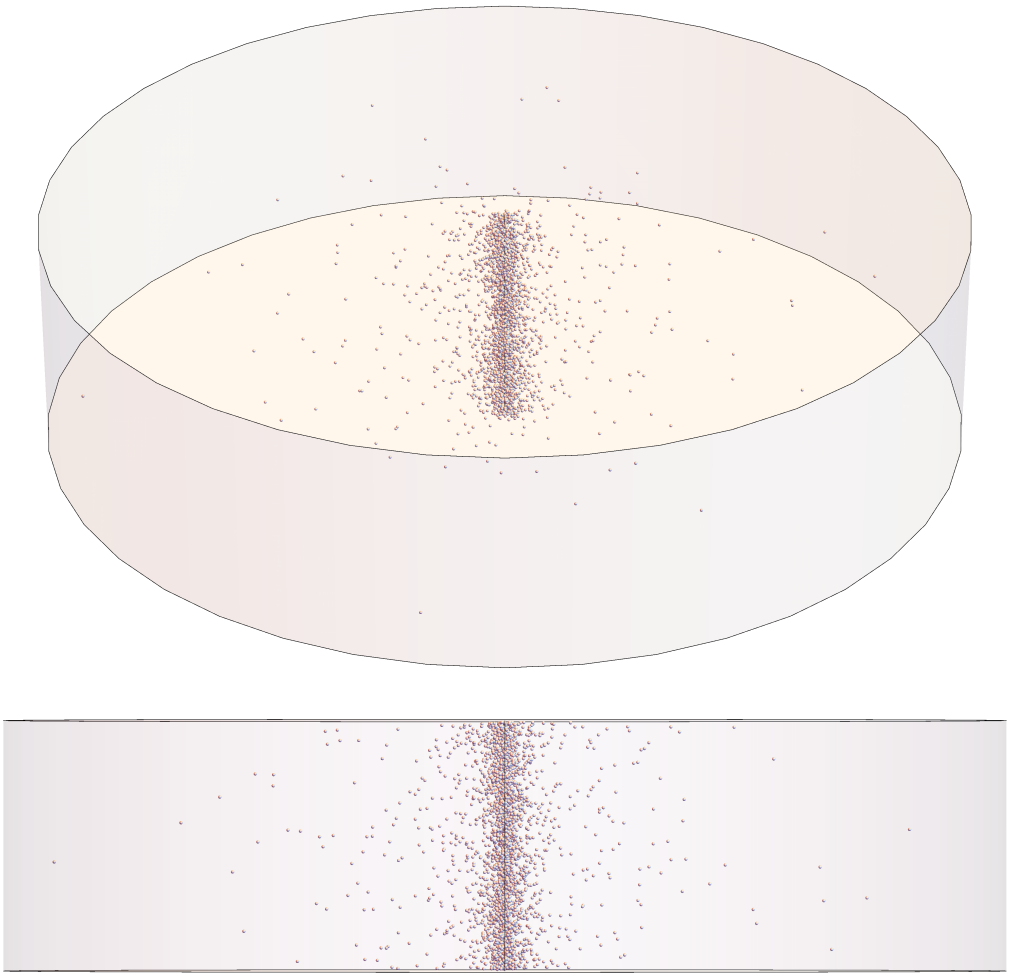

Figure 3.12: Illustration of the opaque phase with parameters: $\bar{R} = 5$, $\gamma = 6$, and $\overline{\psi} = 2.55$. The positions of the particles have been sampled independently from a 3D density $\rho_{3D}(x, y, z) = \rho_z \rho(r)$, where $\rho(r)$ is the solution determined by $\rho = \frac{d\psi}{dr}$ in equations (3.53), and the vertical density is a constant $\rho_z = \frac{N}{\Delta z}$. The dimensionless radius is related to these 3D quantities by $\bar{R} = \frac{R}{\pi r_o^2 \rho_z}$, and the radius of the particles is determined by $r_o = \sqrt{\frac{R}{\pi \bar{R} \rho_z}}$. The lower image is the view along the horizontal direction demonstrating the opacity of the system: every line of sight through the centre is occluded. Notice that the distribution is localised near the centre.

4

Phototaxis

4.1 A Model of Phototaxis

The preceding analysis models the collective self-organisation of thermophoretic colloids under illumination, where each particle absorbs light radiation which it isotropically conducts into the surrounding fluid, and then drifts by thermophoresis along the collectively generated temperature gradients. As previously discussed, this could be interpreted as a first approximation to a model of self-thermophoretic colloids which are self-propelling along their internal axis with an enhanced diffusivity over long time scales due to Brownian rotation of their orientation. Alternatively one may, following the model of Golestanian and Cohen [120], consider the anisotropic heating of the colloids in which isotropic colloids will heat most on the side facing the light radiation, thus making the particles self-thermophoretic, but always in the direction of the greater light intensity. If the particles are self-propelling but without alignment interactions then the system will exhibit a uniform distribution of orientations with as many particles self-propelling in every direction. If a Janus particle is illuminated asymmetrically, then if it's metallic side is oriented towards the greater light intensity it will absorb more energy and induce a larger local temperature gradient than if it had been oriented toward the lesser light intensity. Therefore, in

a population of particles asymmetrically illuminated, with a uniform distribution of orientations, as many particles will be facing the greater light intensity as the lesser one, but those facing the greater light intensity will experience a larger response. Thus there is a contribution to particle current from a differential response of differently oriented particles due to asymmetric illumination at each point in the swarm, see figure (4.1). Note that though the illumination of the system from the outside may be symmetric, the collective effect of shading will result in asymmetric illumination at points within the swarm. Additional processes such as radiation pressure may also contribute to a drift directed along the orientation of greatest light intensity.

The radiation pressure of a wave incident on the surface of a non-transmitting material is described by the Maxwell-Bartoli expression [133, 134] $P = (1+R)\frac{I}{c}\cos^2\theta$ for wave intensity I, wave speed c, angle of incidence θ, and reflectivity R ($R = 0 \Rightarrow$ complete absorption which we have assumed throughout this work, and $R = 1 \Rightarrow$ complete reflection). In experiments on self-thermophoresis the laser irradiating the colloid typically has intensity $\sim 10^8 Wm^{-2}$ [106, 111, 114], dividing by the speed of light suggests a radiation pressure of order from $10^{-1}Pa$ to $1Pa$. The colloids used in such experiments typically have a size of the order of a micron, thus the radiation force is of the order $\frac{I}{c}\pi r_0^2 \sim \left(10^{-1} \to 1\right) Pa \times 10^{-12}m^2 \sim 0.1 \to 1$ pico-Newton. This is potentially significant. In the experiments of Yiang et al [106] the colloids are confined in a narrow chamber but when irradiated from below they are pushed up to the upper surface and move by self-thermophoresis within an effectively 2D area perpendicularly to the radiation. Hence radiation pressure is dominant to self-thermophoresis in this experiment since the colloids do not self-propel downwards in opposition to the radiation pressure (here they move with speed of microns per second). In [111] Qian et al compared the force due to radiation pressure with $6\pi\eta r_0 v_{th}$, where v_{th} is the speed due to self-thermophoresis. Although thermophoresis is force-free and hence v_{th} is not due to an external force balancing the Stoke's drag, as this expression seems to imply, this expression can be thought of as the magnitude of an external force that would be required to propel the colloid to the speed that self-thermophoresis has achieved and so can be compared to the force of radiation pressure. Qian et al found $6\pi\eta r_0 v_{th} = 0.103pN$ and a force due to radiation pressure of $0.051pN$, so in this case self-thermophoresis is dominant, though radiation pressure is significant. In Ashkin's seminal paper on optical trapping of colloids [135] Ashkin was able to manipulate transparent colloids by momentum transfer as the laser light is refracted but not absorbed, thus avoiding thermal effects caused by energy absorption. In this paper, Ashkin claims that thermal effects are usu-

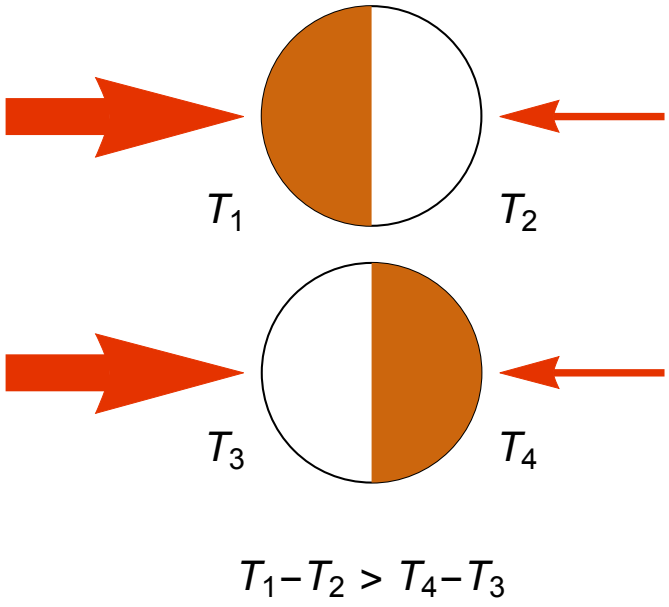

Figure 4.1: Schematic illustration of how self-themophoretic Janus colloids may be effectively phototactic. The Janus particle creates a local temperature gradient due to the metallic side heating more than the non-metallic side. This local temperature gradient will be greater when the metallic side is facing the greater light intensity than when it is facing the lesser light intensity, hence the particle will self-propel with greater speed when oriented one way than when oriented the other way.

ally orders of magnitude larger than radiation pressure when not using transparent particles. It seems the relative effect of radiation pressure is system dependent, but potentially significant.

The combined effect of these processes could induce an effective phototactic response from the particles. As a simplifying assumption, we ignore for now the effect of macroscopic temperature fields and simply model the particles as phototactic, exhibiting a net drift towards or away from the greater light intensity. Assume the colloid current is proportional to the difference in light intensity from both sides[1], i.e. it is the vector sum of light intensities

$$\vec{j} = -D\nabla\rho - \nu\rho\sum_i \vec{I}_i \tag{4.1}$$

[1]This follows Golestanian's models [64, 120] in which particle self-propulsion speed is assumed to be proportional to light intensity, and in particular in [106] the temperature difference across a heating Janus colloid is explicitly accounted for, and the self-propulsion speed calculated as being proportional to light intensity, which is confirmed in their experiments.

This model need not be self-thermophoretic Janus colloids, but can be any system of particles responding phototactically. The parameter, ν, describes the phototactic response of the system where $\nu > 0$ corresponds to positive phototaxis in which particles move towards the greater light intensity. Particle conservation implies,

$$\frac{\partial \rho}{\partial t} = -\nabla.\vec{j} \tag{4.2}$$

$$= D\nabla^2\rho + \nu\nabla.\rho\sum_i \vec{I}_i \tag{4.3}$$

4.1.1 One Dimensional Phototaxis

The particle current is

$$j = -D\frac{\partial}{\partial x}\rho + \nu\rho\left(I_+ - I_-\right) \tag{4.4}$$

, so the density evolution is

$$\frac{\partial \rho}{\partial t} = D\frac{\partial^2\rho}{\partial x^2} - \nu\frac{\partial}{\partial x}\left(\rho\left(I_+ - I_-\right)\right) \tag{4.5}$$

The shading shall be modelled by the same processes as in chapter 2, thus $I_+(x) = I_{\infty}e^{-\alpha\int_x^{\infty}\rho dx'}$ and $I_-(x) = I_{-\infty}e^{-\alpha\int_{-\infty}^{x}\rho dx'}$, which means the intensity difference at each point is

$$I_+(x) - I_-(x) = I_{\infty}e^{-\alpha\int_x^{\infty}\rho dx'} - I_{-\infty}e^{-\alpha\int_{-\infty}^{x}\rho dx'} \tag{4.6}$$

These exponentials can be combined,

$$I_+(x) - I_-(x) = -2\sqrt{I_{\infty}I_{-\infty}}e^{-\alpha N/2}\sinh\left[\alpha\int_x^{\infty}\rho dx' - \frac{\alpha N}{2} - \frac{1}{2}\ln\left[\frac{I_{\infty}}{I_{-\infty}}\right]\right] \tag{4.7}$$

The equation of motion is then

$$\frac{\partial \rho}{\partial t} = D\frac{\partial^2\rho}{\partial x^2} + 2\nu\sqrt{I_{\infty}I_{-\infty}}e^{-\alpha N/2}\frac{\partial}{\partial x}\left(\rho\sinh\left[\alpha\int_x^{\infty}\rho dx' - \frac{\alpha N}{2} - \frac{1}{2}\ln\left[\frac{I_{\infty}}{I_{-\infty}}\right]\right]\right) \tag{4.8}$$

This equation does not have a stationary solution on an infinite domain with $\nu > 0$ because positive phototaxis will result in particles moving outwards, i.e. at almost every position in the particle distribution the greater light intensity will be in the

direction away from the centre of the swarm, and so particles that move towards the greater light intensity will collectively disperse. If this phototactic mechanism is included in a model of thermophoretic colloids, then thermophilic particles will be attracted to the centre of the swarm by the collectively produced macroscopic temperature field, but they will be attracted to the greater light intensity by the effective positive phototactic self-thermophoretic mechanism described in the introduction to this chapter. Hence, the effect of this phototaxis is to introduce a tendency for collective dispersal counteracting the tendency to mutually attract.

In seeking a stationary distribution we proceed with the assumption that the particles are negatively phototactic with $\nu < 0$. Scaling this equation to dimensionless form, $x = \lambda\xi$, $\rho = \frac{N}{\lambda}\bar{\rho}$, $t = \frac{\lambda^2}{D}\tau$:

$$\frac{\partial\bar{\rho}}{\partial\tau} = \frac{\partial^2\bar{\rho}}{\partial\xi^2} - \frac{2\left|\nu\right|\sqrt{I_\infty I_{-\infty}}}{D}e^{-\alpha N/2}\lambda\frac{\partial}{\partial\xi}\left(\bar{\rho}\sinh\left[\alpha N\int_\xi^\infty \bar{\rho}d\xi' - \frac{\alpha N}{2} - \frac{1}{2}\ln\left[\frac{I_\infty}{I_{-\infty}}\right]\right]\right) \tag{4.9}$$

Choosing the length scale to be $\lambda = \frac{D}{2|\nu|\sqrt{I_\infty I_{-\infty}}}$ and, as in chapter 2, defining $a = \alpha N$, the dimensionless form of this equation is

$$\frac{\partial\bar{\rho}}{\partial\tau} = \frac{\partial^2\bar{\rho}}{\partial\xi^2} - \frac{\partial}{\partial\xi}\left(e^{-a/2}\bar{\rho}\sinh\left[a\left(\int_\xi^\infty \bar{\rho}d\xi' - \frac{1}{2}\right) - \frac{1}{2}\ln\left[\frac{I_\infty}{I_{-\infty}}\right]\right]\right) \tag{4.10}$$

with dimensionless current $\bar{j} = -\frac{\partial\bar{\rho}}{\partial\xi} + e^{-a/2}\bar{\rho}\sinh\left[a\left(\int_\xi^\infty \bar{\rho}d\xi' - \frac{1}{2}\right) - \frac{1}{2}\ln\left[\frac{I_\infty}{I_{-\infty}}\right]\right]$. Seeking a stationary distribution, with zero current,

$$\frac{d\bar{\rho}}{d\xi} = e^{-a/2}\bar{\rho}\sinh\left[a\left(\int_\xi^\infty \bar{\rho}d\xi' - \frac{1}{2}\right) - \frac{1}{2}\ln\left[\frac{I_\infty}{I_{-\infty}}\right]\right] \tag{4.11}$$

As before, we convert this integro-differential equation into a purely differential equation by defining the function $\psi(\xi) = -a\left(\int_\xi^\infty \bar{\rho}d\xi' - \frac{1}{2}\right) \implies \bar{\rho} = \frac{1}{a}\frac{d\psi}{d\xi}$, then

$$\frac{d^2\psi}{d\xi^2} + e^{-a/2}\frac{d\psi}{d\xi}\sinh\left[\psi + \frac{1}{2}\ln\left[\frac{I_\infty}{I_{-\infty}}\right]\right] = 0 \tag{4.12}$$

$$\Rightarrow \frac{d}{d\xi}\left[\frac{d\psi}{d\xi} + e^{-a/2}\cosh\left[\psi + \frac{1}{2}\ln\left[\frac{I_\infty}{I_{-\infty}}\right]\right]\right] = 0 \tag{4.13}$$

$$\Rightarrow \frac{d\psi}{d\xi} = c - e^{-a/2}\cosh\left[\psi + \frac{1}{2}\ln\left[\frac{I_\infty}{I_{-\infty}}\right]\right] \tag{4.14}$$

The constant of integration can be determined by considering the limits $\xi \to \pm\infty$: here normalisation of the dimensionless density implies the function ψ takes the

values $\psi = \pm\frac{a}{2}$ as $\frac{d\psi}{d\xi} \to 0$, thus $c = e^{-a/2}\cosh\left[\pm\frac{a}{2} + \frac{1}{2}\ln\left[\frac{I_\infty}{I_{-\infty}}\right]\right]$. For this to be true in both limits requires $I_\infty = I_{-\infty}$. This means that there are no stationary distributions on an infinite domain with asymmetric illumination. With this constant determined, and considering the case of symmetric illumination, the equation for ψ becomes

$$\frac{d\psi}{d\xi} = e^{-a/2}\left(\cosh\frac{a}{2} - \cosh\psi\right) \tag{4.15}$$

This is precisely the same equation as (2.73) for the stationary distribution of thermophoretic particles in the limit of an infinite domain! The solution is therefore the same, specifically,

$$\psi(\xi) = 2\text{arctanh}\left[\tanh\left[\frac{a}{4}\right]\tanh\left[\frac{(1-e^{-a})}{4}\xi\right]\right] \tag{4.16}$$

with density,

$$\bar{\rho}(\xi) = \frac{\frac{1}{2a}\left(1-e^{-a/2}\right)^2}{1 + \frac{\sinh^2\left[\frac{(1-e^{-a})}{4}\xi\right]}{\cosh^2\left[\frac{a}{4}\right]}} \tag{4.17}$$

4.1.2 Combining Phototaxis and Thermophoresis in 1D

Combining the effects of collective thermophoresis and phototaxis the particle current is modelled by

$$j = -D\nabla\rho + D_T\rho\nabla T + \nu\rho\left(I_+ - I_-\right) \tag{4.18}$$

The equations of motion are then derived, as above, from conservation of particle number, and the temperature evolution is modelled by the heat equation as per chapter 2, hence,

$$\begin{cases} \frac{\partial T}{\partial t} = \kappa\nabla^2 T + \Gamma\left[\rho\right] \\ \frac{\partial \rho}{\partial t} = D\nabla^2\rho - \nabla.\rho\left(D_T\nabla T + \nu\left(I_+ - I_-\right)\right) \end{cases} \tag{4.19}$$

Using the same heating functional as was derived in chapter 2, these equations are more precisely,

$$\begin{cases} \frac{\partial T}{\partial t} = \kappa\frac{\partial^2 T}{\partial x^2} + \frac{2\alpha}{c\rho_f}\sqrt{I_\infty I_{-\infty}}e^{-\alpha N/2}\rho\left(x\right)\cosh\left[\alpha\int_x^\infty \rho dx' - \frac{\alpha N}{2} - \frac{1}{2}\ln\left[\frac{I_\infty}{I_{-\infty}}\right]\right] \\ \frac{\partial \rho}{\partial t} = D\frac{\partial^2\rho}{\partial x^2} - \frac{\partial}{\partial x}\rho\left(D_T\frac{\partial T}{\partial x} - 2\nu\sqrt{I_\infty I_{-\infty}}e^{-\alpha N/2}\sinh\left[\alpha\int_x^\infty \rho dx' - \frac{\alpha N}{2} - \frac{1}{2}\ln\left[\frac{I_\infty}{I_{-\infty}}\right]\right]\right) \end{cases} \tag{4.20}$$

where the boundary conditions at x_b are, as previously, the zero current of particles, $D\nabla\rho|_{\pm x_b} = D_T\rho\left(\pm x_b\right)\nabla T|_{\pm x_b} + \nu\rho\left(\pm x_b\right)\left(I_+\left(\pm x_b\right) - I_-\left(\pm x_b\right)\right)$, and the temperature matching the fixed temperature of the heat bath, $T\left(\pm x_b\right) = 0$, however, we shall take the limit $x_b \to \infty$. Scaling the various physical quantities in the usual way, $x = \lambda\xi$, $\rho = \frac{N}{\lambda}\bar{\rho}$, $t = \frac{\lambda^2}{\kappa}\tau$, and $T = \frac{D}{D_T}\overline{T}$, the equations of motion are

$$\begin{cases} \frac{\partial \bar{T}}{\partial \tau} = \frac{\partial^2\bar{T}}{\partial\xi^2} + \alpha N e^{-\alpha N/2}\lambda\frac{2D_T}{c\rho_f\kappa D}\sqrt{I_\infty I_{-\infty}}\bar{\rho}\cosh\left[\alpha N\left(\int_\xi^\infty \bar{\rho}d\xi' - \frac{1}{2}\right) - \frac{1}{2}\ln\left[\frac{I_\infty}{I_{-\infty}}\right]\right] \\ \frac{\kappa}{D}\frac{\partial\bar{\rho}}{\partial\tau} = \frac{\partial^2\bar{\rho}}{\partial\xi^2} - \frac{\partial}{\partial\xi}\bar{\rho}\left(\frac{\partial\overline{T}}{\partial\xi} - \lambda\frac{2\nu\sqrt{I_\infty I_{-\infty}}}{D}e^{-\alpha N/2}\sinh\left[\alpha N\left(\int_\xi^\infty \bar{\rho}d\xi' - \frac{1}{2}\right) - \frac{1}{2}\ln\left[\frac{I_\infty}{I_{-\infty}}\right]\right]\right) \end{cases} \tag{4.21}$$

If the choice $\lambda = \frac{c\rho_f\kappa D}{2D_T\sqrt{I_\infty I_{-\infty}}}$ is made for the length scale, then the coefficient of the hyperbolic sine is $\lambda\frac{2\nu\sqrt{I_\infty I_{-\infty}}}{D} = \frac{\nu}{D_T}c\rho_f\kappa \equiv \mu$. Defining $a = \alpha N$ as usual, the

dimensionless equations are

$$\begin{cases} \frac{\partial \overline{T}}{\partial \tau} = \frac{\partial^2 \overline{T}}{\partial \xi^2} + a e^{-a/2} \overline{\rho} \cosh \left[a \left(\int_\xi^\infty \overline{\rho} d\xi' - \frac{1}{2} \right) - \frac{1}{2} \ln \left[\frac{I_\infty}{I_{-\infty}} \right] \right] \\ \frac{\kappa}{D} \frac{\partial \overline{\rho}}{\partial \tau} = \frac{\partial^2 \overline{\rho}}{\partial \xi^2} - \frac{\partial}{\partial \xi} \overline{\rho} \left(\frac{\partial \overline{T}}{\partial \xi} - \mu e^{-a/2} \sinh \left[a \left(\int_\xi^\infty \overline{\rho} d\xi' - \frac{1}{2} \right) - \frac{1}{2} \ln \left[\frac{I_\infty}{I_{-\infty}} \right] \right] \right) \end{cases} \tag{4.22}$$

We seek stationary solutions for this system under symmetric illumination ($I_\infty = I_{-\infty}$). The dimensionless current is $\bar{j} = -\frac{\partial \bar{\rho}}{\partial \xi} + \bar{\rho} \frac{\partial \bar{T}}{\partial \xi} - \mu e^{-a/2} \bar{\rho} \sinh \left[a \left(\int_\xi^\infty \overline{\rho} d\xi' - \frac{1}{2} \right) \right]$. In a stationary state this current is zero, hence,

$$\frac{d\bar{\rho}}{d\xi} = \bar{\rho} \frac{d\bar{T}}{d\xi} - \mu e^{-a/2} \bar{\rho} \sinh \left[a \left(\int_\xi^\infty \overline{\rho} d\xi' - \frac{1}{2} \right) \right] \tag{4.23}$$

The heat equation can be solved with the same method employed in chapter 2 to obtain the same variation of the temperature field, specifically

$$\frac{d\bar{T}}{d\xi} = e^{-a/2} \sinh \left[a \left(\int_\xi^\infty \bar{\rho} d\xi' - \frac{1}{2} \right) \right] \tag{4.24}$$

Substituting this into the zero current condition one obtains,

$$\frac{d\overline{\rho}}{d\xi} = \overline{\rho} e^{-a/2} (1 - \mu) \sinh \left[a \left(\int_\xi^\infty \overline{\rho} d\xi' - \frac{1}{2} \right) \right] \tag{4.25}$$

Defining the function ψ in the usual way and integrating one obtains the equation,

$$\frac{d\psi}{d\xi} = e^{-a/2} (1 - \mu) \left(\cosh \left[\frac{a}{2} \right] - \cosh \left[\psi \right] \right) \tag{4.26}$$

This is almost precisely the same equation that describes the distribution of thermophoretic colloids, without phototactic effects, studied in chapter 2! The effect of the inclusion of phototaxis is to rescale the horizontal extent of the distribution, i.e. equation (2.73) can be recovered with a rescaled length scale such that $\xi \to \xi (1 - \mu)$, but only if $1 - \mu > 0$, that is $D_T > c \rho_f \kappa \nu$. Thus, as long as a photophilic response is not too strong, it will introduce a tendency towards dispersal of the distribution, but only by modifying the horizontal extent of the distribution, not by changing the functional form of the distribution. Indeed, whether the system self-organises to the bell-shaped distribution of the low shading-limit, or the flat distribution of the opaque limit, is determined by the parameter $a = \alpha N$ and is unaffected by the action of phototaxis. If the phototphilic response is too large then the system will disperse and will not form a stationary distribution on an infinite domain.

The fact that the self-organisation of collective phototaxis is the formation of the

same distributions that are formed by purely thermophoretic particles is very much reminiscent of the similarities in stationary distributions found by Golestanian in his model of collective thermophoresis, and Vincent and Hill in their model of collective phototaxis. Indeed, both found that the stationary distributions take the form of the square of the secant function, which is precisely the form found in the present work in the limit of low shading!

4.1.3 Explanation for Similarity of Phenomenology of Thermophoresis and Phototaxis

Consider the model of collective thermophoresis in an arbitrary dimensional space (though for simplicity we shall describe the light intensity as if it were in 1D): the temperature fields which determine the distribution of particles are determined by the heat equation,

$$\partial_t T = \kappa \nabla^2 T + \Gamma\left[\rho\right] \tag{4.27}$$

with heating functional, $\Gamma\left[\rho\right]$. The energy for the heating comes from the radiation field $\vec{I}_{\pm}$ ($\vec{I}_{+}$ comes from $+\infty$ and is directed towards $-\infty$, whereas $\vec{I}_{-}$ comes from $-\infty$ and is directed towards $+\infty$), such that the heating rate at some point is the rate of energy loss from the radiation field, i.e. the divergence of the radiation field,

$$\Gamma\left[\rho\right] = -\frac{1}{c\rho_f}\nabla.\left(\vec{I}_{+} + \vec{I}_{-}\right) \tag{4.28}$$

Substituting this into the heat equation

$$\partial_t T = \kappa \nabla^2 T - \frac{1}{c\rho_f}\nabla.\left(\vec{I}_{+} + \vec{I}_{-}\right) \tag{4.29}$$

Consider an arbitrary volume, V, and integrate both sides of this equation over this volume, then

$$c\rho_f \int_V \partial_t T dV = c\rho_f \kappa \int_V \nabla.\nabla T dV - \int_V \nabla.\left(\vec{I}_{+} + \vec{I}_{-}\right) dV \tag{4.30}$$

The heat stored in this volume (or rather the excess heat over and above what would be present in the absence of active heating in the system) is $Q\left(V\right) = \int_V T c\rho_f dV$, which means the LHS of equation (4.30) is the rate of change of heat in the volume, $\partial_t Q\left(V\right) = \partial_t \int_V T c\rho_f dV$. Applying the divergence theorem to the RHS of equation

(4.30),

$$\frac{1}{c\rho_f\kappa}\partial_t Q\left(V\right)=\oint_S\left(\nabla T-\frac{1}{c\rho_f\kappa}\left(\vec{I}_+ + \vec{I}_-\right)\right).d\vec{S} \tag{4.31}$$

If the rate of change of the temperature field is much faster than the evolution of the density field (which may be the case if $\kappa \gg D$) then on time scales over which the density evolves appreciably the heat equation is effectively in a stationary state at all times. Therefore, when temperature is enslaved to particle distribution, $\nabla T = \frac{1}{c\rho_f\kappa}\left(\vec{I}_+ + \vec{I}_-\right)$, in which case any coupling to the temperature gradient is effectively a coupling to the vector sum of light intensity. Irrespective of whether the enslaving principle holds, this equality always applies when the system as a whole is in a stationary state. This explains the equivalence of stationary distributions of collective thermophoresis and collective phototaxis. Since this analysis applies generally, it also applies to the case of incorporating phototaxis into a cylindrically symmetric system, in which case the only change to the stationary distribution is a modification of the parameter γ, i.e. $\gamma \to \gamma_{eff} = \left(1-\frac{\nu}{D_T}c\rho_f\kappa\right)\gamma$.

5

Conclusions

We have studied the collective behaviour of self-thermophoretic colloids under laser illumination. This is an artificial active matter system that could be realised in experiment and for which few analytic results have been found. We studied the self-organisation of the system to stationary distributions using a mean field model in rectangular and cylindrical symmetry, generalising the work of Golestanian appropriate in the limit of negligible shading. We have modelled the non-local and non-pairwise collective effect of shading on the dynamics of the system: in rectangular symmetry a mostly transparent system will form a diffuse bell shaped distribution with exponential tails (the square of a hyperbolic secant) which is the same distribution found by Golestanian and also Vincent and Hill in a model of phototaxis in algae; in the opaque limit the system forms a dense phase with a uniform density of freely diffusing particles at uniform temperature confined by exponentially decaying edges that heat to create steep temperature gradients. In cylindrical symmetry the stationary distributions bifurcate in a hysteresis curve between diffuse and transparent distributions that fill the cylindrical container, and dense and opaque distributions that are localised close to the centre of the container. The controlling parameter in this hysteresis is the radiation power where for low power only diffuse and transparent states are possible, for high power only localised and opaque states

are possible, and for intermediate power the system is bistable between diffuse and localised states.

The effect of shading on the collective behaviour of self-thermophoretic colloids is two fold: First, not all colloids have the same causative impact on the rest of the system, that is they are not all equal sources of heat: in 1D the shaded interior of opaque systems does not contribute heating to the collective dynamics, only the edges of the distributions which absorb energy create the temperature gradients which constrain the swarm, i.e. the tails dominate the centre, the swarm is formed from the edge like a surface tension; in 2D, localised swarms can form in the centre which absorb the geometrically focused energy creating temperature gradients which mostly determine the shape of the tails- i.e. the centre of the swarm constrains the tails. The second effect of shading is the variable opacity of distributions in higher dimensions: in cylindrical geometry, when the radiation power is large enough the system self-organises either to diffuse and transparent states or to localised and opaque states, where the marginally opaque distributions are a separatrix between the two basins of attraction. The critical role of the state of marginal opacity in discriminating between different modes of self-organisation is reminiscent of the flocking model of Pearce et al in which their system self-organises to a state of marginal opacity (though in their model the marginally opaque state is the attractor). This correspondence in phenomenology arguably provides one of the first bridges between a thermodynamic system and an animal system.

We have also studied collective phototaxis using the same formalism and found that the stationary distributions are exactly the same as the self-thermophoretic system. This suggests the possibility that there may be universal phenomena in systems governed by line-of-sight interactions which could shed light on the behaviour of other active matter systems.

The theory presented in this thesis has generalised the model of Golestanian [64], but has not directly addressed the agent based model of Golestanian and Cohen [120]. The mathematical theory developed in this thesis could potentially be extended to at least provide insight to Golestanian and Cohens model and perhaps to model it directly. Allowing for asymmetric illumination in the 1D model on an infinite domain, and assuming $\kappa \gg D$ which implies that the temperature field is enslaved to the density field (an assumption made in both of [64, 120]), equation (2.17), recast in terms of ψ, becomes a generalised Burgers equation for ψ, where the non-linear term involves the product of a hyperbolic sine of ψ with the ψ gradient instead of just ψ with the ψ gradient. The Burgers equation is known to have

travelling solutions (and, indeed, is exactly solvable) so it is likely that there are travelling wave solutions for this generalised Burgers equation. This may, optimistically, be used as a mathematical model of the agent based model of Golestanian and Cohen which found travelling distributions from collimated illumination from one side of a finite swarm. Although their model is not strictly a quasi-1D system, as it is of finite extent in perpendicular directions, this approach may provide insight into their model. A more realistic approach to modelling the simulations of Golestanian and Cohen could be as follows: consider finitely many particles (in 3D) in a cylindrical container with impermeable boundaries illuminated from one side along the z-direction. The mathematical theory developed in this thesis could be adapted to this situation. In this case the radiation is not radially directed, so the 1D model of light absorption would be most appropriate, except with the parameter a now being a function of cylindrical radius. The heat equation would be solved with 2D rotational symmetry, though geometrically spreading three dimensionally in the far field, which is considerably different from the 1D model considered in this work. It is anticipated that there would be circulating currents since this was seen in [120], hence detailed balance would be violated even in the moving frame of reference. Since the solid boundaries would prevent lateral dissipation and evaporation of the swarm (as is seen in [120]), it is possible that this system would produce travelling distributions that are stationary in the moving frame of reference. Such an analysis could provide insight to Golestanian and Cohen's model.

It is interesting to compare the length scales that emerge in the quasi-1D system with those of the cylindrically symmetric quasi-2D system. Observe equations (2.16) and (3.15): in the 1D case the length scale, λ, and the parameter, a, were chosen so as to respectively "tidy up" the heating term and exponents/arguments of the hyperbolic functions; whereas in the 2D case the length scale was chosen to "tidy up" the arguments of the functions and the remaining parameters are gathered together into the dimensionless parameter γ. Intuitively one might qualitatively expect that: increasing the laser power causes larger flows of energy, and so larger temperature gradients and so a more localised distribution; increasing the thermal conductivity couples the same energy flow to a shallower temperature gradient and hence to more diffuse distributions; and increasing the Soret coefficient, the ratio of thermophoretic mobility to diffusivity, increases the relative strength of thermophoresis, thus causing more localised distributions. These qualitative effects occur but take different forms in 1D and 2D: in 1D the thermal conductivity divided by the product of radiation power and Soret coefficient is the *length* scale, thus the length scale of the system is proportional to thermal conductivity and inversely proportional to both laser power

and Soret coefficient, though the *form* of the distribution is unaffected by such changes. Whereas in 2D, the same combination of physical quantities determines the *dimensionless* parameter γ, which is, broadly speaking, related to how localised the distribution is, though through changes in the functional form as γ is changed rather than in the length scale *per se*.

It seems that this is determined by the dimensional dependence of the thermal conductivity. A quasi-1/2D system is modelled by considering a purely 1/2D system and then relating the purely 1/2D quantities in such a model to their 3D counterparts, as all experimental systems must be three dimensional, by incorporating the appropriate perpendicular length scales. Not all quantities need this relation- for instance the dimensionality of the diffusivity, $[D] = \frac{L^2}{T}$, is independent of system dimensions- though the thermal conductivity does $[k] = \frac{E}{T\ \Theta\ L^{n-2}}$. The combination of thermal conductivity, laser power, and Soret coefficient described above is such that in 1D and 3D there is a length scale left over, but in 2D the dimensions cancel, due to the independence of length of the thermal conductivity, and this combination of parameters is dimensionless, hence the dimensionless parameter γ.

The constraints on system opacity are determined by the terms inside the exponential and hyperbolic functions of the heating term (which relate to particle number and particle radius): in 1D this involves defining a dimensionless parameter, $a = \alpha N$, which, when the equations are solved, determines the functional form of the solutions (localised or diffuse) and the overall system opacity. When one relates the parameters α and N to higher dimensional quantities it becomes clear that the parameter, a, should determine the overall opacity, as it is essentially the perpendicular density in units of particle diameter. In 2D the terms in the exponential arguments determine the length scale, but also place *constraints* on the overall opacity, though do not *determine* the opacity of the system. There is an interesting correspondence between 1D and 2D systems: in both cases the thermal conductivity, laser power, and Soret coefficient are grouped together in the same way, as are, broadly speaking, the particle number and particle diameter; though these exchange roles with the former determining the length scale in 1D but not 2D where it defines a dimensionless parameter, and the latter defining a dimensionless parameter in 1D and the length scale in 2D.

The system has been analysed in spherical symmetry, though with no definitive conclusions. In this case the length scale could be defined analogously with the cylindrically symmetric case defining $\lambda = r_0\sqrt{N\pi}$, which implies a dimensionless system size $\overline{R} = \frac{R}{r_0\sqrt{N\pi}}$. Similarly, a dimensionless parameter can be defined: $\gamma = \frac{PD_T}{2\pi c\rho_f \kappa D}\frac{1}{\lambda}$,

but notice in this case it must include the length scale. One can define ψ in precisely analogous terms, which leads to a second order ODE: $\bar{r}^2 \frac{d^2\psi}{d\bar{r}^2} + \gamma e^{-\overline{\psi}} \frac{d\psi}{d\bar{r}} \sinh\psi = 0$. However, if one Taylor expands ψ and analyses this equation near the origin, where $\psi \to 0$, the coefficients do not match, which means the equation does not have well behaved solutions near the origin. Similarly, assuming a power law divergence in density at the origin (but $\psi \to 0$), the exponents do not match either. If one assumes complete absorption of incoming radiation (which means the integral of density from the origin diverges and one must define ψ as the integral from some radius to the boundary) then the same problem is encountered. In 2D there is a singularity in the heating functional at the origin, but the only artefact of this is a finite gradient in density as $r \to 0$, which means a discontinuity in gradient passing through the origin to the other side. It appears that in 3D the singularity is strong enough to significantly distort the solutions. One can attempt to consider far field asymptotics in the 3D case, analogously with the 2D case: the temperature in the far field due to heating near the origin will vary as $1/r$; the balance of diffusion and thermophoresis implies $\rho(r) = \rho_{boundary} e^{S_T T(r)} \Rightarrow \rho = \rho_{boundary} e^{\frac{\gamma_s}{2}\frac{1}{r}} \sim \rho_{boundary}\left(1 + \frac{\gamma_s}{2}\frac{1}{r}\right)$. This suggests that the system may form a uniform distribution with a higher density in the centre which decays to the uniform background density as $1/r$.

Consider the 2D cylindrically symmetric stationary distributions: the physical parameters of particle number and system radius determine the dimensionless system size, $\{N, r_0\} \Rightarrow \bar{R}$, and the laser power (plus thermal properties) determines dimensionless laser power, $P \Rightarrow \gamma$. These two parameters together determines a restricted set of possible system opacities, i.e. $\left\{\bar{R}, \gamma\right\} \Rightarrow \overline{\psi}$. Now consider a subsystem defined by everything up to the radius R_s: there will be some number of particles within this radius, which together define a new $\bar{R}$, and a reduced laser power at this radius $P(R_s) \Rightarrow \gamma_s$, and if the system over all is in a stationary state, then so must be the subsystem, thus $\left\{\bar{R}_s, \gamma_s\right\} \Rightarrow \overline{\psi}_s = \psi(R_s)$. Therefore any given triple of parameters, $\left\{\bar{R}, \gamma, \overline{\psi}\right\}$, determines a function whose every subsystem corresponds to a renormalised function of another triple of parameters, $\left\{\bar{R}_s, \gamma_s, \overline{\psi}_s\right\}$. In particular, in the γ-$\overline{\psi}$ plane the curves defined by constant $\beta = \gamma e^{-\overline{\psi}}$ are invariants of this subsystem rescaling. This observation is insightful, but I have been unable to take it further.

The major shortcoming of the present work is that the stability of the distributions have not been analysed. On qualitative grounds it is arguable that instabilities found in Golestanian's model are arrested by the effect of shading: the instabilities in his model occurred as a positive feedback that dense states become hot, attracting more particles into the dense region, which increases the density further. However,

we have found that the rate of heating depends not only on the local density, but also on the shading by the exterior of the distribution, so if the most dense parts of the distribution are also the most shaded, then the region of heating moves towards the edge of the distribution, which should nullify any positive feedback of the type found by Golestanian. However, this has not been proven. Neither have the stabilities and instabilities of the different branches of the hysteresis loop been proven. An additional extension of the present work would model the self-propulsion of the particles more correctly by accounting for their movement as an enhanced diffusivity that depends on the position in the distribution. That is, the self-thermophoretic Janus colloids move under illumination with a speed dependent on the light intensity, so the most shaded regions should have the least effective diffusivity. This might have significant consequences for the self-organisation of such particles.

6

Bibliography

[1] Z E Musielak and B Quarles. The three-body problem. *Reports on Progress in Physics*, 77(6):065901, 2014. URL http://stacks.iop.org/0034-4885/77/i=6/a=065901.

[2] Joel L. Lebowitz. Statistical mechanics: A selective review of two central issues. *Rev. Mod. Phys.*, 71:S346–S357, Mar 1999. doi: 10.1103/RevModPhys.71.S346. URL https://link.aps.org/doi/10.1103/RevModPhys.71.S346.

[3] H. Eugene Stanley. Scaling, universality, and renormalization: Three pillars of modern critical phenomena. *Rev. Mod. Phys.*, 71:S358–S366, Mar 1999. doi: 10.1103/RevModPhys.71.S358. URL https://0-link-aps-org.pugwash.lib.warwick.ac.uk/doi/10.1103/RevModPhys.71.S358.

[4] Steve Pressé, Kingshuk Ghosh, Julian Lee, and Ken A. Dill. Principles of maximum entropy and maximum caliber in statistical physics. *Rev. Mod. Phys.*, 85:1115–1141, Jul 2013. doi: 10.1103/RevModPhys.85.1115. URL https://0-link-aps-org.pugwash.lib.warwick.ac.uk/doi/10.1103/RevModPhys.85.1115.

[5] Christopher Jarzynski. Diverse phenomena, common themes. *Nature Physics*, 11:105–107, February 2015. doi: 10.1038/nphys3229.

[6] Steven M Manson. Simplifying complexity: a review of complexity theory. *Geoforum*, 32(3):405 – 414, 2001. ISSN 0016-7185. doi: https://doi.org/10.1016/S0016-7185(00)00035-X. URL http://www.sciencedirect.com/science/article/pii/S001671850000035X.

[7] J. P. Gollub and J. S. Langer. Pattern formation in nonequilibrium physics. *Rev. Mod. Phys.*, 71:S396–S403, Mar 1999. doi: 10.1103/RevModPhys.71.S396. URL https://0-link-aps-org.pugwash.lib.warwick.ac.uk/doi/10.1103/RevModPhys.71.S396.

[8] T. R. Kirkpatrick and J. R. Dorfman. Nonequilibrium is different. *Phys. Rev. E*, 92:022109, Aug 2015. doi: 10.1103/PhysRevE.92.022109. URL https://0-link-aps-org.pugwash.lib.warwick.ac.uk/doi/10.1103/PhysRevE.92.022109.

[9] Sybren R. de Groot and Peter Mazur. Non-equilibrium thermodynamics. *American Journal of Physics*, 31(7):558–559, 1963. doi: 10.1119/1.1969680. URL https://doi.org/10.1119/1.1969680.

[10] P. Romanczuk, M. Bär, W. Ebeling, B. Lindner, and L. Schimansky-Geier. Active brownian particles. *The European Physical Journal Special Topics*, 202(1):1–162, Mar 2012. ISSN 1951-6401. doi: 10.1140/epjst/e2012-01529-y. URL https://doi.org/10.1140/epjst/e2012-01529-y.

[11] J Elgeti, R G Winkler, and G Gompper. Physics of microswimmers single particle motion and collective behavior: a review. *Reports on Progress in Physics*, 78(5):056601, 2015. URL http://stacks.iop.org/0034-4885/78/i=5/a=056601.

[12] John Toner, Yuhai Tu, and Sriram Ramaswamy. Hydrodynamics and phases of flocks. *Annals of Physics*, 318(1):170 – 244, 2005. ISSN 0003-4916. doi: https://doi.org/10.1016/j.aop.2005.04.011. URL http://www.sciencedirect.com/science/article/pii/S0003491605000540. Special Issue.

[13] Sriram Ramaswamy. The mechanics and statistics of active matter. *Annual Review of Condensed Matter Physics*, 1(1):323–345, 2010. doi: 10.1146/annurev-conmatphys-070909-104101. URL https://doi.org/10.1146/annurev-conmatphys-070909-104101.

[14] Tams Vicsek and Anna Zafeiris. Collective motion. *Physics Reports*, 517 (3):71 – 140, 2012. ISSN 0370-1573. doi: https://doi.org/10.1016/j.physrep.2012.03.004. URL http://www.sciencedirect.com/science/article/pii/S0370157312000968. Collective motion.

[15] M. C. Marchetti, J. F. Joanny, S. Ramaswamy, T. B. Liverpool, J. Prost, Madan Rao, and R. Aditi Simha. Hydrodynamics of soft active matter. *Rev. Mod. Phys.*, 85:1143–1189, Jul 2013. doi: 10.1103/RevModPhys.85.1143. URL https://link.aps.org/doi/10.1103/RevModPhys.85.1143.

[16] Sriram Ramaswamy. Active matter. *Journal of Statistical Mechanics: Theory and Experiment*, 2017(5):054002, 2017. URL http://stacks.iop.org/1742-5468/2017/i=5/a=054002.

[17] Gautam I. Menon. *Active Matter*, pages 193–218. Springer New York, New York, NY, 2010. ISBN 978-1-4419-6494-6. doi: 10.1007/978-1-4419-6494-6_9. URL https://doi.org/10.1007/978-1-4419-6494-6_9.

[18] David Saintillan and Michael J. Shelley. Active suspensions and their nonlinear models. *Comptes Rendus Physique*, 14(6):497 – 517, 2013. ISSN 1631-0705. doi: https://doi.org/10.1016/j.crhy.2013.04.001. URL http://www.sciencedirect.com/science/article/pii/S1631070513000704. Living fluids / Fluides vivants.

[19] Clemens Bechinger, Roberto Di Leonardo, Hartmut Löwen, Charles Reichhardt, Giorgio Volpe, and Giovanni Volpe. Active particles in complex and crowded environments. *Rev. Mod. Phys.*, 88:045006, Nov 2016. doi: 10.1103/RevModPhys.88.045006. URL https://link.aps.org/doi/10.1103/RevModPhys.88.045006.

[20] Elod Mehes and Tamas Vicsek. Collective motion of cells: from experiments to models. *Integr. Biol.*, 6:831–854, 2014. doi: 10.1039/C4IB00115J. URL http://dx.doi.org/10.1039/C4IB00115J.

[21] M. Ballerini, N. Cabibbo, R. Candelier, A. Cavagna, E. Cisbani, I. Giardina, V. Lecomte, A. Orlandi, G. Parisi, A. Procaccini, M. Viale, and V. Zdravkovic. Interaction ruling animal collective behavior depends on topological rather than metric distance: Evidence from a field study. *Proceedings of the National Academy of Sciences*, 105(4):1232–1237, 2008. doi: 10.1073/pnas.0711437105. URL http://www.pnas.org/content/105/4/1232.abstract.

[22] Nicholas C. Makris, Purnima Ratilal, Deanelle T. Symonds, Srinivasan Jagannathan, Sunwoong Lee, and Redwood W. Nero. Fish population and behavior revealed by instantaneous continental shelf-scale imaging. *Science*, 311 (5761):660–663, 2006. ISSN 0036-8075. doi: 10.1126/science.1121756. URL http://science.sciencemag.org/content/311/5761/660.

[23] Nicholas C. Makris, Purnima Ratilal, Srinivasan Jagannathan, Zheng Gong, Mark Andrews, Ioannis Bertsatos, Olav Rune Godø, Redwood W. Nero, and J. Michael Jech. Critical population density triggers rapid formation of vast oceanic fish shoals. *Science*, 323(5922):1734–1737, 2009. ISSN 0036-8075. doi: 10.1126/science.1169441. URL http://science.sciencemag.org/content/323/5922/1734.

[24] T Chou, K Mallick, and R K P Zia. Non-equilibrium statistical mechanics: from a paradigmatic model to biological transport. *Reports on Progress in Physics*, 74(11):116601, 2011. URL http://stacks.iop.org/0034-4885/74/i=11/a=116601.

[25] R J Harris and G M Schtz. Fluctuation theorems for stochastic dynamics. *Journal of Statistical Mechanics: Theory and Experiment*, 2007(07):P07020, 2007. URL http://stacks.iop.org/1742-5468/2007/i=07/a=P07020.

[26] R K P Zia and B Schmittmann. Probability currents as principal characteristics in the statistical mechanics of non-equilibrium steady states. *Journal of Statistical Mechanics: Theory and Experiment*, 2007(07):P07012, 2007. URL http://stacks.iop.org/1742-5468/2007/i=07/a=P07012.

[27] Crispin Gardiner. *Stochastic Methods*. Springer-Verlag Berlin Heidelberg, 4 edition, 2009. ISBN 978-3-540-70712-7.

[28] Frank Schweitzer. *Brownian Agents and Active Particles: Collective Dynamics in the Natural and Social Sciences*. Springer Publishing Company, Incorporated, 2007. ISBN 3540738444.

[29] Tamás Vicsek, András Czirók, Eshel Ben-Jacob, Inon Cohen, and Ofer Shochet. Novel type of phase transition in a system of self-driven particles. *Physical Review Letters*, 75(6):1226, 1995.

[30] Francesco Ginelli. The physics of the vicsek model. *The European Physical Journal Special Topics*, 225(11):2099–2117, Nov 2016. ISSN 1951-6401. doi: 10.1140/epjst/e2016-60066-8. URL https://doi.org/10.1140/epjst/e2016-60066-8.

[31] R. Großmann, P. Romanczuk, M. Bär, and L. Schimansky-Geier. Pattern formation in active particle systems due to competing alignment interactions. *The European Physical Journal Special Topics*, 224(7):1325–1347, Jul 2015. ISSN 1951-6401. doi: 10.1140/epjst/e2015-02462-3. URL https://doi.org/10.1140/epjst/e2015-02462-3.

[32] P. M. Chaikin and T. C. Lubensky. *Principles of Condensed Matter Physics*. Cambridge University Press, 1995. doi: 10.1017/CBO9780511813467.

[33] Thomas Ihle. Invasion-wave-induced first-order phase transition in systems of active particles. *Phys. Rev. E*, 88:040303, Oct 2013. doi: 10.1103/PhysRevE.88.040303. URL https://link.aps.org/doi/10.1103/PhysRevE.88.040303.

[34] Thomas Ihle. Kinetic theory of flocking: Derivation of hydrodynamic equations. *Phys. Rev. E*, 83:030901, Mar 2011. doi: 10.1103/PhysRevE.83.030901. URL https://link.aps.org/doi/10.1103/PhysRevE.83.030901.

[35] Leiming Chen, John Toner, and Chiu Fan Lee. Critical phenomenon of the orderdisorder transition in incompressible active fluids. *New Journal of Physics*, 17(4):042002, 2015. URL http://stacks.iop.org/1367-2630/17/i=4/a=042002.

[36] Francesco Ginelli and Hugues Chaté. Relevance of metric-free interactions in flocking phenomena. *Phys. Rev. Lett.*, 105:168103, Oct 2010. doi: 10.1103/PhysRevLett.105.168103. URL https://0-link-aps-org.pugwash.lib.warwick.ac.uk/doi/10.1103/PhysRevLett.105.168103.

[37] Yen-Liang Chou, Rylan Wolfe, and Thomas Ihle. Kinetic theory for systems of self-propelled particles with metric-free interactions. *Phys. Rev. E*, 86:021120, Aug 2012. doi: 10.1103/PhysRevE.86.021120. URL https://link.aps.org/doi/10.1103/PhysRevE.86.021120.

[38] Jean-Baptiste Caussin, Alexandre Solon, Anton Peshkov, Hugues Chaté, Thierry Dauxois, Julien Tailleur, Vincenzo Vitelli, and Denis Bartolo. Emergent spatial structures in flocking models: A dynamical system insight. *Phys. Rev. Lett.*, 112:148102, Apr 2014. doi: 10.1103/PhysRevLett.112.148102. URL https://link.aps.org/doi/10.1103/PhysRevLett.112.148102.

[39] Victor Dossetti and Francisco J. Sevilla. Emergence of collective motion in a model of interacting brownian particles. *Phys. Rev. Lett.*, 115:058301, Jul

2015. doi: 10.1103/PhysRevLett.115.058301. URL https://link.aps.org/doi/10.1103/PhysRevLett.115.058301.

[40] R Gromann, L Schimansky-Geier, and P Romanczuk. Active brownian particles with velocity-alignment and active fluctuations. *New Journal of Physics*, 14(7):073033, 2012. URL http://stacks.iop.org/1367-2630/14/i=7/a=073033.

[41] Antoine Bricard, Jean-Baptiste Caussin, Nicolas Desreumaux, Olivier Dauchot, and Denis Bartolo. Emergence of macroscopic directed motion in populations of motile colloids. *Nature*, 503:95–98, November 2013. doi: 10.1038/nature12673.

[42] Gil Ariel and Amir Ayali. Locust collective motion and its modeling. *PLOS Computational Biology*, 11(12):1–25, 12 2015. doi: 10.1371/journal.pcbi.1004522. URL https://doi.org/10.1371/journal.pcbi.1004522.

[43] J. Buhl, D. J. T. Sumpter, I. D. Couzin, J. J. Hale, E. Despland, E. R. Miller, and S. J. Simpson. From disorder to order in marching locusts. *Science*, 312 (5778):1402–1406, 2006. ISSN 0036-8075. doi: 10.1126/science.1125142. URL http://science.sciencemag.org/content/312/5778/1402.

[44] J. Tailleur and M. E. Cates. Statistical mechanics of interacting run-and-tumble bacteria. *Phys. Rev. Lett.*, 100:218103, May 2008. doi: 10.1103/PhysRevLett.100.218103. URL https://0-link-aps-org.pugwash.lib.warwick.ac.uk/doi/10.1103/PhysRevLett.100.218103.

[45] M. E. Cates and J. Tailleur. When are active brownian particles and run-and-tumble particles equivalent? consequences for motility-induced phase separation. *EPL (Europhysics Letters)*, 101(2):20010, 2013. URL http://stacks.iop.org/0295-5075/101/i=2/a=20010.

[46] Andreas Zttl and Holger Stark. Emergent behavior in active colloids. *Journal of Physics: Condensed Matter*, 28(25):253001, 2016. URL http://stacks.iop.org/0953-8984/28/i=25/a=253001.

[47] Michael E. Cates and Julien Tailleur. Motility-induced phase separation. *Annual Review of Condensed Matter Physics*, 6(1):219–244, 2015. doi: 10.1146/annurev-conmatphys-031214-014710. URL https://doi.org/10.1146/annurev-conmatphys-031214-014710.

[48] Davide Marenduzzo. An introduction to the statistical physics of active matter: motility-induced phase separation and the "generic instability" of active gels. *The European Physical Journal Special Topics*, 225(11):2065–2077, Nov 2016. ISSN 1951-6401. doi: 10.1140/epjst/e2016-60084-6. URL https://doi.org/10.1140/epjst/e2016-60084-6.

[49] Wen Yang, Vyacheslav R. Misko, Jacques Tempere, Minghui Kong, and Francois M. Peeters. Artificial living crystals in confined environment. *Phys. Rev. E*, 95:062602, Jun 2017. doi: 10.1103/PhysRevE.95.062602. URL https://link.aps.org/doi/10.1103/PhysRevE.95.062602.

[50] Bo Li, Di Zhou, and Yilong Han. Assembly and phase transitions of colloidal crystals. *Nature Reviews Materials*, 1(15011), January 2016. doi: 10.1038/natrevmats.2015.11.

[51] Marjolein Dijkstra. *Entropy-Driven Phase Transitions in Colloids: From spheres to anisotropic particles*, pages 35–71. John Wiley & Sons, Inc., 2014. ISBN 9781118949702. doi: 10.1002/9781118949702.ch2. URL http://dx.doi.org/10.1002/9781118949702.ch2.

[52] Jeremie Palacci, Stefano Sacanna, Asher Preska Steinberg, David J. Pine, and Paul M. Chaikin. Living crystals of light-activated colloidal surfers. *Science*, 339(6122):936–940, 2013. ISSN 0036-8075. doi: 10.1126/science.1230020. URL http://science.sciencemag.org/content/339/6122/936.

[53] Daan Frenkel. Order through disorder: entropy strikes back. *Physics World*, 6(2):24, 1993. URL http://stacks.iop.org/2058-7058/6/i=2/a=24.

[54] G. De Magistris and D. Marenduzzo. An introduction to the physics of active matter. *Physica A: Statistical Mechanics and its Applications*, 418(Supplement C):65 – 77, 2015. ISSN 0378-4371. doi: https://doi.org/10.1016/j.physa.2014.06.061. URL http://www.sciencedirect.com/science/article/pii/S0378437114005366. Proceedings of the 13th International Summer School on Fundamental Problems in Statistical Physics.

[55] J. Palacci, S. Sacanna, S.-H. Kim, G.-R. Yi, D. J. Pine, and P. M. Chaikin. Light-activated self-propelled colloids. *Philosophical Transactions of the Royal Society of London A: Mathematical, Physical and Engineering Sciences*, 372 (2029), 2014. ISSN 1364-503X. doi: 10.1098/rsta.2013.0372. URL http://rsta.royalsocietypublishing.org/content/372/2029/20130372.

[56] B. M. Mognetti, A. Šarić, S. Angioletti-Uberti, A. Cacciuto, C. Valeriani, and D. Frenkel. Living clusters and crystals from low-density suspensions of active colloids. *Phys. Rev. Lett.*, 111:245702, Dec 2013. doi: 10.1103/PhysRevLett.111.245702. URL https://0-link-aps-org.pugwash.lib.warwick.ac.uk/doi/10.1103/PhysRevLett.111.245702.

[57] Wei Wang, Wentao Duan, Suzanne Ahmed, Ayusman Sen, and Thomas E. Mallouk. From one to many: Dynamic assembly and collective behavior of self-propelled colloidal motors. *Accounts of Chemical Research*, 48(7):1938–1946, 2015. doi: 10.1021/acs.accounts.5b00025. URL http://dx.doi.org/10.1021/acs.accounts.5b00025. PMID: 26057233.

[58] J. Schwarz-Linek, C. Valeriani, A. Cacciuto, M. E. Cates, D. Marenduzzo, A. N. Morozov, and W. C. K. Poon. Phase separation and rotor self-assembly in active particle suspensions. *Proceedings of the National Academy of Sciences*, 109(11):4052–4057, 2012. doi: 10.1073/pnas.1116334109. URL http://www.pnas.org/content/109/11/4052.abstract.

[59] Alexander P. Petroff, Xiao-Lun Wu, and Albert Libchaber. Fast-moving bacteria self-organize into active two-dimensional crystals of rotating cells. *Phys. Rev. Lett.*, 114:158102, Apr 2015. doi: 10.1103/PhysRevLett.114.158102. URL https://0-link-aps-org.pugwash.lib.warwick.ac.uk/doi/10.1103/PhysRevLett.114.158102.

[60] Chen, Xiao, Yang, Xiang, Yang, Mingcheng, and Zhang, H. P. Dynamic clustering in suspension of motile bacteria. *EPL*, 111(5):54002, 2015. doi: 10.1209/0295-5075/111/54002. URL https://doi.org/10.1209/0295-5075/111/54002.

[61] R C Gerum, B Fabry, C Metzner, M Beaulieu, A Ancel, and D P Zitterbart. The origin of traveling waves in an emperor penguin huddle. *New Journal of Physics*, 15(12):125022, 2013. URL http://stacks.iop.org/1367-2630/15/i=12/a=125022.

[62] John Toner and Yuhai Tu. Long-range order in a two-dimensional dynamical XY model: How birds fly together. *Phys. Rev. Lett.*, 75:4326–4329, Dec 1995. doi: 10.1103/PhysRevLett.75.4326. URL https://link.aps.org/doi/10.1103/PhysRevLett.75.4326.

[63] John Toner and Yuhai Tu. Flocks, herds, and schools: A quantitative theory

of flocking. *Phys. Rev. E*, 58:4828–4858, Oct 1998. doi: 10.1103/PhysRevE.58.4828. URL https://link.aps.org/doi/10.1103/PhysRevE.58.4828.

[64] Ramin Golestanian. Collective behavior of thermally active colloids. *Phys. Rev. Lett.*, 108:038303, Jan 2012. doi: 10.1103/PhysRevLett.108.038303. URL https://link.aps.org/doi/10.1103/PhysRevLett.108.038303.

[65] Evelyn F. Keller and Lee A. Segel. Initiation of slime mold aggregation viewed as an instability. *Journal of Theoretical Biology*, 26(3):399 – 415, 1970. ISSN 0022-5193. doi: https://doi.org/10.1016/0022-5193(70)90092-5. URL http://www.sciencedirect.com/science/article/pii/0022519370900925.

[66] F. Jlicher, K. Kruse, J. Prost, and J.-F. Joanny. Active behavior of the cytoskeleton. *Physics Reports*, 449(1):3 – 28, 2007. ISSN 0370-1573. doi: https://doi.org/10.1016/j.physrep.2007.02.018. URL http://www.sciencedirect.com/science/article/pii/S0370157307001330. Nonequilibrium physics: From complex fluids to biological systems III. Living systems.

[67] J. Prost, F. Julicher, and J-F. Joanny. Active gel physics. *Nature Physics*, 11: 11–117, 2015. doi: doi:10.1038/nphys3224.

[68] Pawel Romanczuk, Hugues Chat, Leiming Chen, Sandrine Ngo, and John Toner. Emergent smectic order in simple active particle models. *New Journal of Physics*, 18(6):063015, 2016. URL http://stacks.iop.org/1367-2630/18/i=6/a=063015.

[69] Amin Doostmohammadi, Michael F. Adamer, Sumesh P. Thampi, and Julia M. Yeomans. Stabilization of active matter by flow-vortex lattices and defect ordering. *Nature Communications*, 7(10557), February 2016. doi: 10.1038/ncomms10557.

[70] Francis G. Woodhouse and Raymond E. Goldstein. Spontaneous circulation of confined active suspensions. *Phys. Rev. Lett.*, 109:168105, Oct 2012. doi: 10.1103/PhysRevLett.109.168105. URL https://link.aps.org/doi/10.1103/PhysRevLett.109.168105.

[71] C. W. Wächtler, F. Kogler, and S. H. L. Klapp. Lane formation in a driven attractive fluid. *Phys. Rev. E*, 94:052603, Nov 2016. doi: 10.1103/PhysRevE.94.052603. URL https://link.aps.org/doi/10.1103/PhysRevE.94.052603.

[72] A M Menzel. Unidirectional laning and migrating cluster crystals in confined self-propelled particle systems. *Journal of Physics: Condensed Matter*, 25

(50):505103, 2013. URL http://stacks.iop.org/0953-8984/25/i=50/a=505103.

[73] Supropriya Saha, Ramin Golestanian, and Sriram Ramaswamy. Clusters, asters, and collective oscillations in chemotactic colloids. *Phys. Rev. E*, 89: 062316, Jun 2014. doi: 10.1103/PhysRevE.89.062316. URL https://link.aps.org/doi/10.1103/PhysRevE.89.062316.

[74] Andreas M. Menzel and Hartmut Löwen. Traveling and resting crystals in active systems. *Phys. Rev. Lett.*, 110:055702, Feb 2013. doi: 10.1103/PhysRevLett.110.055702. URL https://link.aps.org/doi/10.1103/PhysRevLett.110.055702.

[75] Yilin Wu. Collective motion of bacteria in two dimensions. *Quantitative Biology*, 3(4):199–205, Dec 2015. ISSN 2095-4697. doi: 10.1007/s40484-015-0057-7. URL https://doi.org/10.1007/s40484-015-0057-7.

[76] H H Wensink and H Lwen. Emergent states in dense systems of active rods: from swarming to turbulence. *Journal of Physics: Condensed Matter*, 24 (46):464130, 2012. URL http://stacks.iop.org/0953-8984/24/i=46/a=464130.

[77] R Gromann, L Schimansky-Geier, and P Romanczuk. Self-propelled particles with selective attractionrepulsion interaction: from microscopic dynamics to coarse-grained theories. *New Journal of Physics*, 15(8):085014, 2013. URL http://stacks.iop.org/1367-2630/15/i=8/a=085014.

[78] Alexandre Morin, Jean-Baptiste Caussin, Christophe Eloy, and Denis Bartolo. Collective motion with anticipation: Flocking, spinning, and swarming. *Phys. Rev. E*, 91:012134, Jan 2015. doi: 10.1103/PhysRevE.91.012134. URL https://link.aps.org/doi/10.1103/PhysRevE.91.012134.

[79] Michael Shelley. On a roll. *Nature*, 503:43–44, November 2013. doi: 10.1038/503043a.

[80] Samuel Sanchez, Alexander A. Solovev, Stefan M. Harazim, Christoph Deneke, Yong Feng Mei, and Oliver G. Schmidt. The smallest man-made jet engine. *The Chemical Record*, 11(6):367–370, 2011. ISSN 1528-0691. doi: 10.1002/tcr.201100010. URL http://dx.doi.org/10.1002/tcr.201100010.

[81] Samuel Snchez and Martin Pumera. Nanorobots: The ultimate wireless self-propelled sensing and actuating devices. *Chemistry An Asian Journal*, 4

(9):1402–1410, 2009. ISSN 1861-471X. doi: 10.1002/asia.200900143. URL http://dx.doi.org/10.1002/asia.200900143.

[82] Yongfeng Mei, Alexander A. Solovev, Samuel Sanchez, and Oliver G. Schmidt. Rolled-up nanotech on polymers: from basic perception to self-propelled catalytic microengines. *Chem. Soc. Rev.*, 40:2109–2119, 2011. doi: 10.1039/C0CS00078G. URL http://dx.doi.org/10.1039/C0CS00078G.

[83] Remi Dreyfus, Jean Baudry, Marcus L. Roper, Marc Fermigier, Howard A. Stone, and Jerome Bibette. Micoscopic artificial swimmers. *Nature*, 437:862–865, 2005.

[84] Brian J. Williams, Sandeep V. Anand, Jagannathan Rajagopalan, and M. Taher A. Saif. A self-propelled biohybrid swimmer at low reynolds number. *Nature Communications*, 5(3081), January 2014. doi: 10.1038/ncomms4081.

[85] Timothy Sanchez, David Welch, Daniela Nicastro, and Zvonimir Dogic. Cilia-like beating of active microtubule bundles. *Science*, 333(6041):456–459, 2011. ISSN 0036-8075. doi: 10.1126/science.1203963. URL http://science.sciencemag.org/content/333/6041/456.

[86] Gauger, E. M., Downton, M. T., and Stark, H. Fluid transport at low reynolds number with magnetically actuated artificial cilia. *Eur. Phys. J. E*, 28(2):231–242, 2009. doi: 10.1140/epje/i2008-10388-1. URL https://doi.org/10.1140/epje/i2008-10388-1.

[87] Yong Woon Kim and Roland R. Netz. Pumping fluids with periodically beating grafted elastic filaments. *Phys. Rev. Lett.*, 96:158101, Apr 2006. doi: 10.1103/PhysRevLett.96.158101. URL https://0-link-aps-org.pugwash.lib.warwick.ac.uk/doi/10.1103/PhysRevLett.96.158101.

[88] Sina Sareh, Jonathan Rossiter, Andrew Conn, Knut Drescher, and Raymond E. Goldstein. Swimming like algae: biomimetic soft artificial cilia. *Journal of The Royal Society Interface*, 10(78), 2013. ISSN 1742-5689. doi: 10.1098/rsif.2012.0666. URL http://rsif.royalsocietypublishing.org/content/10/78/20120666.

[89] J L Anderson. Colloid transport by interfacial forces. *Annual Review of Fluid Mechanics*, 21(1):61–99, 1989. doi: 10.1146/annurev.fl.21.010189.000425. URL https://doi.org/10.1146/annurev.fl.21.010189.000425.

[90] J. L. Anderson, M. E. Lowell, and D. C. Prieve. Motion of a particle generated by chemical gradients part 1. non-electrolytes. *Journal of Fluid Mechanics*, 117:107121, 1982. doi: 10.1017/S0022112082001542.

[91] Franz M. Weinert and Dieter Braun. Observation of slip flow in thermophoresis. *Phys. Rev. Lett.*, 101:168301, Oct 2008. doi: 10.1103/PhysRevLett.101.168301. URL https://link.aps.org/doi/10.1103/PhysRevLett.101.168301.

[92] Jeffrey L. Moran and Jonathan D. Posner. Phoretic self-propulsion. *Annual Review of Fluid Mechanics*, 49(1):511–540, 2017. doi: 10.1146/annurev-fluid-122414-034456. URL https://doi.org/10.1146/annurev-fluid-122414-034456.

[93] Pierre Illien, Ramin Golestanian, and Ayusman Sen. 'fuelled' motion: phoretic motility and collective behaviour of active colloids. *Chem. Soc. Rev.*, 46:5508–5518, 2017. doi: 10.1039/C7CS00087A. URL http://dx.doi.org/10.1039/C7CS00087A.

[94] W. C. K. Poon. *From Clarkia to Escherichia and Janus: The physics of natural and synthetic active colloids*, pages 317–386. Proceedings of the International School of Physics Enrico Fermi. IOS Press, 2013. ISBN 978-1-61499-277-6. doi: 10.3254/978-1-61499-278-3-317.

[95] Krishna Kanti Dey, Flory Wong, Alicia Altemose, and Ayusman Sen. Catalytic motors- quo vadimus? *Current Opinion in Colloid & Interface Science*, 21:4 – 13, 2016. ISSN 1359-0294. doi: https://doi.org/10.1016/j.cocis.2015.12.001. URL https://www.sciencedirect.com/science/article/pii/S1359029415001120.

[96] Jonathan R. Howse, Richard A. L. Jones, Anthony J. Ryan, Tim Gough, Reza Vafabakhsh, and Ramin Golestanian. Self-motile colloidal particles: From directed propulsion to random walk. *Phys. Rev. Lett.*, 99:048102, Jul 2007. doi: 10.1103/PhysRevLett.99.048102. URL https://link.aps.org/doi/10.1103/PhysRevLett.99.048102.

[97] Benedikt Sabass and Udo Seifert. Dynamics and efficiency of a self-propelled, diffusiophoretic swimmer. *The Journal of Chemical Physics*, 136(6):064508, 2012. doi: 10.1063/1.3681143. URL https://doi.org/10.1063/1.3681143.

[98] L. Baraban, M. Tasinkevych, M. N. Popescu, S. Sanchez, S. Dietrich, and O. G. Schmidt. Transport of cargo by catalytic janus micro-motors. *Soft*

Matter, 8:48–52, 2012. doi: 10.1039/C1SM06512B. URL http://dx.doi.org/10.1039/C1SM06512B.

[99] JEFFREY L. MORAN and JONATHAN D. POSNER. Electrokinetic locomotion due to reaction-induced charge auto-electrophoresis. *Journal of Fluid Mechanics*, 680:3166, 2011. doi: 10.1017/jfm.2011.132.

[100] Walter F. Paxton, Kevin C. Kistler, Christine C. Olmeda, Ayusman Sen, Sarah K. St. Angelo, Yanyan Cao, Thomas E. Mallouk, Paul E. Lammert, and Vincent H. Crespi. Catalytic nanomotors: autonomous movement of striped nanorods. *Journal of the American Chemical Society*, 126(41):13424–13431, 2004. doi: 10.1021/ja047697z. URL http://dx.doi.org/10.1021/ja047697z. PMID: 15479099.

[101] Sebastien Fournier-Bidoz, Andre C. Arsenault, Ian Manners, and Geoffrey A. Ozin. Synthetic self-propelled nanorotors. *Chem. Commun.*, pages 441–443, 2005. doi: 10.1039/B414896G. URL http://dx.doi.org/10.1039/B414896G.

[102] R Piazza and A Parola. Thermophoresis in colloidal suspensions. *Journal of Physics: Condensed Matter*, 20(15):153102, 2008. URL http://stacks.iop.org/0953-8984/20/i=15/a=153102.

[103] Stefan Duhr and Dieter Braun. Why molecules move along a temperature gradient. *Proceedings of the National Academy of Sciences*, 103(52):19678–19682, 2006. doi: 10.1073/pnas.0603873103. URL http://www.pnas.org/content/103/52/19678.abstract.

[104] Klaus Kroy, Dipanjan Chakraborty, and Frank Cichos. Hot microswimmers. *The European Physical Journal Special Topics*, 225(11):2207–2225, Nov 2016. ISSN 1951-6401. doi: 10.1140/epjst/e2016-60098-6. URL https://doi.org/10.1140/epjst/e2016-60098-6.

[105] R. Golestanian. Debut of a hot "fantastic voyager". *Physics Online Journal*, 3:108, December 2010. doi: 10.1103/Physics.3.108.

[106] Hong-Ren Jiang, Natsuhiko Yoshinaga, and Masaki Sano. Active motion of a janus particle by self-thermophoresis in a defocused laser beam. *Phys. Rev. Lett.*, 105:268302, Dec 2010. doi: 10.1103/PhysRevLett.105.268302. URL https://link.aps.org/doi/10.1103/PhysRevLett.105.268302.

[107] Mingcheng Yang and Marisol Ripoll. Simulations of thermophoretic nanoswimmers. *Phys. Rev. E*, 84:061401, Dec 2011. doi: 10.1103/PhysRevE.84.061401. URL https://0-link-aps-org.pugwash.lib.warwick.ac.uk/doi/10.1103/PhysRevE.84.061401.

[108] Daniel Rings, Markus Selmke, Frank Cichos, and Klaus Kroy. Theory of hot brownian motion. *Soft Matter*, 7:3441–3452, 2011. doi: 10.1039/C0SM00854K. URL http://dx.doi.org/10.1039/C0SM00854K.

[109] Daniel Rings, Romy Schachoff, Markus Selmke, Frank Cichos, and Klaus Kroy. Hot brownian motion. *Phys. Rev. Lett.*, 105:090604, Aug 2010. doi: 10.1103/PhysRevLett.105.090604. URL https://link.aps.org/doi/10.1103/PhysRevLett.105.090604.

[110] Alberto Parola and Roberto Piazza. A microscopic approach to thermophoresis in colloidal suspensions. *Journal of Physics: Condensed Matter*, 17(45): S3639, 2005. URL http://stacks.iop.org/0953-8984/17/i=45/a=059.

[111] Bian Qian, Daniel Montiel, Andreas Bregulla, Frank Cichos, and Haw Yang. Harnessing thermal fluctuations for purposeful activities: the manipulation of single micro-swimmers by adaptive photon nudging. *Chem. Sci.*, 4:1420–1429, 2013. doi: 10.1039/C2SC21263C. URL http://dx.doi.org/10.1039/C2SC21263C.

[112] Marco Braun and Frank Cichos. Optically controlled thermophoretic trapping of single nano-objects. *ACS Nano*, 7(12):11200–11208, 2013. doi: 10.1021/nn404980k. URL http://dx.doi.org/10.1021/nn404980k. PMID: 24215133.

[113] Ognjen Ilic, Ido Kaminer, Yoav Lahini, Hrvoje Buljan, and Marin Soljai. Exploiting optical asymmetry for controlled guiding of particles with light. *ACS Photonics*, 3(2):197–202, 2016. doi: 10.1021/acsphotonics.5b00605. URL http://dx.doi.org/10.1021/acsphotonics.5b00605.

[114] Andreas P. Bregulla, Haw Yang, and Frank Cichos. Stochastic localization of microswimmers by photon nudging. *ACS Nano*, 8(7):6542–6550, 2014. doi: 10.1021/nn501568e. URL http://dx.doi.org/10.1021/nn501568e. PMID: 24861455.

[115] Spas Nedev, Sol Carretero-Palacios, Paul Khler, Theobald Lohmller, Alexander S. Urban, Lindsey J. E. Anderson, and Jochen Feldmann. An optically

controlled microscale elevator using plasmonic janus particles. *ACS Photonics*, 2(4):491–496, 2015. doi: 10.1021/ph500371z. URL http://dx.doi.org/10.1021/ph500371z. PMID: 25950013.

[116] Sabrina Simoncelli, Samuel Johnson, Franziska Kriegel, Jan Lipfert, and Jochen Feldmann. Stretching and heating single dna molecules with optically trapped goldsilica janus particles. *ACS Photonics*, 0(0):null, 0. doi: 10.1021/acsphotonics.7b00839. URL http://dx.doi.org/10.1021/acsphotonics.7b00839.

[117] Linhan Lin, Xiaolei Peng, Xiaoling Wei, Zhangming Mao, Chong Xie, and Yuebing Zheng. Thermophoretic tweezers for low-power and versatile manipulation of biological cells. *ACS Nano*, 11(3):3147–3154, 2017. doi: 10.1021/acsnano.7b00207. URL http://dx.doi.org/10.1021/acsnano.7b00207. PMID: 28230355.

[118] Wei Li, Xiaoran Wu, Hong Qin, Zhongqiang Zhao, and Hewen Liu. Light-driven and light-guided microswimmers. *Advanced Functional Materials*, 26 (18):3164–3171, 2016. ISSN 1616-3028. doi: 10.1002/adfm.201505378. URL http://dx.doi.org/10.1002/adfm.201505378.

[119] Jaideep Katuri, Xing Ma, Morgan M. Stanton, and Samuel Snchez. Designing micro- and nanoswimmers for specific applications. *Accounts of Chemical Research*, 50(1):2–11, 2017. doi: 10.1021/acs.accounts.6b00386. URL http://dx.doi.org/10.1021/acs.accounts.6b00386. PMID: 27809479.

[120] Jack A. Cohen and Ramin Golestanian. Emergent cometlike swarming of optically driven thermally active colloids. *Phys. Rev. Lett.*, 112:068302, Feb 2014. doi: 10.1103/PhysRevLett.112.068302. URL https://link.aps.org/doi/10.1103/PhysRevLett.112.068302.

[121] Daniel J. G. Pearce, Adam M. Miller, George Rowlands, and Matthew S. Turner. Role of projection in the control of bird flocks. *Proceedings of the National Academy of Sciences*, 111(29):10422–10426, 2014. doi: 10.1073/pnas.1402202111. URL http://www.pnas.org/content/111/29/10422.abstract.

[122] George B. Witman. Chlamydomonas phototaxis. *Trends in Cell Biology*, 3(11):403 – 408, 1993. ISSN 0962-8924. doi: https://doi.org/10.1016/0962-8924(93)90091-E. URL http://www.sciencedirect.com/science/article/pii/096289249390091E.

[123] Gáspár Jékely. Evolution of phototaxis. *Philosophical Transactions of the Royal Society of London B: Biological Sciences*, 364(1531):2795–2808, 2009. ISSN 0962-8436. doi: 10.1098/rstb.2009.0072. URL http://rstb.royalsocietypublishing.org/content/364/1531/2795.

[124] Jorge Arrieta, Ana Barreira, Maurizio Chioccioli, Marco Polin, and Idan Tuval. Phototaxis beyond turning: persistent accumulation and response acclimation of the microalga chlamydomonas reinhardtii. *Scientific Reports*, 7 (3447), 2017. doi: 10.1038/s41598-017-03618-8.

[125] Silvano Furlan, Diego Comparini, Marzena Ciszak, Lucia Beccai, Stefano Mancuso, and Barbara Mazzolai. Origin of polar order in dense suspensions of phototactic micro-swimmers. *PLOS ONE*, 7(6):1–9, 06 2012. doi: 10.1371/journal.pone.0038895. URL https://doi.org/10.1371/journal.pone.0038895.

[126] R. V. Vincent and N. A. Hill. Bioconvection in a suspension of phototactic algae. *Journal of Fluid Mechanics*, 327:343371, 1996. doi: 10.1017/S0022112096008579.

[127] S. Ghorai and N. A. Hill. Penetrative phototactic bioconvection. *Physics of Fluids*, 17(7):074101, 2005. doi: 10.1063/1.1947807. URL https://doi.org/10.1063/1.1947807.

[128] S. Ghorai, M. K. Panda, and N. A. Hill. Bioconvection in a suspension of isotropically scattering phototactic algae. *Physics of Fluids*, 22(7):071901, 2010. doi: 10.1063/1.3457163. URL https://doi.org/10.1063/1.3457163.

[129] Andrea Giometto, Florian Altermatt, Amos Maritan, Roman Stocker, and Andrea Rinaldo. Generalized receptor law governs phototaxis in the phytoplankton euglena gracilis. *Proceedings of the National Academy of Sciences*, 112(22):7045–7050, 2015. doi: 10.1073/pnas.1422922112. URL http://www.pnas.org/content/112/22/7045.abstract.

[130] Michael F Modest. *Radiative Heat Transfer*. Elsevier, 3 edition, 2013. ISBN 978-0-12-386944-9. doi: 10.1016/C2010-0-65874-3.

[131] Stefan Duhr and Dieter Braun. Thermophoretic depletion follows boltzmann distribution. *Phys. Rev. Lett.*, 96:168301, Apr 2006. doi: 10.1103/PhysRevLett.96.168301. URL https://0-link-aps-org.pugwash.lib.warwick.ac.uk/doi/10.1103/PhysRevLett.96.168301.

[132] R. M. Corless, G. H. Gonnet, D. E. G. Hare, D. J. Jeffrey, and D. E. Knuth. On the lambertw function. *Advances in Computational Mathematics*, 5(1): 329–359, Dec 1996. ISSN 1572-9044. doi: 10.1007/BF02124750. URL https://doi.org/10.1007/BF02124750.

[133] David S Bradshaw and David L Andrews. Manipulating particles with light: radiation and gradient forces. *European Journal of Physics*, 38(3):034008, 2017. URL http://stacks.iop.org/0143-0807/38/i=3/a=034008.

[134] David McGloin, Craig McDonald, and Yuri Belotti. *Colloidal Interactions with Optical Fields: Optical Tweezers*, chapter 7, pages 111–130. Wiley-Blackwell, 2016. ISBN 9781119220510. doi: 10.1002/9781119220510.ch7. URL https://onlinelibrary.wiley.com/doi/abs/10.1002/9781119220510.ch7.

[135] A. Ashkin. Acceleration and trapping of particles by radiation pressure. *Phys. Rev. Lett.*, 24:156–159, Jan 1970. doi: 10.1103/PhysRevLett.24.156. URL https://0-link-aps-org.pugwash.lib.warwick.ac.uk/doi/10.1103/PhysRevLett.24.156.